TAMPEREEN TEKNILLINEN YLIOPISTO
TAMPERE UNIVERSITY OF TECHNOLOGY

Sami Rissanen

Modulation of Membrane Lipid Receptors Explored via Multiscale Computer Simulations

Julkaisu 1606 • Publication 1606

Tampere 2018

Tampereen teknillinen yliopisto. Julkaisu 1606
Tampere University of Technology. Publication 1606

Sami Rissanen

Modulation of Membrane Lipid Receptors Explored via Multiscale Computer Simulations

Thesis for the degree of Doctor of Science in Technology to be presented with due permission for public examination and criticism in Rakennustalo Building, Auditorium RG202, at Tampere University of Technology, on the 13th of December 2018, at 12 noon.

Tampereen teknillinen yliopisto - Tampere University of Technology
Tampere 2018

Doctoral candidate:	Sami Rissanen Laboratory of Physics/Biological Physics and Soft Matter Group Faculty of Natural Sciences Tampere University of Technology Finland
Supervisor:	Ilpo Vattulainen, Prof. Laboratory of Physics/Biological Physics and Soft Matter Group Faculty of Natural Sciences Tampere University of Technology Finland
Pre-examiners:	Gerhard Schütz, Prof. Institute of Applied Physics Vienna University of Technology Austria
	Roland Faller, Prof. Department of Chemical Engineering University of California Davis The United States of America
Opponent:	Giulia Rossi, Ph.D. Physics Department University of Genoa Italy

ISBN 978-952-15-4272-5 (printed)
ISBN 978-952-15-4301-2 (PDF)
ISSN 1459-2045

ABSTRACT

This work focuses on two lipid receptors known as GM1 and phosphatidylinositol 4,5-bisphosphate ($PI(4,5)P_2$). GM1 is a ganglioside present in the outer plasma membrane, sensing signals from the outside of the cell, while $PI(4,5)P_2$ is an important phosphoinositide found in the inner leaflet of the plasma membrane. Due to their vital role in cellular life, studies of the lipid–lipid and lipid–protein interactions of these receptors have become an attractive venture for researchers. Nevertheless, despite a significant amount of work, the molecular details of these interactions have remained largely unknown due to the limited temporal and spatial resolution of the current experimental methods. Here we overcome this problem by using atomistic and coarse-grained molecular dynamics simulations applied to explore the structural and dynamical properties of these lipid receptors in various membranes.

In the first part of this Thesis, the functional properties of $PI(4,5)P_2$ were studied through lipid–protein interactions between $PI(4,5)P_2$, talin, and integrin. The simulations revealed a new means on how $PI(4,5)P_2$ together with talin interferes with the stability of the integrin transmembrane domains, suggesting a new mechanism for the first steps of integrin activation.

The second part of this Thesis focuses on various mechanisms that can alter and regulate lipid receptor binding properties. First, the binding of cholera toxin to GM1 and the fluorescent analog of the receptor was examined. A clear difference in the behavior between the native and the labeled GM1 was observed. These results highlight the importance of artifacts that fluorescent labeling can cause. Second, the intracellular calcium was shown to affect the $PI(4,5)P_2$ headgroup tilting and the related ligand binding. Importantly, these results were directly linked to cell signaling events through experimental findings observed by our collaborators. Finally, the fundamental question as to how the $PI(4,5)P_2$ receptor is recognized only in the plasma membrane but not in the other cell compartments was explored. Enhanced ligand binding to cholesterol-rich $PI(4,5)P_2$ membranes was found, suggesting that the steep cholesterol gradient along the secretory pathway in a cell may be a part of the machinery coordinating the specific cell organelle recognition.

Altogether, the Thesis provides novel insight on the function of lipid receptors, modulation of lipid–protein interactions, and highlights the added value gained by bridging scientific computing and novel computing tools with experimental science.

TIIVISTELMÄ

Tässä työssä käsitellään GM1 ja fosfatidyyli-inositoli-4,5-bisfosfaatti ($PI(4,5)P_2$) -lipidireseptoreita. GM1 on gangliosidi, joka esiintyy solukalvon ulommaisella puolella ja vastaanottaa solun ulkopuolelta tulevia signaaleja. $PI(4,5)P_2$ on tärkeä fosfatidyyli-inositoli ja esiintyy solukalvon sytosolisella osalla. Soluille elintärkeisiin toimintoihin osallistumisen takia lipidireseptoreiden vuorovaikutukset muiden lipidien sekä proteiinien kanssa ovat olleet monien tutkimusten kohteena. Suuresta huomiosta ja panostuksesta huolimatta reseptoreiden toiminnallisista yksityiskohdista tiedetään kuitenkin edelleen verrattain vähän. Tämä johtuu nykyisten kokeellisten menetelmien haasteista tutkia pieniä nanoskaaloja sekä niiden nopeaa dynamiikkaa. Tässä työssä käytetään atomistisia sekä karkeistettuja molekyylidynamiikkasimulaatioita kyseisten lipidireseptoreiden rakenteellisten ja dynaamisten ominaisuuksien selvittämiseen.

Väitöstyön ensimmäisessä osassa tutkitaan $PI(4,5)P_2$-reseptorin vuorovaikutuksia integriinin kanssa. Simulaatiot paljastivat uuden mekanismin, jolla $PI(4,5)P_2$ yhdessä talin-proteiinin kanssa voi häiritä integriinin kalvossa olevan osan vakautta. Tulokset tarjoavat uuden mahdollisen selityksen sille, miten integriinien aktivoitumista voidaan säädellä solukalvoissa.

Jälkimmäinen osa tästä väitöstyöstä keskittyy lipidireseptorien toimintamekanismien säätelyyn. Ensiksi tutkitaan koleratoksiinin sitoutumista sekä sen luonnolliseen GM1-reseptoriin että sen fluoresoivaksi muokattuun GM1-vastinpariin. Tulokset osoittavat selkeän eron proteiinin sitoutumisessa näiden reseptorien välillä, korostaen yleisesti käytettyjen fluoresoivien aineiden merkitystä ja vaikutusta tutkittaviin kohteisiin. Seuraavaksi selvitetään sytosolissa olevan kalsiumin vaikutus $PI(4,5)P_2$-reseptoriin ja sen aiheuttamiin muutoksiin proteiinin sitoutumisessa. Tulokset yhdistetään myös solusignalointireittiin kokeellisen yhteistyön kautta. Viimeiseksi tutkitaan perusperiaatetta siitä, miten $PI(4,5)P_2$-reseptori sitoo tiettyjä proteiineja pelkästään solukalvossa, mutta ei muissa solun soluelimissä. Tulokset havainnollistavat, että solukalvon kolesteroli parantaa proteiinien sitoutumista $PI(4,5)P_2$-reseptoriin. Tämä voi selittää soluelinten identiteettiä, kun jo ennestään tiedetään, että kolesterolikonsentraatio muuttuu eri solukalvoissa ja on korkeimmillaan juuri plasmakalvossa.

Kokonaisuutena tämä työ tarjoaa uusia näkemyksiä lipidireseptorien toiminnallisuudesta sekä lipidi–proteiini -vuorovaikutusten säätelystä. Työ korostaa laskennallisten ja kokeellisten tutkimusten yhteistyön tärkeyttä ja hyödyllisyyttä.

PREFACE

This Doctoral Thesis was carried out in the Biological Physics and Soft Matter (BIO) research group of the Laboratory of Physics of Tampere University of Technology (TUT). TUT graduate school, Alfred Kordelin Foundation, The Federation of European Biochemical Societies (FEBS), and Tekniikan edistämissäätiö (TES) are acknowledged for funding this Thesis project. The molecular dynamics simulations were conducted using the computing services of the Finnish IT Centre for Scientific Computing (CSC), the Tampere Center for Scientific Computing (TCSC), and the High-Performance Computing Center of the TU Dresden.

First of all, I would like to thank professor Ilpo Vattulainen for giving me the opportunity to carry out this exciting project in a friendly environment of his research group. Without his knowledge on the field and the resources of the group, this Thesis could not have been done.

Special thanks go to Tomasz Róg who adviced and supported me through the various stages of this project. Thanks should be also directed to Matti for all the spiritual support and fruitful discussions. I would also like to thank all of my other colleagues for their advice and making my days at work enjoyable. The work of all the co-authors is also greatly appreciated.

I am grateful to Dr. Ünal Coskun for the opportunity to visit in his group in Dresden. Thanks also to other people working there, especially Michal Grzybek and Eva Nedvedova, for making the visit both fun and useful.

Last but not least, I want to thank my family, friends, and especially Annina for all their company and support during my studies and the writing process of this Thesis.

Tampere, November 25, 2018

Sami Rissanen

CONTENTS

LIST OF SYMBOLS AND ABBREVIATIONS

AA	All-atom
AFM	Atomic force microscopy
bdGM1	Bodipy-GM1
BPTI	Bovine pancreatic trypsin inhibitor
β_2AR	β_2-adrenergic receptors
CER	Ceramide
Chol	Cholesterol
CG	Coarse-grained
COM	Center of mass
CTxB	Cholera toxin B subunit
DAG	Diacylglycerol
DOPC	1,2-dioleoyl-sn-glycero-3-phosphocholine
ECCR	Electronic continuum correction with the rescaling-method
ER	Endoplasmic reticulum
ESR	Electron spin resonance
F0–F3	PLC PH FERM domains F0–F3
F2–F3	PLC PH FERM domains F2–F3
GalNAc	*N*-acetylgalactosamine
GlcCer	Glucoceramide
GalCer	Galactosylceramide
GPCR	G-protein coupled receptor
GPMV	Giant plasma membrane vesicle
GPL	Glycerophospholipid
GSL	Glycosphingolipid
GUV	Giant unilamellar vesicle
H-bond	Hydrogen bond
IMC	Inner membrane clasp
IP3	Inositol 1,4,5-trisphosphate
L_d	Liquid-disordered
L_o	Liquid-ordered
LJ	Lennard–Jones
MD	Molecular dynamics
NMR	Nuclear magnetic resonance

NpT	Grand canonical ensemble
NVE	Microcanonical ensemble
NVT	Canonical ensemble
OH	Hydroxyl group
OMC	Outer membrane clasp
OPLS	Optimized potentials for liquid simulations
P1	Phosphorus atom in the PI(4,5)P_2 backbone
P4	Phosphorus atom in the position 4 of the PI(4,5)P_2 inositol ring
P5	Phosphorus atom in the position 5 of the PI(4,5)P_2 inositol ring
PBC	Periodic boundary condition
PA	Phosphatidic acid
PC	Phosphatidylcholine
PE	Phosphatidylethanolamine
PH	Pleckstrin homology
PI	Phosphoinositide
PI(4,5)P_2	Phosphatidylinositol 4,5-bisphosphate
PME	Particle-mesh Ewald
PLC	Phospholipase C
POPC	1-palmitoyl-2-oleoyl-sn-glycero-3-phosphocholine
PS	Phosphatidylserine
PtdIns	Phosphatidylinositol
SASA	Solvent accessible surface area
SM	Sphingomyelin
UA	United-atom
VMD	Visual Molecular Dynamics
vdW	van der Waals
v-rescale	Velocity rescaling

ϵ_{ij},σ_{ij}	Lennard–Jones parameters for particles i and j
ϵ_0	Permittivity of the vacuum
ϵ_r	Relative permittivity of the medium
Δt	Time step
ν	Frequency
$\mathcal{V}_{\mathrm{coulomb}}$	Coulombic contribution to the potential energy
$\mathcal{V}_{\mathrm{LJ}}$	van der Waals contribution to the potential energy
$\mathcal{V}_{\mathrm{TOT}}$	Total potential energy defined by force field

$\mathcal{V}_{\text{bonded}}$	Potential energy caused by bonded interactions
$\mathcal{V}_{\text{non-bonded}}$	Potential energy caused by non-bonded interactions
$\mathcal{V}_{\text{bond}}(r_{ij})$	Bond stretching contribution to the potential energy
$\mathcal{V}_{\text{angle}}(\theta_{ijk})$	Angle contribution to the potential energy
$\mathcal{V}_{\text{dihedral}}(\omega_{ijkl})$	Dihedral angle contribution to the potential energy
θ_{ijk}	Angle between particles i, j, and k
θ^0_{ijk}	Reference angle between particles i, j, and k
θ_z	Angle between the z-axis of the simulation box and the selected vector for deuterium order parameter
ω_{ijkl}	Dihedral angle between atoms i, j, k, and l
ω^0_{ijkl}	Reference dihedral angle between atoms i, j, k, and l
τ	Time constant for temperature coupling
$\mathbf{F}_i$	Force vector acting on a particle i
A	Area of a sphere
h	Planck's constant
k_{B}	Boltzmann's constant
$k_{r,ij}$	Force constant for bond stretching between atoms i and j
$k_{\theta,ijk}$	Force constant for the bending angle (ijk) vibration
$k_{\omega,ijkl}$	Force constant for the dihedral angle $(ijkl)$ vibration
K	Kinetic energy of particles
m_i	Mass of a particle i
M	Total mass of N particles
n	Integer denoting the periodicity of the rotational barrier in the dihedral potential function
N	Number of particles
N_f	Number of degrees of freedom
$\mathbf{r}_i$	Position vector of a particle i
q_i, q_j	Charges of particles i and j
r_{vdW}	van der Waals radius
r^0_{ij}	Reference bond length between atoms i and j
S_z	Order parameter
S_{CD}	Deuterium order parameter
t	Time
T	Temperature
T_0	Reference temperature
$\mathbf{v}_i$	Velocity vector of a particle i
x, y, z	Cartesian coordinates

LIST OF PUBLICATIONS

I **A. Orłowski, S. Kukkurainen, A. Pöyry, S. Rissanen, I. Vattulainen, V. Hytönen, and T. Róg.** "PIP2 and Talin Join Forces to Activate Integrin", *The Journal of Physical Chemistry B*, vol. 119, no. 38, pp. 12381–12389, 2015. DOI: 10.1021/acs.jpcb.5b06457.

II **S. Rissanen[‡], M. Grzybek[‡], A. Orłowski, T. Róg, O. Cramariuc, I. Levental, C. Eggeling, E. Sezgin, and I. Vattulainen.** "Phase Partitioning of GM1 and Its Bodipy-Labeled Analog Determine Their Different Binding to Cholera Toxin", *Frontiers in Physiology*, vol. 8, no. 252, 2017. DOI: 10.3389/fphys.2017.00252.

III **E. Bilkova[‡], R. Pleskot[‡], S. Rissanen[‡], S. Sun[‡], A. Czogalla, L. Cwiklik, T. Róg, I. Vattulainen, P. S. Cremer, P. Jungwirth, and Ü. Coskun.** "Calcium Directly Regulates Phosphatidylinositol 4,5-Bisphosphate Headgroup Conformation and Recognition", *Journal of the American Chemical Society*, vol. 139, no. 11, pp. 4019–4024, 2017. DOI: 10.1021/jacs.6b11760.

In this thesis, the candidate presents additional results to complement those presented in Article III. These unpublished data will be later submitted for publication (E. Nedvedova[‡], S. Rissanen[‡], A. Czogalla, P. Jurkiewicz, M. Grzybek, S. Cyboran-Mikołajczyk, L. Salmela, T. Róg, M. Hof, K. Fahmy, I. Vattulainen, and Ü. Coskun. "Cholesterol Determines PI(4,5)P_2 Presentation and Protein Recruitment", manuscript under preparation (2018)), but since the manuscript at the time of writing this Thesis is still incomplete, the draft of the paper is not included in this Thesis. Yet, the system details and the key results of that study will be discussed.

Authors marked as [‡] have contributed equally to the work (for details, see Chapter Author's Contribution).

AUTHOR'S CONTRIBUTION

I My part of designing the project was minor. In practice, I was responsible for the reference systems for the study. Therein, I prepared, performed, and analyzed all the systems without talin. I also implemented these results to the manuscript together with the first author (Adam Orłowski).

II I designed and prepared all the simulation systems, and conducted the simulations. Analysis of the computational data was done by the author. The *in silico* part of the study was lead by the author, who also coordinated the discussion between the computational and experimental labs. Michal Grzybek was the equally contributing first author, and he was responsible for the wet lab experiments. The two first authors equally wrote the first version of the manuscript.

III I shared the first-author status with 3 other researchers. I was the leading author regarding the atomistic simulation work. I designed the molecular dynamics simulations, excluding the Berger systems which were done by the co-author Roman Pleskot. The rest of the systems were prepared, performed and analyzed by the author. Moreover, all the equally contributing first authors participated equally to the paper writing. Four separate research groups were involved in this project, and I coordinated the discussion from our lab.

1. INTRODUCTION

Cells are the fundamental functional and structural units of all living organisms. To work properly, a cell has to respond to changes in its immediate environment and must be able to receive and process signals. Universally, all cells are surrounded by a plasma membrane that separates the interior of a cell from the extracellular space. The main function of the membrane is to act as a barrier and regulate the transport of matter and signals to and from a cell. In addition to the plasma membrane, also many other membrane structures exist within a cell, including several cell organelles and the nucleus of a eukaryotic cell.

The core of all the membranes is a lipid bilayer. It is a soft interface that is a few nanometers thick, consisting of various kinds of lipids. In cell membranes in cells, the lipid bilayer is complemented by other molecules, such as carbohydrates and, in particular, membrane-associated proteins. Although the importance of membranes in living systems is outstanding and they have been studied intensively during the past decades, the interactions and the communication between lipids and proteins is not well understood. By understanding the lipid–lipid and lipid–protein interactions in more detail, new treatments and drugs against diseases, such as cancer, could be designed.

Frequently, the problem to experimentally study the structure and the dynamics of a membrane is related to the small size and dynamical nature of the studied molecules. Computational simulations can be used to overcome this problem and unravel the dynamics and the structure of a biological system even in atomic-level resolution. While simulations also have limitations, the high-quality simulation models and the computer capacity have improved rapidly, shrinking the gap between experiments and simulations. Consequently, the computational tools have become more and more interesting for researchers, pharmaceutical companies, and biotechnology industries.

In this work, the properties of two lipid receptors are explored with the aid of molecular dynamics simulations. GM1, a well-known lipid marker for nanoscale liquid-ordered

membrane domains, and $PI(4,5)P_2$, the most abundant phosphoinositide in the inner leaflet of the plasma membrane, are studied in different membrane environments. Furthermore, most of the simulation studies discussed in this Thesis are also bridged to experiments done by our collaborators. The main focus in this Thesis is on the results achieved *in silico*.

1.1 Research Objectives and Scope of the Thesis

Integrins are crucial for several key cellular activities, including proliferation, survival, and gene expression [1]. Hence, revealing new insights on the first steps of integrin activation could reveal new target binding sites for drug molecules against diseases, such as cancer. The first objective of this work is to study how the $PI(4,5)P_2$ lipid receptor can bind talin (a well-known integrin activator [2, 3]) and further affect integrin stability.

The second main objective of this Thesis project is to study the effect of BODIPY, an often used fluorescent label, on the GM1 lipid receptor. Cholera toxin recognizes the native GM1 in the liquid-ordered phase. Nevertheless, in a recent study, the acyl-chain labeled BODIPY-GM1 was recognized in the opposing liquid-disordered phase [4]. The molecular details for the newly observed behavior remained unclear. Due to the critical role of interactions between GM1 and cholera toxin in diarrhea, and the interactions between the BODIPY labeled GM1 and cholera toxin in biomolecular studies, it is of exceptional importance to understand how GM1 interacts with its key partners in cell membranes.

Finally, the main focus of this work is to clarify how naturally existing molecules can modulate lipid receptor recognition. The intracellular calcium ions act as messengers to regulate cell migration, gene transcription, and apoptosis [5]. Moreover, phospholipase C (PLC) binding to $PI(4,5)P_2$ is known to result in the release of calcium ions to the cytosol [6]. Nevertheless, the effect of calcium on interactions between $PI(4,5)P_2$ and PLC has remained unknown. Also, $PI(4,5)P_2$ receptors are present not only in the plasma membrane but also in the other cell compartments, such as Golgi apparatus [7, 8]. How various $PI(4,5)P_2$ specific proteins, including PLC, can recognize $PI(4,5)P_2$ in the plasma membrane but not in the other cell compartments [9] is a fundamental question that has remained unsolved. Our aim is to unravel the enigma of the specific protein binding to the plasma membrane. In particular, the focus here is to clarify if the steep cholesterol concentration gradient

along the secretory pathway [10, 11] can correlate with the altered protein binding.

Altogether, the primary objective of this Thesis project is to provide one with new knowledge on the structure and dynamics of the well-known lipid receptors, GM1 and PI(4,5)P_2.

1.2 Structure of the Dissertation

This Thesis is structured as follows. First, the relevant biological background information related to cell membranes, lipids, and related proteins is described in Chapter 2. In Chapter 3, the utilized research methods, including the basics of molecular dynamics simulations and analysis tools are introduced. Chapter 4 gives an overview of the studied simulation systems. In Chapter 5, the key results of this project are presented and discussed. Section 5.1 is based on Article I and gives insight into the joint action of PI(4,5)P_2 and talin on integrin activation. In Section 5.2, based on Article II, GM1 properties in different lipid phase environments are examined, and the effect of fluorescent labels on GM1 are demonstrated. Based on Article III and unpublished results, the structural and dynamical changes in the PI(4,5)P_2 conformation upon the presence of calcium and cholesterol are discussed in Chapters 5.3 and 5.4, respectively. Finally, conclusions and ideas for future research are given in Chapter 6.

2. BIOLOGICAL BACKGROUND

Cell membranes possess a ubiquitous bilayer architecture that is vital for cells and living organisms. The core of all the membrane structures is composed of lipids that make up the underlying membrane scaffold, where other molecules, such as proteins, are embedded. Membrane heterogeneity (lateral compartmentalization and leaflet asymmetry) is essential for cell signaling and trafficking and can be achieved by recruiting specific lipids from/into functional compartments. To understand the cell functioning mechanisms properly, it is of particular importance to understand lipid–lipid and lipid–protein interactions.

In this Chapter, the relevant biological background for this Thesis is discussed, the main focus being lipids and membranes. The Chapter is closed with a discussion of membrane-associated proteins and their interactions with membranes.

2.1 Lipids and Other Building Blocks of Membranes

Lipids are amphiphilic biomolecules. They have several major functions in cells. They are used to store energy [12], they act as signaling molecules [13], and they are also substrates in post-translational protein modifications [14]. Nevertheless, one of the most important functions of lipids is to form lipid bilayers that work as barriers between two fluids, and at the same time as protein recruitment platforms [15, 16]. A lipid bilayer can be formed by a single lipid type. Still, a huge diversity of lipids exist in cells. The human plasma membrane alone is known to contain thousands of different lipid species [17]. To understand the biological consequences of various lipids, it is crucial to understand the reason for the enormous diversity of membrane lipid compositions and chemical heterogeneity of different lipid types. Why so many different lipids are needed, and what are their functions, are fundamental questions that have been studied extensively [15].

The diversity among lipids arises from the combination of different headgroups,

lipid backbones, and the fatty acids attached to the lipid backbone. The degree of structural differences ranges from subtle changes (double bonds in the acyl chain) to larger ones (different backbones or headgroups). The most abundant membrane lipids are classified into three groups: glycerophospholipids (GPLs), sphingolipids, and sterols (cholesterol in mammals).

Lipids are categorized into structural and signaling lipids [18]. The primary structural lipids in eukaryotic cells are the glycerophospholipids: phosphatidylcholine (PC), phosphatidylethanolamine (PE), phosphatidylserine (PS), phosphatidic acid (PA), and phosphatidylinositol (PtdIns). Their hydrophobic fragment is a diacylglycerol (DAG) with acyl chains of various lengths and saturation states (number of double bonds). The *sn*-1 acyl chain is usually saturated, whereas the *sn*-2 fatty acid is often mono- or polyunsaturated (*cis*) [19]. In most eukaryotic membranes, PC accounts for more than half of all the phospholipids [15].

The second class of structural lipids is constituted of sphingolipids. The major sphingolipids in mammalian cells are sphingomyelin (SM) and glycosphingolipids (GSLs), whose hydrophobic portion is ceramide (CER). As denoted by the name, GSLs contain sugar moieties in their headgroup. Mono-, di-, or oligosaccharides are constructed on either glucosylceramide (GlcCer) or galactosylceramide (GalCer) [20]. Notably, the N-acyl chain of sphingolipids tends to be longer and more saturated than the *sn*-2 acyl chains of GPLs [21], often leading to a highly packed membrane organization.

The third main lipid type found in biological membranes are sterols. In mammals, sterols are predominantly cholesterol (Chol) molecules, while in yeast they are ergosterols. The cholesterol structure consists of four hydrocarbon rings with a hydroxyl group (polar) at one end and a branched and fully saturated aliphatic tail at the other end. The ring structure is rigid with one side almost flat (smooth α-face), whereas the other side contains two methyl groups making the surface rougher (β-face). Cholesterol is synthesized in the endoplasmic reticulum and is eventually transported through the Golgi to the plasma membrane [22]. In the plasma membrane, it is present in both leaflets. Nevertheless, the details of its transmembrane distribution remain debated [23, 24, 25]. Due to its unique structure (see Fig. 2.1), cholesterol has a substantial impact on fundamental membrane properties (see Section 2.2.2).

The lipid molecules used in this Thesis project are illustrated in Fig. 2.1 and the main lipid receptors, GM1 and PI(4,5)P_2, are discussed in more detail below.

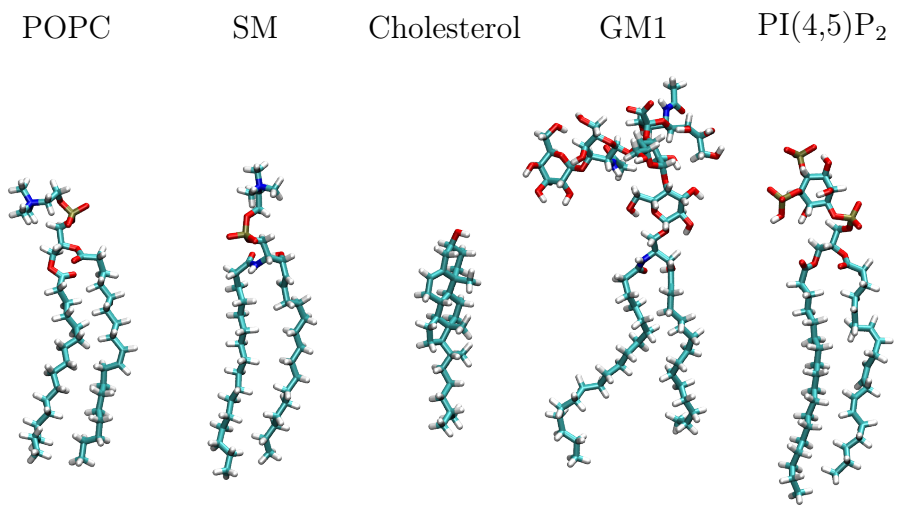

Figure 2.1 *Snapshots of lipid molecules used in this work. Standard coloring scheme and licorice drawing method are used. Pictures are visualized using Visual Molecular Dynamics (VMD) [26] and rendered utilizing the Tachyon ray tracing library [27].*

2.1.1 Phosphoinositides and PI(4,5)P_2

Phosphorylation is a process where a phosphoryl group (PO_3^{2-}) is attached to a host molecule. Phosphoinositide (PI) is a term used for phosphorylated phosphatidylinositol (PtdIns). PIs are minor constituents of cellular membranes, possessing about 1 mol% of all the phospholipids [28]. The degree of diversity among the phosphatidylinositols arises from the level of phosphorylation of the PI headgroup. The inositol ring in the PI headgroup can be phosphorylated on positions 3, 4, and 5, generating seven possible PIs. In humans, PI(4,5)P_2 is the most abundant PI [8] mainly localized at the plasma membrane [29]. Nevertheless, PI(4,5)P_2 has also been detected in the nucleus [30] and Golgi [7, 8]. Furthermore, PI(4,5)P_2 plays a significant role in regulating various signaling pathways. This is most likely due to the ability of rapid switching of the phosphorylation state with the help of different kinases and phosphatases. For instance, doubly phosphorylated PI(4,5)P_2 can be synthesized from various PIs by different kinases: type I PIP5Kα, β, and γ convert PI(4)P into PI(4,5)P_2 [31], type II PIP4K kinase turn PI(5)P into PI(4,5)P_2 [32, 33], and phosphatases such as PTEN modify PI(3,4,5)P_3 into PI(4,5)P_2 [34].

PIs are composed of the glycerol backbone, *sn*-1 and *sn*-2 acyl chains, and an inositol ring attached to a phosphate group [28] (see Fig. 2.1). Although acyl chains of PIs

can vary, they possess less heterogeneity than the other GPLs [35]. In humans, the most common fatty acid chains for PIs are stearic acid consisting of a saturated 18-carbon chain (18:0) in the *sn*-1 position and arachidonic acid with four double bonds in a 20-carbon long fatty acid chain (20:4) linked to the *sn*-2 position [19, 36].

Although the levels of these signaling molecules are small compared with the levels of bulk membrane lipids, they are essential to identify endocytic membranes and to recruit proteins from the cytosol [8]. The identity among organelles is mostly defined by molecules present on the cytoplasmic leaflet of membranes. Phosphoinositides are key players among these molecules [15]. In the inner leaflet of the plasma membrane, PI(4,5)P_2 has multiple roles. For instance, phospholipase C (PLC) is known to bind to PI(4,5)P_2 in the plasma membrane, hydrolyze the receptor, and eventually lead to Ca^{2+} release from the endoplasmic reticulum (ER) [6]. Moreover, PI(4,5)P_2 is required for the actin regulation of clathrin-mediated endocytosis [8]. Also, to name a few examples, different effector proteins for endocytosis have an ENTH, ANTH, or PH domain, and these are specific to PI(4,5)P_2 [8, 37, 38] (for more examples see Refs. [8, 18]).

2.1.2 Glycolipids and GM1

Glycolipids constitute the most complex and varied group of membrane lipids. This is due to their headgroup that consists of one or more sugar units. Glycolipids fall into two categories based on their structure [39]. Glycolipids built on phosphatidylglycerol are denoted as glycophospholipids, and glycolipids built on ceramide are known as glycosphingolipids.

Glycosphingolipids are the most common glycolipids in cell membranes. Their structure is composed of a fatty acid attached to a long-chain amino alcohol sphingosine and glycans. The primary sugar units in glycosphingolipids found in animals are glucose, galactose, fucose, *N*-acetylgalactosamine (GalNAc), and *N*-acetylglucosamine [40]. When one (or more) sialic acid (usually *N*-acetylneuraminic acid) is linked to the glycosphingolipid sugar chains, the molecule is denoted as ganglioside [41]. Depending on the headgroup structure, gangliosides are named as follows [39]. The shortest member, containing a single galactose residue linked to the glucose core, is designated as G3. Addition of one sugar monomer (GalNAc) generates G2, and extension with a further galactose residue results in the G1 member. Moreover, the number of sialylation fragments is designated with a second letter in the receptor name: M for

monosialylated, D for disialylated, and so forth. Therefore, a headgroup with all the three sugar moieties and a single sialylation is called GM1 (see Fig. 2.2).

GM1 occurs most abundantly in the outer leaflet of the plasma membrane and it is known to drive several vital cellular functions, such as neuronal differentiation [42, 43], ion transport modulation [44, 45], immune cell reactivity [46, 47], and microdomain regulation [48]. These and multiple other roles are discussed in Ref. [49]. In addition to the vital roles in cell functions, GM1 has been used as a lipid raft marker in model membranes owing to its enrichment in ordered lipid microdomains, where it is recognized by ligands, such as the cholera toxin B subunit (CTxB). Supporting the high-affinity binding to GM1, the crystal structure of CTxB has been resolved at 1.25 Å resolution in complex with the GM1 pentasaccharide [50]. The crystal structure reveals a "two-fingered grip" of carbohydrates (thumb being sialic acid and forefinger the last two sugars of the other headgroup branch) holding CTxB. This is among the highest affinity protein–carbohydrate interactions with a micromolar dissociation constant [51, 52].

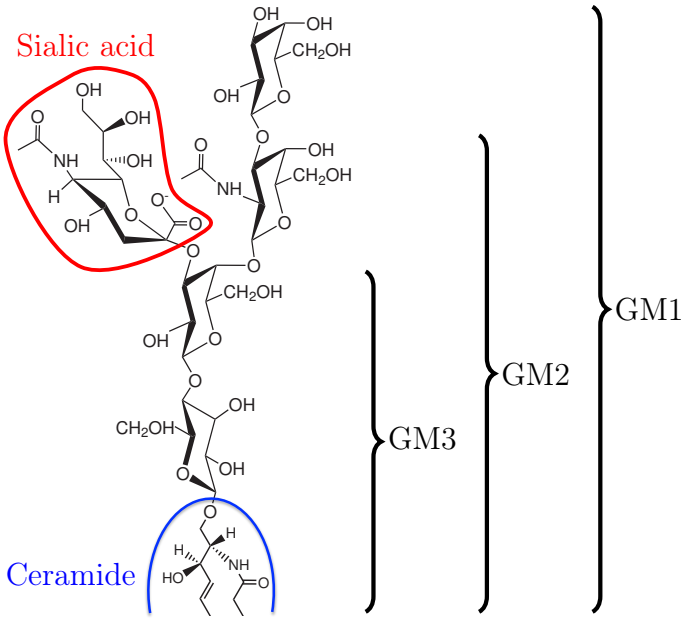

Figure 2.2 *A sketch of different ceramide -based monosialylated gangliosides. Ceramide unit and sialic acid are highlighted in blue and red, respectively. In the lipid structure, acyl chains are not fully shown.*

2.2 Membrane Models

Various membrane models have been proposed in the past decades [53]. One of the first major steps in the field was done by Robertson in 1959 [54] when he proposed a three-layered membrane structure where two protein layers are adsorbed to the lipid bilayer. Based on the Robertson model and additional observations, in 1966 Lenard and Singer proposed a new model [55] suggesting that some of the proteins may be able to span the lipid bilayer. Eventually, one of the most significant steps in the field was done by Singer and Nicolson in 1972 [56] when they proposed the famous "fluid mosaic" model (also called the Singer–Nicolson model) for membranes. The core of the model is the lipid bilayer structure consisting of amphiphilic lipids. Instead of proteins coating the bilayer, as proposed by Robertson, the proteins were suggested to reside within the lipid bilayer and diffuse with lipids in a fluid 2D matrix. Although the fluid mosaic model is still relevant [57], it has been further developed to satisfy other requirements. One of the most famous models proposes that membranes are laterally segregated and contain functional domains (called "rafts") [58]. This concept has been studied extensively since 1997 and its main core is now quite well established and accepted: cell membranes are dynamic, heterogeneous, protein-rich lipid bilayers involved in numerous cellular functions. Also, there is considerable evidence supporting the picture that in cell membranes there are membrane proteins forming functional complexes with specific lipids that foster the activation of the proteins, and/or modulate their activation. For further discussion on this broad topic, see, e.g., Refs. [59, 60, 61].

Based on the current view, membranes are composed of two sheets of lipids in which proteins are embedded (see Fig. 2.3). In the bilayer, amphiphilic phospholipids are oriented so that the hydrophobic groups (acyl chains) face each other, and the hydrophilic groups (polar headgroups) face with the aqueous phase. Notably, the membrane composition varies according to the organism (prokaryote or eukaryote) [19, 62], the cell type (e.g., different tissues) [21, 63], the organelle type (e.g., Golgi, endoplasmic reticulum, plasma membrane) [15, 64], the state of the cell (responding to stimuli) [65, 66], and between membrane leaflets and subdomains [61]. Importantly, changes in lipid compositions have been linked to diseases, such as type 2 diabetes, cancer, and Alzheimer's disease [21, 67, 68].

Although membrane structures exist in many cell organelles, lipids are not distributed homogeneously throughout the main organelles [15]. Instead, various lipids are found

in different quantities in different subcellular space, and particular patterns of lipid compositions have been found among various cell organelles. For instance, cholesterol concentration is found to increase along the secretory pathway [10, 11] and is highest in the plasma membrane [10, 11]. Moreover, endoplasmic reticulum (ER) contains more unsaturated GPLs, whereas sphingolipids are enriched in the plasma membrane [15, 64]. Also, cardiolipin resides almost exclusively in mitochondria [69] or the lysobisphosphatidic acid in late endosomes [70, 71].

2.2.1 Lipids Modulating Membrane Properties

The relative size of the cross-sectional area of the lipid headgroup and lipid acyl chains affects the lipid shape and consequently membrane curvature [72]. Cylindrically shaped lipids (cross-sectional areas of the headgroup and acyl chains being similar), such as PC, typically form planar lipid bilayers. Conically shaped lipids (cross-sectional area of the headgroup is smaller than the area of acyl chains), such as PA, form negative spontaneous membrane curvature, while inverse conical shaped lipids (cross-sectional area of the headgroup is larger than the area of acyl chains), such as lysolipids, induce positive curvature. These disrupting shapes may promote non-bilayer membrane structures and intermediates for membrane fusion [73, 74].

Lipids with different acyl chains can influence intrinsic membrane properties. Long saturated fatty acids (typically in sphingolipids) pack tightly, make membranes thicker, and decrease lipid mobility [15, 61]. On the other hand, double bonds in unsaturated fatty acids form a kink in the acyl chain, leading to more distorted and fluid membranes. In model membranes with appropriate lipid compositions and temperature, saturated lipids, unsaturated lipids (essentially lipids with different melting points), and cholesterol can form phase separated systems with high lipid packing (liquid-ordered phase, L_o) and less lipid packing (liquid-disordered phase, L_d) [15]. This phenomenon is one of the basic fundamentals behind the lipid raft hypothesis [58]. Phase separation has been detected in vesicles derived from cell membranes [75, 76]. Nevertheless, phase transitions are rarely observed in living cells [77, 78], and the existence of phases in the cell membrane is to date unclear.

In the plasma membrane and Golgi, lipids are asymmetrically distributed in the lipid bilayer. In these membranes, SM and GSLs are localized on the luminal side (non-cytosolic), whereas PS and PE are enriched in the cytosolic leaflet [79, 80]. Importantly, the asymmetric lipid distribution has an essential role in cell

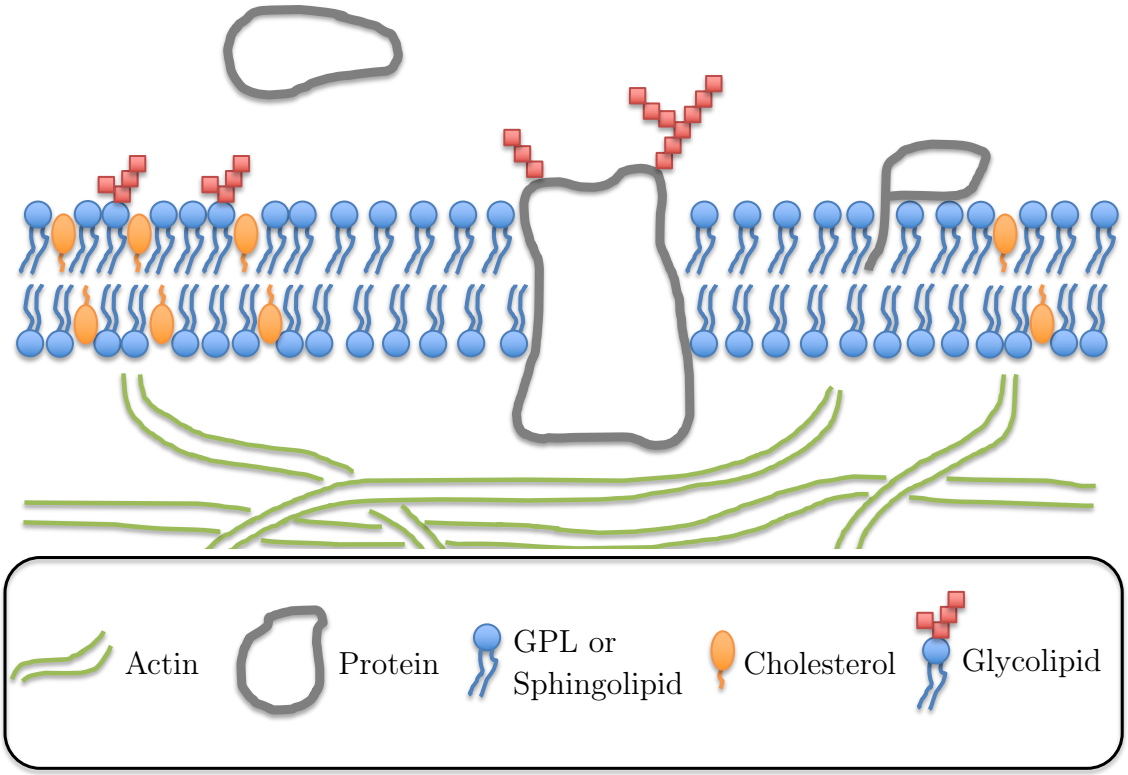

Figure 2.3 *Illustrative artistic figure presenting a cell plasma membrane. In the upper leaflet (extracellular side) glycolipids can be found. Moreover, three different proteins are illustrated: a peripheral protein (left), an integral membrane protein (middle), and a lipid-anchored protein (right). Cholesterol molecules and actin cytoskeleton are also shown. Gray color represents the proteins, blue structural GPL/sphingolipids, orange cholesterol, green the actin cytoskeleton, and red the sugar units.*

functions. For instance, PS is presented mainly in the inner leaflet of the plasma membrane, whereas in the outer leaflet it mediates a signal for phagocytosis and leads to apoptosis [81]. Lipids can move across the bilayer (in a process called lipid flip–flop). The rate of flip–flop strongly depends on the lipid type. For example, PC movement across the bilayer is slow and takes from hours to days [82, 83], whereas cholesterol can flip–flop at a rate of time scales from nanoseconds to microseconds, depending on the acyl chains of the adjacent lipids [84]. In biological membranes, flippases (ATP-dependent and unidirectional) and scramblases (energy-independent and bidirectional) can enhance flip–flop rates significantly [79]. Furthermore, lipids are also known to interact across the bilayer. For instance, PS aggregates in the cytosolic leaflet of the plasma membrane induce clustering of glycolipids in the outer

leaflet of the plasma membrane [85]. Notably, this requires at least one long acyl chain, and cholesterol.

2.2.2 Cholesterol Affects Membrane Properties

Due to its unique structure, cholesterol has a substantial impact on physical membrane properties. It is known to increase the order of acyl chains [86, 87], condense bilayers [88], increase the mechanical strength [89], and decrease the membrane permeability [90]. Furthermore, cholesterol increases membrane viscosity, slowing down the lateral and rotational lipid diffusion [91, 92, 93]. Also, due to the relatively small cross-sectional area of the polar headgroup compared to the ring structure, cholesterol generates intrinsic negative membrane curvature [94]. Consequently, cholesterol has potential for promoting the emergence of highly curved membrane structures and can cause intermediate states in the membrane fusion process [95, 96].

According to the current view, cholesterol is a fundamental component of ordered nanodomains that form a platform for membrane signaling and trafficking [60]. Cholesterol straightens out the lipid acyl chains [97] in the cholesterol-rich liquid-ordered L_o phase. This makes such bilayers or compartments of membranes thicker than the membrane structure in the cholesterol-poor L_d phase [98]. Affecting the bilayer thickness, cholesterol has been suggested to play a major role in identifying the cell organelles via altering the hydrophobic thickness (and hydrophobic mismatch for proteins), and therefore selectively guide different transmembrane proteins to different cell organelles [99]. Cholesterol–protein interactions are discussed in more detail in Section 2.3.

2.2.3 Ions Modulating Membranes

Biomembranes assemble and operate in the aqueous solution, where ions are also present. The most common ions in biologically relevant electrolytes are Na^+, K^+, and Cl^-. The polar lipid headgroups interact directly with ions in the solution and can lead to changes in lipid phase transitions [100], membrane potential [101], and dynamics of the hydration layer [102]. Also, divalent ions Ca^{2+} and Mg^{2+} are of importance in biomembranes. They are found to catalyze membrane fusion [103, 104] and to modify membrane structure by binding multiple anionic sites simultaneously. Notably, intracellular calcium ions act as secondary messengers and have been linked

to many vital aspects of life, including gene transcription, cell proliferation, and death [105]. Moreover, intracellular Ca^{2+} homeostasis has been found to alter cancer cells, and targeting calcium signaling has become an emerging research area [5].

Many experimental methods exist for studying the effect of ions on membrane structure and mechanical properties, including deuterium nuclear magnetic resonance (NMR), atomic force microscopy (AFM), calorimetry, and electron spin resonance (ESR) [106, 107]. Also, simulations have been used to study effects of ions on membranes. Nevertheless, these studies are only as accurate as the simulation method and the force field. For instance, smaller ions, such as F^- and Li^+, induce polarisation of the water, and can therefore induce over- or underestimated lipid binding [108]. Moreover, multivalent ions are often more complicated [109], and transition metals, such as Zn^{2+} and Cd^{2+}, are challenging to model even with quantum chemical calculations [110]. It is not only the ion parameters, but also the membrane models that need to be accurate, and for example, overbinding of Na^+ in the CHARMM force field has been corrected with an extra potential [111].

2.3 The Interplay of Lipids and Proteins

Biological membranes are mainly composed of lipids and proteins. It is estimated that about a third of plasma membrane area is covered by proteins [112]. Although the number of different proteins in cells is enormous, they are generally classified into three main categories. The first class, integral membrane proteins (often called transmembrane proteins) are permanently associated with the membrane. They span through the entire membrane with one or more alpha helices or a beta barrel [113]. The second class, peripheral proteins, are temporarily associated with the membrane by partially penetrating into the membrane surface. Lipid-anchored proteins constitute the third class. These proteins have a covalently linked anchor, typically being a lipid acyl chain that is embedded in the membrane [114]. All protein types are illustrated in Fig. 2.3.

Transmembrane proteins have been suggested to require a suitable lipid environment to work properly; this is largely the view proposed by Simons et al. when introducing the raft concept [58]. The influence of lipids on proteins can be divided into two main categories: membrane-mediated effects and direct (specific) interactions. Membranes as such can influence proteins through bulk properties [115], such as hydrophobic mismatch (membrane thickness), headgroup hydration, headgroup tilting, membrane

curvature, and electrostatic properties. The specific lipid–protein interactions are formed through chemical recognition of proteins and lipids, modulating protein structure and functions [116]. To highlight the specific lipid binding sites on protein surface, many protein structures have been resolved together with bound lipids [117]. The lipids that are tightly bound to a specific lipid binding site in the protein are called non-annular lipids, whereas the lipids around the protein are generally called annular lipids [118, 119]. The other lipids further from protein move faster than the annular or non-annular lipids [120] and are called bulk lipids.

To study protein–lipid interactions, multiple methods can be used, including crystallography, NMR, AFM, and molecular dynamics simulations. Unfortunately, our knowledge of protein–lipid interactions is still based on single case studies. For instance, in a recent study by Contreras et al. [121], a direct and highly specific interaction between the transmembrane domain of the COPI machinery protein p24 and sphingomyelin with an 18-carbon long acyl chain attached to the spinghosine backbone (SM 18) was found. Sphingolipid was observed to bind with high binding affinity to the protein, consequently leading to protein dimerization. Importantly, this was found to be acyl chain specific and only the SM 18 caused the effect, not other acyl chain lengths like 16 or 20. The study demonstrates how elaborate lipid–protein interactions can be and increases our understanding of why such a vast variety of different lipids exist in biological membranes. Indeed, changes in lipid acyl chains have been linked to severe diseases, such as cancer [122].

Cholesterol influences the behavior of membrane-associated proteins in multiple ways [123]. It can affect protein behavior both through specific and non-specific effects. For cholesterol, different binding motifs from proteins have been recognized [124], and cholesterol has been co-crystallized together with several proteins, a large fraction of them belonging to G protein-coupled receptors (GPCRs) [125].

In a study by Lingwood et al. [126], cholesterol was found to modulate glycolipid conformation and receptor activity. In the study, membrane cholesterol induced GM1 headgroup tilting, resulting in loss of access for ligand binding. Furthermore, Manna et al. [127] demonstrated how cholesterol limits β_2-adrenergic receptors (β_2ARs) conformational variability and therefore modulates β_2AR functioning in an allosteric fashion. This effect was caused by specific interaction between the protein and cholesterol molecules, not via the bulk membrane properties. Moreover, cholesterol has been proposed to modulate binding affinities of some G protein-coupled receptors,

such as serotonin$_{1A}$ [128] and glutamate [129] receptors. Also, cholesterol has been shown to accelerate the interaction between Aβ5-16 peptide and GM1 molecules [124]. This likely takes place through the hydrogen bond formed between the cholesterol hydroxyl group (OH) and the oxygen atom linking the oligosaccharide to the GM1 ceramide.

There are also other determinants that can alter protein functioning in membranes, such as transmembrane protein oligomerization [130], and protein phase partitioning. Therefore, lipids are not only forming a platform for proteins, but they also serve as functional units and regulators in cell signaling pathways. Thus, the interplay between proteins and lipids and lipid–protein interactions are crucial to understand before we can understand how cell signaling events are mediated and controlled.

2.4 Selected Protein in Spotlight

In this Thesis, a transmembrane protein from the integrin family is studied. Integrins have a remarkable ability to transmit signals in both directions across the cell membrane [131]. These signals are crucial for several key cellular activities, including proliferation, survival, and gene expression [1]. Also, certain tumor types have been found to exhibit high levels of specific integrins which make the integrin-associated signal complex an important spot for cancer therapy development [132].

Integrins are heterodimeric transmembrane receptors composed of α- and β-subunits. In human, 18 different α- and eight β-subunits have been found, forming 24 different integrin heterodimers [131]. Since the activation of integrin is essential for cell adhesion and integrin linkage to the actin cytoskeleton, much of the research has focused on the different integrin activation steps. The activation has been shown to change the conformation of the integrin complex [133]. In its folded inactive state, the intracellular portions of the α- and β-subdomains lie close together and adhere to one another. In the active state, this contact is broken, and both the transmembrane and the intracellular portions of the α- and β-subdomains stay further from each other.

Transmembrane helices from each subunit are characterized to be stabilized by the inner membrane clasp (IMC) and the outer membrane clasp (OMC) [134, 135]. The inactive conformation is the passively adopted integrin receptor's default state [136] that is shifted towards the activated state upon recruitment of activating proteins,

such as talin (inside-out activator) [2, 3]. Notably, PI(4,5)P_2 lipid receptors have been observed to enhance talin binding to membranes [137, 138] and further to influence talin–integrin binding [139, 140]. Nevertheless, how integrin activation is regulated, and how different lipid species and lipid environments affect the process, remain largely unknown.

3. METHODS

Atomic details of biological systems are extremely challenging to study by the current experimental methods. For example, X-ray crystallography can solve the structure of a molecule in atomistic resolution, but the data it yields characterizes the structure, not the dynamics. Meanwhile, single-molecule fluorescence techniques can grasp the movement of molecules, but their spatial resolution is not sufficient to understand the atomistic picture. Also, in fluorescent techniques additional fluorescent labels (probes) are needed, and therefore the observations are no longer based on the natural compounds but on their fluorescent analogs. To overcome these challenges, one approach to study dynamical properties of biological systems in atomistic resolution is to use computer simulations and modeling tools, such as atomistic molecular dynamics (MD) simulations.

3.1 Molecular Dynamics Simulations

Classical MD simulation is a computational approach to calculate the time evolution of particles' positions and velocities in a many-body system using classical mechanics. MD simulations can be used to estimate equilibrium and transport properties of complex systems that are analytically unsolvable.

The first MD simulation study was published already in 1957 [141]. In the study, a hard-sphere model was employed such that atoms moved in straight lines, and collisions were perfectly elastic. The first MD simulation of a real liquid (argon) was reported in 1964 [142], and the first biomolecular simulation of a small 58 amino acid protein bovine pancreatic trypsin inhibitor (BPTI) was simulated in vacuum for 8.8 ps and published in 1977 [143]. The first 1 µs simulation was performed in 1998 [144] demonstrating protein folding. The current methodology and computer capacity have allowed studies of a full virus in atomistic detail [145], tens of thousands of lipids for microseconds [146], and simulations of proteins over time scales of milliseconds [147].

The molecular dynamics simulation approach is in principle quite simple. Molecules consist of particles that are attached to each other by springs, and the movement of the particles is computed using Newton's equations of motion. Nevertheless, the roots of the classical molecular dynamics (or molecular mechanics in general) method are in quantum mechanics [148], where molecular properties are derived by solving the Schrödinger equation. However, in classical MD simulations only the nuclear coordinates are followed and electrons are neglected. The basis of this is in the Born–Oppenheimer approximation stating that the movement of atomic nuclei can be separated from the movement of the electrons. Moving on, Newton's equations of motion for a conservative force can be derived from elegant theoretical Lagrangian and Hamiltonian frameworks of classical mechanics [149], which play a fundamental role in statistical mechanics. For further discussion of this exciting topic, please see discussion in, e.g., Ref. [149].

Below I go through the basic theory behind MD and aim to give a broad view of the MD method. For further information, I recommend reading Refs. [148, 150, 151, 152] that give more detailed insight combined with practical examples.

3.1.1 Initial Conditions

Before initiating any MD simulation, the system needs to be adequately prepared. To run a simulation, one needs initial structure and topology. Initial structures for a biomolecular system are usually based on experimental results. For instance, X-ray and NMR methods are used to resolve protein structures, which are generally available in the protein data bank (PDB) [153]. In addition to the initial structure (and velocities), description of the system is required. This information is called the system topology. It contains parameters attributed to the particles and their interactions. In practice, these parameters describe physical properties of particles, such as charge, mass, as well as relations between other particles, like bonds and angles. Notably, in a typical MD simulation the information given in the topology does not change, that is, it is not modified during the course of the simulations. For example, bonds do not break, or new bonds can not form during an MD simulation. However, there are also reactive force fields (for force fields, see Section 3.1.3) that allow modifications in molecular structure, such as bond breaking [154]. Importance of the initial conditions is unquestioned since a wrong initial structure would require simulations to be exceptionally long to make sure that sampling at long times would

generate correct results, and failures in the topology would make the simulation results useless.

After the system has been constructed properly, it is usually energy minimized to eliminate the high-energy interactions before the production run. In the run, the system starts to evolve in time through forces acting on the particles.

3.1.2 Time Propagation

The motion of particles in a simulated system is calculated from the forces acting on the particles. To this end, one uses Newton's equations of motion. Newton's second law states that the mass describes the "slowness" of a particle, and the equation of motion is

$$\mathbf{F}_i = m_i \frac{\mathrm{d}^2 \mathbf{r}_i}{\mathrm{d}t^2}, \tag{3.1}$$

where t is time, $\mathbf{F}_i$ is the force acting on particle i of mass m_i, and $\mathbf{r}_i$ is the position vector of particle i [155].

When the total force acting on each particle is known, new particle positions can be calculated. Nevertheless, this can not be solved analytically for a many-body system [156]. Therefore, numerical methods are needed to solve the equations of motion. The basic idea of the numerical approach is that continuous time is discretized and particle positions and forces are calculated at points separated by short time intervals Δt (called the time step). This method is called the finite difference approach [152].

When the forces and the time step are known, many algorithms (called integrators) are available for integrating the equations of motion. Commonly, these algorithms approximate dynamical properties, such as velocities and accelerations, as Taylor series expansions. In this work, the so-called leap-frog algorithm [157, 158] was utilized:

$$\mathbf{r}_i\left(t + \Delta t\right) = \mathbf{r}_i\left(t\right) + \mathbf{v}_i\left(t + \frac{\Delta t}{2}\right)\Delta t, \tag{3.2}$$

$$\mathbf{v}_i\left(t + \frac{\Delta t}{2}\right) = \mathbf{v}_i\left(t - \frac{\Delta t}{2}\right) + \frac{\mathbf{F}_i\left(t\right)}{2m_i}\Delta t, \tag{3.3}$$

where $\mathbf{r}_i$ is the position and $\mathbf{v}_i$ the velocity of particle i. As can be seen from Eqs. (3.2)

and (3.3), the velocities are defined at half steps, while the positions are defined at whole steps of Δt. Therefore, the technique is named the leap-frog algorithm.

When performing an MD simulation, the selection of a proper time step Δt is crucial. For example, if a time step of one millisecond is used to simulate how the earth orbits around the sun, many iterations are needed to get a trajectory of the earth going around the sun just once. Meanwhile, because the particles in a system (here the earth) continue their movement in a straight line and the force is assumed to be constant during the time step, having a too long Δt will result in an incorrect particle path, giving wrong simulation results.

The time step Δt needs to be short enough to describe the fastest degree of freedom. In the case of a typical atomistic biomolecular system, the fastest movement is the O–H or N–H bond stretching with a wave number of 3400–3700 $\frac{1}{\text{cm}}$ [148]. This corresponds to a period of 10 fs. Considering that a reasonable Δt is one-tenth of the period of the highest frequency mode, a proper time step for an atomistic biomolecular system would then be $\Delta t = 1$ fs. In practice, various constraint algorithms, such as LINCS [159] and SETTLE (for water) [160] are used to constrain the bond stretching and consequently to remove the high-frequency movements. After the implementation of constraints, the fastest frequencies are usually the H–O–H angle vibrations (1600 $\frac{1}{\text{cm}}$), and the longest acceptable time step to sample this movement properly would then be $\Delta t = 2$ fs. In this work, the time step of 2 fs was used in all the atomistic models (for details, see Chapter 4).

Even if a really short time step is used, events that contain high-frequency movements are not in the scope of atomistic simulations. In quantum mechanics, harmonic oscillator energies are quantized by $h\nu$, where h is Planck's constant and ν is the frequency of the vibration. On the other hand, in a classical approach, the thermal energy is $k_{\text{B}}T$, where k_{B} is Boltzmann's constant, and T is the temperature. That is, by having $hv \ll k_{\text{B}}T$, discretized energy levels are not present and classical mechanics can be used. Therefore, especially in low-temperature simulations, this needs to be considered carefully.

3.1.3 Potential Energy Function

In MD simulations, the forces in Eq. (3.1) are calculated by taking a negative gradient of the potential energy

$$\mathbf{F}_i = -\nabla \mathcal{V}_{\mathrm{TOT}}, \tag{3.4}$$

where $\mathcal{V}_{\mathrm{TOT}}$ is the potential energy. The potential energy function together with parameters used in the potential energy function is called the force field. Quite often, the force field is also considered to include the algorithms used in the simulation (barostat, thermostat, etc.) and their parameters, since if these algorithms or their parameters are changed, then also the results often changes. For biomolecular systems, several force fields are available, but none of them is perfect and universal. When simulating a system containing proteins and lipids in atomistic detail in the same system, the set of the available force fields is more limited. One commonly used set of potential functions is the CHARMM36 protein force field [161] in combination with the recently published CHARMM36 lipid force field [162]. In CHARMM, force fields for nucleic acids [163] and carbohydrates [164] are also available. Another commonly used force field is the OPLS (optimized potentials for liquid simulations) all-atom protein force field [165] that is compatible with a newly released lipid force field [166, 167]. Unfortunately, the selection of the refined lipid types in this force field is more limited compared to CHARMM36. Further, a new OPLS3 force field has been designed [168] offering a large set of parameters for small molecules, but it is currently available only for commercial purposes. Finally, the Amber ff99SB-ILDN force field for proteins [169] is compatible with the recently developed Lipid14 parameter set for lipids [170, 171]. Also, newly designed Slipids parameters [172, 173, 174] can be used with the Amber protein force field. For more details about various force fields, see Refs. [175, 176, 177].

In each force field, the described interactions can be divided into two categories: bonded and non-bonded interactions. The total potential energy function is the sum of these interactions

$$\mathcal{V}_{\mathrm{TOT}} = \mathcal{V}_{\mathrm{bonded}} + \mathcal{V}_{\mathrm{non\text{–}bonded}}. \tag{3.5}$$

3.1.4 Bonded Interactions

Covalent bonds between atoms or molecules are modeled by introducing three bonded interactions: bond, angle, and dihedral potentials

$$\mathcal{V}_{\text{bond}}\left(r_{ij}\right) = k_{r,ij}\left(r_{ij} - r_{ij}^{0}\right)^{2}, \tag{3.6}$$

$$\mathcal{V}_{\text{angle}}\left(\theta_{ijk}\right) = k_{\theta,ijk}\left(\theta_{ijk} - \theta_{ijk}^{0}\right)^{2}, \tag{3.7}$$

$$\mathcal{V}_{\text{dihedral}}\left(\omega_{ijkl}\right) = k_{\omega,ijkl}\left(1 + \cos\left(n\omega_{ijkl} - \omega_{ijkl}^{0}\right)\right), \tag{3.8}$$

where $k_{r,ij}$, $k_{\theta,ijk}$, and $k_{\omega,ijkl}$ are force constants and r_{ij}^{0}, θ_{ijk}^{0}, and ω_{ijkl}^{0} are reference values in equilibrium for a bond, an angle, and a dihedral, respectively. In the dihedral potential, the torsional angle is defined as the angle between the ijk and jkl planes with a value of zero corresponding to particles i and l on the same side (*cis* configuration). Moreover, n is an integer denoting the periodicity of the rotational barrier. The parameter values for bonded interactions are usually determined by using spectroscopic techniques and X-ray crystallography, as well as quantum-mechanical calculations [148]. Also, different types of potential functions exist for the bonded interactions [150].

3.1.5 Non-Bonded Interactions

In addition to the bonded interactions among the covalently bonded atoms, also independent molecules can experience interactions with each other. These long-range interactions are called non-bonded interactions. In general, three types of non-bonded interactions are considered: Pauli repulsion, van der Waals (vdW) dispersion, and electrostatic interaction. The first two are quantum-chemical in nature and are usually modeled using a simple expression, such as the Lennard–Jones (LJ) potential

$$\mathcal{V}_{\text{LJ}} = 4\epsilon_{ij}\left(\frac{\sigma_{ij}^{12}}{r_{ij}^{12}} - \frac{\sigma_{ij}^{6}}{r_{ij}^{6}}\right). \tag{3.9}$$

The attractive component r^{-6} (r being distance) is due to dispersive forces that arise from fluctuations in the electron clouds. The fluctuations induce the formation of a dipole, which in turn induces dipoles in the electron clouds of the surrounding atoms. The theory for this phenomenon was explained already in 1930 using quantum mechanics [152] (also known as London dispersion). The repulsive interaction has also its roots in quantum mechanics (Pauli principle), noting that two electrons can not

have the same set of quantum numbers and therefore particles repel each other if they get too close to each other. The attractive van der Waals interaction can have various forms, such as those proportional to r^{-4}, r^{-6}, etc., depending on whether, for instance, there are fluctuating or permanent dipoles, or spatially fixed or freely rotating dipoles interacting with one an other. Nevertheless, in commonly used force fields, the term proportional to r^{-6} is usually chosen for simplicity, efficiency, and sufficient accuracy. Similarly, again for mathematical convenience and practical efficiency, the repulsive term in the Lennard-Jones interaction potential is typically chosen to be proportional to r^{-12}. The LJ-parameters ϵ_{ij} and σ_{ij} are usually obtained by fitting simulation results to lattice energies and crystal structures, or to experimentally measured liquid properties such as the enthalpy of vaporization (heat of vaporization) and density [178].

The third non-bonded interaction, electrostatic interaction between two particles, is calculated using Coulomb's law

$$\mathcal{V}_{\text{coulomb}} = \frac{1}{4\pi\epsilon_0}\frac{q_i q_j}{\epsilon_r r_{ij}}, \tag{3.10}$$

where ϵ_0 is the permittivity of vacuum, q_i and q_j are the charges of particles i and j, ϵ_r is the relative permittivity of the medium, and r_{ij} the distance between two particles. In a typical atomistic system, each atom carries a fixed partial charge that is obtained from quantum-chemical calculations. Nevertheless, QM calculations do not solve partial atomic charges uniquely, since different methods, such as full density screening and outer density screening, can give different results [179]. Therefore, great care needs to be taken when deriving partial charges for MD simulations. It is also important to note that while the Lennard–Jones potential decays rapidly, the Coulombic interaction does not, thus increasing the computational load significantly. Using computational tricks (cut-offs), the interaction can be calculated only to a certain distance, but even with large cut-off distances (2.5 nm), significant artifacts have been obtained [180]. Alternative algorithms, such as Ewald methods [181, 182], are implemented to address this problem.

3.1.6 Fine-Tuning Simulations: Ensembles and Periodic Boundary Conditions

Although the basics of MD is really simple (see Section 3.1), many corrections are needed to include further properties to the system and to mimic the real biological environment. A direct use of MD leads to the microcanonical ensemble (NVE ensemble), where the number of particles, the system volume, and the energy of the system are kept constant. However, NpT (isothermal-isobaric) or NVT (canonical ensemble) ensembles are often applied as they are more realistic and typically used in experiments. The simulated systems presented in this work are conducted in the NpT ensemble. To achieve this, the temperature and the pressure are treated using a thermostat and a barostat, respectively.

The velocities and the kinetic energy of the particles in an MD simulation can be connected to the temperature via the equipartition theorem

$$K = \frac{1}{2}\sum_{i=1}^{N} m_i v_i^2 = \frac{1}{2} N_f k_\mathrm{B} T, \tag{3.11}$$

where N_f is the number of degrees of freedom. From Eq. (3.11), the temperature can be derived as a function of velocities

$$T = \sum_{i=1}^{N} \frac{m_i v_i^2}{N_f k_\mathrm{B} T}. \tag{3.12}$$

A simple way to keep the temperature constant is to use the so-called weak coupling scheme by Berendsen [183]. In this scheme, the reference temperature T_0 is achieved by scaling the velocities at a rate determined by the time constant τ:

$$\frac{\mathrm{d}T}{\mathrm{d}t} = \frac{T_0 - T}{\tau}. \tag{3.13}$$

Although the Berendsen scheme is efficient in stabilizing the temperature of the system, it does not generate any thermodynamic ensemble correctly as it suppresses the fluctuations of the kinetic energy. To this end, more sophisticated methods, such as the Nosé–Hoover [184, 185] and velocity rescaling [186] thermostats are utilized. For more details and comparison of other thermostats, see e.g. Ref. [187].

Analogous to temperature coupling, different coupling schemes exist for the pressure

control. The Berendsen coupling scheme [183] scales the simulation box size and consequently the atom coordinates, leading to exponential decay towards the reference pressure. The Berendsen barostat is often used to equilibrate the simulation system. Nevertheless, it does not yield the correct NpT ensemble, and therefore, more sophisticated barostats, such as Parrinello–Rahman [188, 189] can be used. The pressure coupling is usually implemented isotropically (scaled in all directions by the same amount), semi-isotropically (x and y dimensions scaled by the same amount, z independently), or anisotropically (all directions scaled independently). The semi-isotropic coupling is often used for systems containing lipid bilayers.

To offer a realistic environment for the studied system, simulation of, e.g., a membrane and water in an infinite vacuum is not an optimal idea. For this, finite simulation boxes could be used, but then the question is, how to deal with the box boundaries? There are several ways to treat the boundaries. The most common in biomolecular systems is to use the periodic boundary conditions (PBCs). With PBCs, the simulation box is replicated infinitely by its translational copies, meaning that if a particle goes through one side of the box, it comes back to the same box from the other side.

3.2 Atomistic vs. Coarse-Grained Models

MD simulations can be used to simulate physical point-like particles. In biomolecular systems, molecular models of different levels (resolutions) are used. As the basis of all phenomena in living systems originates from chemical and mechanical processes on an atomic level, atomistic models are commonly used in the field. Nevertheless, for certain large-scale phenomena, atomistic models are too costly to be conducted. Therefore, also more coarse models are designed to reach longer times and larger length scales.

In all-atom (AA) models, simulation particles represent individual atoms. Parameters of the particles, such as mass and partial charge, reflect reality and the interactions between particles can be adopted from experiments. As atomistic models have the ability to describe, e.g., inter and intra hydrogen bonding, they are often used in studies where atomistic details are important for the studied phenomena. Especially in many systems comprised of transmembrane proteins embedded in lipid bilayers, AA models are the method of choice. A typical simulation system including a transmembrane protein, 100-1,000 lipids, and solvent (water and ions) results in

a system of 100,000–1,000,000 atoms. In a representative case, these systems are simulated for a few microseconds and they are repeated a couple of times (see e.g., Ref. [127]).

Although computing power has increased and modeling software have been optimized heavily during the past decades, one of the main issues in biological science is still the length-scale and time-scale gap between theoretical and experimental methods. One way to overcome this issue is to systematically reduce the number of degrees of freedom representing a system of interest. This is called coarse-graining (CG) [150]. In CG systems, a group of atoms is considered as a single particle, called bead (or pseudo-atom), and atomistic details are taken effectively into account in the bead parameters. Such averaging reduces the computational cost because of two main reasons. First, the number of particles decreases substantially. As the number of non-bonded interactions increases by the square of interacting sites, the number of calculated interactions decreases by orders of magnitude when converting from AA to CG (depending on the CG model) and the achieved benefit in computational cost is significant. Second, when the smallest particles are removed from the system, the finest interaction details (fastest motions) in the system get slower, the particle-particle interactions become softer, and therefore longer time-steps can be used in the integration process. Consequently, with the same computational resources, CG models can offer a substantial increase in the time and length scales compared to the corresponding AA system.

One of the simplest ways to use coarse-graining is to include all the hydrogen atoms in the heavy atoms. For instance, in hydrocarbons (CH, CH_2, and CH_3) the number of interaction sites decreases by a factor of 2–3, depending on the saturation state. In this level of coarse-graining, the model describes the underlying molecular unit by a single particle (see, e.g., the Berger lipid model [190]). Models derived in this way are commonly called united-atom (UA) force fields.

Perhaps the most commonly used coarse-grained model in biomolecular systems is the MARTINI force field. It is parametrized mainly based on density, solubility, and diffusion rates of water/oil systems [191]. The resulting model is based on a four-to-one mapping, meaning that each particle (often called a bead) represents on average four heavy atoms. Special cases, such as ring-like structures, require finer description to capture adequate chemical specificity. MARTINI has four types of particles: charged, polar, non-polar, and apolar. Each particle type has a number of

subtypes, allowing one to describe more accurately the underlying atomic structure (such as the degree of polarity) [192]. Currently, MARTINI contains parameters for proteins [172, 193], lipids [192], nucleic acids [194], and carbohydrates [195], and it is also compatible with a polarizable water model [196]. Additionally, MARTINI simulations can be conducted with implicit solvent (so-called dry MARTINI) [197]. Depending on the system composition, a time step of 20–40 fs is typically used (in comparison to a 2 fs time step used with AA models). Notably, due to the coarse-graining process, phenomena in simulations speed up and, for instance, the diffusion rate of water is approximately 4 times higher in MARTINI simulations compared to the experimental diffusion rate of water [191].

The smaller computational load in coarse-grained models comes with a cost, as the atomic details are lost and certain properties, such as hydrogen bonds, can not be seen. Therefore, quite often in a novel research project, the same system is simulated using a coarse-grained model in combination with the corresponding atomistic model. Also in this work, the so-called multiscale approach was used, i.e., the unpublished work was first simulated using the MARTINI model to reach proper protein binding with longer time scales, and then fine-grained and further simulated with a fully atomistic description to see the details of the binding event. As the multiscale approach is of interest, practical tools, such as MARTINI `insane` [198] and `backward` [199], have been developed to help to do the conversion from atomistic to coarse-grained resolution and vice versa.

3.3 Analysis Tools

In this work, a vast set of analysis tools have been utilized. Here, I only describe the methods that are not trivial but play an essential role in this Thesis.

3.3.1 Hydrogen Bonds

Hydrogen bonds are quantum mechanical in nature [200]. Because the MD method follows the rules of classical mechanics, the analysis of hydrogen bonds in this context needs clarification. When analyzing the number of hydrogen bonds from classical simulations, different geometrical criteria can be used (see, e.g. Ref. [201]). Typically, a distance cut-off in the range of 3–4 Å for the acceptor-donor distance is used, resulting from the position of the first minimum of the donor-acceptor distance

distribution (3.4 Å for oxygen-oxygen distance in water [201]). Moreover, a maximum value of 20–30° for the acceptor-donor-hydrogen triplet angle (zero meaning that hydrogen is between the donor and acceptor atoms) is applied. This criterion is also observed from the angle distribution function, and in a previous study for water was found to be 30° [201]. In some cases, also acceptor-hydrogen-acceptor angle criteria could be used, but the angle distribution is rather flat and gets all the values from zero to 180°, and is therefore not adapted [201].

Here, the number of hydrogen bonds was calculated using the GROMACS tool `gmx hbond`. In the calculation, the default GROMACS parameters of 30° and 0.35 nm for angle and distance were used, respectively. When both criteria are satisfied, the contact is considered to describe a hydrogen bond. In the calculations, all the OH and NH groups are considered as donors, and N and O atoms as acceptors.

3.3.2 Solvent Accessible Surface Area

The surface area of a molecule can be calculated in several ways. For a single particle, the area of a sphere is simply $A = 4\pi r^2$, where r is the radius of the sphere. For example, the van der Waals radius r_{vdW} can be used as the radius r. For a many-body system, the analytical solution can be derived, but it needs extensive and sophisticated programming and is thus not often used [202]. Instead, numerical methods are commonly utilized by using either cylindrical slices, cube composition, or point distributions on atomic spheres.

In this work, we have used the solvent accessible surface area (SASA) [202] method to calculate the surface of a molecule or group of molecules. In the algorithm, a spherical solvent probe with a radius of 0.14 nm is set in contact with a solute atom, whose radius corresponds to its van der Waals radius r_{vdW}. The probe is sampled around the studied solvent molecule without penetrating to its atoms [202]. In the unpublished results for the solvent group, the membrane and the protein are selected, whereas for the calculation group only the protein is picked. In this way, the area of the protein that is accessible to water is computed. Further, subtracting this value from the total surface area of the protein, the area covering the membrane is determined. Similarly, in Articles II and III, the surface calculation is done for lipid headgroups by selecting the whole membrane as a solute and the lipid headgroups as the calculation group.

3.3.3 Order Parameter

One way to define the degree of orientation among molecules is to employ so-called order parameter. In this context, it shows how strongly the orientations of selected molecules are aligned in the same direction. The order parameter calculation of this type is implemented in GROMACS (`gmx order`), and it follows the formula

$$S_z = \frac{1}{2} \left\langle 3 \cos^2\theta_z - 1 \right\rangle , \tag{3.14}$$

where θ_z is the angle between the z-axis of the simulation box and the selected vector. For lipid acyl chains, the vector is defined between the positions of carbon atoms C_{n-1} and C_{n+1}. The brackets correspond to taking an average over time and molecules. The minimum S_z value ($-\frac{1}{2}$) represents the perpendicular orientation, a value of one refers to fully aligned vectors, and a value of zero represents the case where the vectors are randomly aligned. Deuterium order parameter (S_{CD}) provides essentially the same information with different minimum and maximum values. From simulations, S_{CD} can be calculated by using formula 3.14 and defining the angle θ_z between z-axis of the simulation box and the C–H vectors of the lipid acyl chains.

If this order parameter was used to consider changes in phase behavior, an abrupt change in the order parameter would be observed when the membrane changed its phase, e.g., from the low-temperature gel phase to the high-temperature fluid phase. Nevertheless, even if the phase of the membrane would not change, S_{CD} would increase gradually as the order of the acyl chains along the membrane normal increased. Moreover, the deuterium order parameter for lipid acyl chains is highly useful because it can be obtained from the quadrupolar splitting of the NMR spectrum. Further, it can be directly compared with simulation data [203] and used for model validation.

4. OVERVIEW OF THE SYSTEMS STUDIED IN THIS WORK

In this Chapter, the details of the simulation systems explored in the Thesis are presented. The main components (lipids, proteins etc.) are listed, their preparation is described, and all the force fields and other important parameters are characterized. Because the last piece of the Thesis project has not been submitted for publication yet, a detailed description of the models used in this study is also provided below.

4.1 Article I

In the first case study (Article I), atomistic MD simulations were performed to show how a single phosphatidylinositol 4,5-bisphosphate ($PI(4,5)P_2$) lipid receptor plays a role in the first steps of integrin activation. Here, αIIbβ3 integrin was embedded into 1,2-dioleoyl-sn-glycero-3-phosphocholine (DOPC) and DOPC/$PI(4,5)P_2$ (9:1) bilayers. Furthermore, an N-terminal FERM domain of a well-known integrin activator talin [2, 3] was added to the systems. To get more details about the talin binding, two versions of the protein were prepared; the first consisted of four talin FERM domains (F0–F3), and the second one of two FERM domains (domains F2–F3). In addition, systems without talin (integrin embedded in the membrane with $PI(4,5)P_2$) were simulated as a reference.

Short talin version (F2–F3) was prepared using the PDB ID 1MK7 [204] crystal structure and the other two talin domains (F0–F1) using PDB IDs 3IVF [205] and 2KMA [206]. Transmembrane domains of αIIbβ3 integrin were prepared using PDB IDs 2K9J [135], 2KNC [207], and 2KV9 [208]. Furthermore, the contacts between talin and integrin were modeled using structures of PDB IDs 1MK7 [204] and 3G9W [209]. All the protein models were prepared using the Modeller [210] software, whereas the lipid bilayers were built using in-house scripts.

To describe the potential energy functions, the OPLS all-atom (OPLS-AA) [165]

force field was applied to the proteins. For lipids, a lipid-refined version of the OPLS all-atom force field was employed [166]. For water, the OPLS-AA compatible TIP3P [211] model was utilized. Simulations were carried out at constant pressure (1 bar) and temperature (310 K). The pressure and temperature were controlled by the Parrinello-Rahman [188] and velocity rescaling (v-rescale) [186] methods with time constants of 1 ps and 0.1 ps, respectively. The integration time step was set to 2 fs, and simulations were simulated for 500 ns and 750 ns for the systems with and without talin, respectively. The last 300 ns of each system was used for the analysis.

4.2 Article II

In Article II, the differences between the natural and the BODIPY-labeled GM1 ganglioside were studied in different lipid environments using atomistic MD simulations. Related simulation studies of free probes (dyes) gauging membrane properties overall, and probes attached to lipids, thereby investigating single-molecule behavior, have been done quite extensively [212, 213, 214, 215]. However, to the best of the author's knowledge, there are no previous simulation studies focusing on labeled GM1. This is quite surprising, since GM1 is an exceptionally important lipid due to its role, for instance, as a receptor for cholera toxin, and therefore as a raft marker [4]. The challenge is to resolve how native (non-labeled) GM1 and BODIPY-labeled GM1 (bdGM1) behave in lipid membranes, how they bind to cholera toxin, and how in these contexts the properties of native and labeled GM1 differ from each other.

For this purpose, two membranes, identical to the lipid bilayers used in the experiments done by our collaborator, were prepared using the method for embedding proteins into bilayers introduced by Javanainen [216], and in-house scripts to implement the method. First, a membrane consisting of DOPC and GM1 (220/40) was assembled to mimic a lipid bilayer in the liquid-disordered (L_d) phase. Second, a membrane containing N-stearoyl-D-erythro-sphingosylphosphorylcholine (SSM), cholesterol, and GM1 (220/220/40) was prepared to mimic a lipid bilayer in the liquid-ordered (L_o) phase. Further, additional lipid bilayers (4 in total) were prepared with the same lipid compositions, but instead of GM1, the BODIPY-GM1 was used. All the four membranes were simulated with and without cholera toxin B-pentamer (CTxB, protein data bank (PDB) ID: 1RF2 [217]), which is a peripheral protein and a well-known GM1 marker. Moreover, to compare with a previous study [126] (for details, see Section 5.2), an extra membrane without sphingolipid (DOPC/Chol/GM1,

220/220/40) was prepared. Finally, all the systems were solvated with water and 140 mM sodium chloride (NaCl) salt.

All the simulations were performed at a constant pressure (1 bar) and temperature (298 K) using the Parrinello-Rahman [188] barostat and the v-rescale [186] thermostat, respectively. The OPLS all-atom force field [165] was used to parametrize all the molecules. For water, the TIP3P [211] model was used. The BODIPY label was parameterized based on the standard OPLS all-atom force field (LJ parameters and bond, angle, and dihedral potentials), and the partial charges were calculated by the authors. Geometry optimization for the BODIPY molecule was carried out by using density functional theory (DFT) with the B3LYP [218] functional and the 6-31G* basis set. All the QM calculations were done by using the Gaussian 09 program [219], and the ChelpG [220] routine was used to derive the partial charges.

4.3 Article III

In the third case study (Article III), atomistic MD simulations were conducted to study the effect of calcium ions on PI(4,5)P_2 receptors in lipid bilayers. To this end, a lipid bilayer consisting of 230 POPC and 26 PI(4,5)P_2 molecules was generated using CHARMM-GUI [221, 222]. The system was solvated in water and 150 mM potassium chloride (KCl) salt. Moreover, to neutralize the system, three different ions were used: Ca^{2+}, Mg^{2+}, and K^+. Following this procedure, simulated systems contained a calcium (and magnesium) concentration of approximately 220 mM. Systems with Mg^{2+} and K^+ are used as control systems for the simulation with calcium.

Due to the rather inaccurate description of divalent ions in classical models, three different atomistic force fields were considered to simulate the same systems. First, similarly to previous studies (Articles I and II), the OPLS all-atom [211] force field with additional refined lipid parameters [166] was used. Second, a standard CHARMM36 lipid force field [162] was employed. Finally, to consider the electronic polarization effects of charged groups, we utilized the recently developed electronic continuum correction with rescaling (ECCR) that dampens the unrealistically high ion pairing that is common in nonpolarizable force fields [223]. In practice, the partial charges of all the ions and PI(4,5)P_2 phosphate groups were scaled by a factor of 0.75. The ECCR correction was done for the Ca^{2+} and K^+ in OPLS-AA systems.

All the simulations were performed under constant pressure (1 bar) and temperature

(310 K). The pressure was coupled using the Parrinello–Rahmen barostat [188] and the temperature with the Nosé–Hoover thermostat [184, 185]. For water, the TIP3P [211] and TIP3PS [224] water models were used for OPLS-AA and CHARMM36, respectively. The TIP3PS water model is based on the TIP3P model [211], with the addition of the Lennard–Jones interactions also applied on the hydrogen atoms. For the integration of the equations of motion, a time step of 2 fs was used and all the systems (8 in total) were simulated for 1 µs. The first 400 ns was considered as equilibration and the last 600 ns were used for the analysis.

4.4 Results to be Published

In the manuscript that is currently being prepared and will be later submitted for publication, the effect of cholesterol on PI(4,5)P_2 molecular presentation and ligand binding was studied. To this end, four PI(4,5)P_2 (18:0, 20:4) lipid bilayers with various cholesterol concentrations were considered. All the membranes were prepared using CHARMM-GUI [221, 222]. Each system was solvated by 50 water molecules per lipid, and potassium ions were used as counterions to neutralize the systems. Using CHARMM-GUI output files, the systems were energy-minimized and then equilibrated by removing implied restraints in a stepwise manner. All the systems were simulated for 1 µs. The first 400 ns was considered as an equilibrium time and the rest was used for analysis.

To study how protein recognition changes upon cholesterol enrichment, additional simulations were performed in a multiscale manner, i.e. by combining atomistic and coarse-grained models. Using this technique, we can simulate larger systems with long simulation times, but still reach atomistic resolution. Here, we started our study by using the coarse-grained (CG) MARTINI model [192]. First, cholesterol-free and cholesterol-rich bilayers were prepared using the CHARMM-GUI MARTINI Bilayer Maker [221, 225]. The equilibrium protocol proposed by the CHARMM-GUI output files was used. The systems were energy-minimized and then equilibrated by removing implied restraints in a stepwise manner. Next, the canonical PI(4,5)P_2 sensor, here the pleckstrin homology (PH) domain of PLC δ1 (PDB ID: 1MAI, [226]), was introduced to the systems. The protein model for the MARTINI force field was built using *martinize.py* (available in `http://cgmartini.nl`). The PLC δ1-PH domain was placed in a random position into the bulk water, with a limitation to keep the minimum distance between the protein and the membrane at 1 nm. The protein was oriented so that the canonical binding site [226] was pointing towards

the membrane. After protein insertion, water was added to the systems and sodium ions were used as counter-ions to neutralize the scheme. Finally, the systems were equilibrated for 2.5 ns using restraints for the protein prior to the production runs. Three replicas were made for both 0 mol% and 35 mol% membrane systems.

In order to improve sampling and get more quantitative observations of the protein binding, the umbrella sampling method [227] was utilized. In essence, using the umbrella sampling method, one can calculate the free-energy profile for a protein binding. To this end, one replica from each system (0 mol% and 35 mol% cholesterol) was randomly chosen and a structure close to the end of 4 µs of the simulations was taken. The selected structures present the protein-bound state of the system. Next, the protein was pulled out from the membrane surface. External force along the membrane normal was applied to the protein towards the bulk water in one run, and towards the membrane interior in the second run. From the two runs, 31 configurations were extracted to act as initial structures for the umbrella sampling simulations. Initial structures were selected so that the distance between the center of the mass (COM) of the protein and the COM of the membrane varied systematically using a 0.1 nm interval in the range of 3–6 nm. The same procedure was repeated for cholesterol-free and cholesterol-rich membrane systems. The cholesterol-free systems were simulated for 400 ns and the cholesterol-rich systems for 500 ns so that the free energy profiles converged. For the free energy profile calculation, the last 100 ns of the umbrella windows were used.

To see the atomistic details of the protein binding, the same structures that were chosen to represent the protein-bound state were fine-grained to atomistic resolution using the Backward [199] tool available in `http://cgmartini.nl`. Because the atomistic systems require more computational resources to simulate the same molecules compared to the coarse-grained models, we reduced the system size before starting the atomistic production runs. Prior to fine-graining, large CG systems were shrunk by removing lipids that were away from the protein. The system size was cut down so that the number of lipids was identical to the atomistic membrane systems without the protein that was simulated earlier. Also, the water and ions close to the removed lipids were deleted. After fine-graining, the original crystal structure of the PLC δ1-PH-domain (PDB ID: 1MAI, [226]) was fitted on top of the fine-grained protein structure to avoid possible mistakes in the fine-graining procedure and to have the correct protein structure as an initial condition for the atomistic system. In addition to the fine-grained CG systems where the protein is

bound to the lipid bilayer in the initial state, three additional repeats (for both 0 mol% and 35 mol% cholesterol systems) with the protein in bulk water were prepared. The initial structures for the lipid bilayers were taken from the membrane simulations by choosing the membrane structures at 400 ns, 700 ns, and 1000 ns, one for each replica. Furthermore, the protein (PDB ID: 1MAI) was placed into the water phase, at least 1 nm away from the membrane surface. Finally, the systems were solvated with water, and potassium ions were added to neutralize the systems. Prior to the 1 µs production run, the systems were equilibrated for 10 ns using restraints on the protein backbone. The last 600 ns of all the five replicas (both 0 mol% and 35 mol% cholesterol) was used for analysis.

4.4.1 CHARMM36 (AT) Parameters

For all the atomistic simulations in this project, the CHARMM36 force field [161, 162] was employed. The GROMACS format force field files were downloaded from the MacKerell Lab Homepage, available in `http://mackerell.umaryland.edu`. For water, the TIP3PS water model [224] was used. The temperature was maintained at 310 K using the Nosé–Hoover thermostat [185, 228] and the protein, the membrane, and the solvent were coupled separately with a time constant of 1 ps. The pressure was coupled semi-isotropically to 1 bar in the plane of the membrane and perpendicular to it using the Parrinello–Rahman barostat [188]. The coupling constant and membrane compressibilities were set to 5 ps and 4.5×10^{-5} bar^{-1}, respectively. The leap-frog algorithm was used to integrate the equations of motion, a time step of 2 fs was employed, and all the trajectories were stored every 100 ps. The neighbor list for non-bonded interactions was updated every 20 steps using the buffered Verlet method [229]. Electrostatic interactions were evaluated utilizing the smooth particle-mesh Ewald (PME) algorithm [230] with a real space cut-off of 1.2 nm. The Lennard–Jones potential was smoothly switched off at 10–12 Å by a force-based switching function [231]. All the covalent bonds involving hydrogen atoms were constrained using the LINCS algorithm [159, 232].

4.4.2 MARTINI (CG) Parameters

All the lipid bilayers that were simulated using coarse-grained models in this study were prepared using the CHARMM-GUI MARTINI Bilayer Maker [221, 225]. The

membranes were energy-minimized and equilibrated using the CHARMM-GUI output files. For the production run with the presence of the protein, the following force field files from the MARTINI web page (`http://cgmartini.nl`) were downloaded: `martini_v2.2.itp`, `martini_v2.0_lipids_all_201506.itp`, `martini_v2.0_solvents.itp`, and `martini_v2.0_ions.itp`. Topology file for the PLC δ1-PH-domain was generated using *martinize.py* (available in `http://cgmartini.nl`). To preserve the protein tertiary structure, an elastic network was applied to the protein beads with a force constant of 500 $\frac{\text{kJ}}{\text{mol}}$.

Similarly to the atomistic systems, all the CG simulations were performed in the isothermal-isobaric (NpT) ensemble (310 K and 1 bar). The temperature was coupled separately for the membrane, solvent, and the protein using the v-rescale thermostat [186] with a time constant of 0.1 ps. The pressure was maintained semi-isotropically using the Berendsen barostat [183] with a relaxation time constant of 5 ps. Lennard-Jones interactions were shifted to zero at 9–12 Å and electrostatic interactions to zero between 0–12 Å. The neighbor list was updated every 10 steps with a radius of 1.4 nm. The time step of 10 fs was used, coordinates were saved every 1 ns, and the periodic boundary conditions were employed in all three dimensions.

In the umbrella sampling simulations, the parameters mentioned above were used and an additional external umbrella force with a force constant of 1000 $\frac{\text{kJ}}{\text{mol}}$ was applied between the COM of the protein and the COM of the membrane. To prevent unwanted membrane bending, a cylinder geometry for the external force was employed with a radius of 3.5 nm.

5. RESULTS AND DISCUSSION

In this Chapter, the results from Articles I – III are discussed. Moreover, additional results to complement those presented in Article III are discussed in more detail in Section 5.4. The focus in this Chapter is on the results from MD simulations, however also some essential experimental results from the original papers are reviewed.

5.1 Article I: PI(4,5)P_2–Talin Complex Initiating Integrin Activation

The members of the integrin family have a remarkable ability to transmit signals in both directions across the cell membrane [131], thus being crucial for several vital cellular activities, including proliferation, survival, and gene expression [1]. These proteins are heterodimeric transmembrane receptors composed of α- and β-subunits. The activation of the protein has been shown to change the conformation of the integrin complex [133]. In its folded inactive state, the intracellular portions of α- and β-subdomains lie close together and adhere to one another. In the active state, this contact is broken and both the transmembrane and the intracellular portions of the α- and β-subdomains stay apart. Moreover, the inactive conformation is the passively adopted integrin receptor's default state [136] that is shifted towards the activated state upon recruitment of activating proteins, such as talin (inside-out activator) [2, 3]. Notably, PI(4,5)P_2 receptors have been observed to enhance talin binding to membranes [137, 138] and further to influence talin–integrin binding [139, 140]. Nevertheless, the details of the integrin activation and the role of lipids in the process are largely unknown.

Integrin α- and β-subunit transmembrane helices are characterized to be stabilized by the inner membrane clasp (IMC) and the outer membrane clasp (OMC) [134, 135]. The IMC is formed between the conserved GFFKR motif of the αIIb domain and the hydrophobic residues Trp715 and Ile719 of the β3 unit, together with the salt bridge between Arg995 αIIb and Asp723 β3. The OMC is between Gly708 in

β3 and the G972xxxG976 motif in αIIb and is located away from the cytoplasm. In a previous study by Hughes et al. [233], specific mutations of the residues in IMC and OMC resulted in perturbed interactions of the integrin transmembrane helices and further led to a continuously active integrin.

The main focus of this study was to study how talin and PI(4,5)P_2 affect the integrin properties. To this end, three different systems were prepared (for system details, see Section 4.1). In the first system, αIIbβ3 integrin was embedded into a lipid bilayer containing PI(4,5)P_2 and talin was placed to the water phase. As a reference, the second system lacked talin, and in the third case a pure DOPC bilayer without PI(4,5)P_2 was used. From these systems, the stability of the salt bridge in the IMC and the distance between the transmembrane helices was measured to recognize early steps of the integrin activation process.

The simulations revealed that when talin and PI(4,5)P_2 are present, the salt bridge in the IMC breaks up (Fig. 5.1A). This behavior was observed in all three replica simulations. Nevertheless, the separation of the integrin α- and β-subunits was not observed (see Fig. 5.1B). This may be due to the somewhat short simulation times that do not allow the rearrangement of the helices to occur, or the fact that only a part of the full-length integrin was included in the simulation model (integrin ectodomain missing). Moreover, when talin was taken away from the system, integrin was observed to be steady, i.e. the salt bridge remained stable during the whole course of simulation (see Fig. 5.1C). Also, the IMC distance remained rather unchanged (see Fig. 5.1D). Finally, in the third case where integrin and talin were present but the anionic PI(4,5)P_2 molecules were removed from the lipid bilayer, the salt bridge broke in one out of the three systems. Still, even in this system, the separation of transmembrane helices was not observed (see Fig. 5.1F).

During the course of the simulations, PI(4,5)P_2 molecules were observed to interact actively with the αIIb residue Arg995 (the component of the IMC salt bridge) in two out of three systems in the presence of talin. Importantly, when talin was absent, hydrogen bonds between PI(4,5)P_2 and the αIIb residue Arg995 were not recorded at all. Nevertheless, contacts between PI(4,5)P_2 and the neighboring residue of the salt bridge (αIIb residue Lys994) were continuously formed. This suggests that talin is not needed to localize PI(4,5)P_2 near the Arg995-Asp723 salt bridge. However, the binding of talin to integrin may expose the salt bridge to the attack by PI(4,5)P_2.

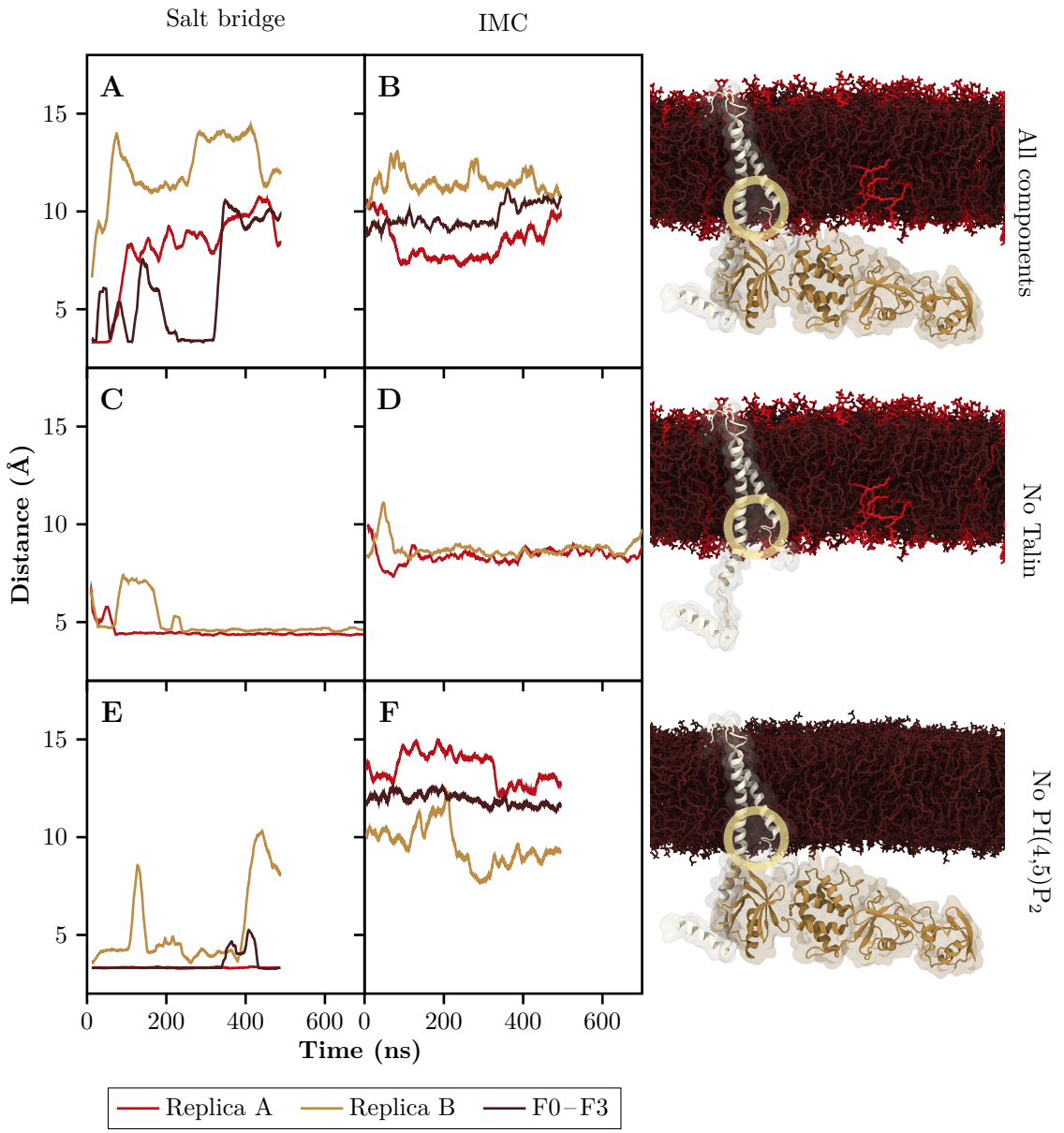

Figure 5.1 *In the left panel (A,C,E), the distance between the salt bridge residues (Arg995 from the αIIb and Asp723 from the β3) as a function of time is presented. When both talin and PI(4,5)P_2 are present, the salt bridge breaks in all the systems (A), whereas without talin (C) the salt bridge remains unbroken. Moreover, in the pure DOPC bilayers (E) the salt bridge breaks in one out of the three systems. To see if this causes integrin activation (separation of the transmembrane helices), the distance between residues Phe993 in αIIb and Lys716 in β3 in the IMC was measured for all the systems studied (B,D,F). A clear correlation between the salt bridge breakage and the separation of helices was not observed. In panels (C,D) red and brown depict replicas of the system without talin, whereas in panels (A,B,E,F) red and brown illustrate replicas of the systems with two FERM domains (F2–F3). Moreover, dark red represents systems with four talin FERM domains (F0–F3). In the most right column, the initial structure of each system is shown. Color coding is as follows: red, PI(4,5)P_2; white, integrin; brown, talin (F0–F3 domains shown). The lipids are drawn as licorice model and the protein with a transparent surface on top the secondary structure. Location of the salt bridge is marked with transparent brown circles on top of the snapshots in the right column. Figure adapted from Ref. [234].*

Although the transmembrane helices remained attached to each other in all the systems, PI(4,5)P_2 together with talin seems to facilitate the break up of the salt bridge. The salt bridge has been shown to be crucial for the integrin stability, and once the salt bridge is broken, integrin activation can take place [233, 235, 236]. Also, new insights into talin binding to PI(4,5)P_2 enriched lipid bilayers was given in this study, but these results are not discussed here (for details, see Article I).

5.2 Article II: Synthetic Modifications Alter the Binding Properties of GM1

Cellular plasma membranes are laterally heterogeneous, featuring a variety of distinct subcompartments that differ in their biophysical properties and composition. These lipid-induced membrane domains are responsible for functional compartmentalization of cellular trafficking and signaling activities in a wide variety of cellular contexts [60, 237]. One of the lipid types present in the domains are glycosphingolipids (GSLs) [58]. GSLs participate in a wide range of biological processes, such as recognition of hormones, cell growth/differentiation, and cell-cell interaction [238, 239, 240]. Among the many glycosphingolipids, GM1 is used as a default lipid marker for the nanoscopic cholesterol/sphingomyelin enriched, liquid-ordered (L_o) membrane domains [4, 240, 241, 242, 243]. These nanodomains are often referred to as "membrane rafts" [58], opposing the liquid-disordered (L_d) membrane environment.

To be able to explore membrane nanostructures visually, in experiments small molecules (lipids and proteins) are often labeled with fluorescent tags. The physicochemical properties of lipids (e.g. hydrophobicity, molecular shape, and planarity) determine their both collective and individual behavior in membranes. Thus, the addition of bulky tags may drastically affect native lipid behavior [244]. For example, GM1 detection by cholera toxin (CT) is a well-established tool for monitoring the L_o membrane domains. Nevertheless, the acyl chain-BODIPY labeled GM1 (bdGM1) is bound to cholera toxin beta-subunit (CTxB) exclusively in the L_d phase in giant unilamellar vesicles (GUVs) and giant plasma membrane vesicles (GPMVs) [4, 243]. Consequently, these fluorescent analog lipids are not identical to the native GM1 regarding their biochemical and biophysical behavior.

Cholera toxin has been discovered to bind to GM1-containing lipid membranes and to induce local membrane curvature (radius of 36 nm) [245, 246]. In this study, the molecular basis of the cholera toxin beta-subunit binding to GM1 and bdGM1 was

unraveled through atomistic MD simulations complemented by experiments done by our collaborator. For the MD simulations, two membranes were prepared (for the system details, see Section 4.2), one mimicking the liquid-ordered (L_o) and the other the liquid-disordered phase. Furthermore, the bilayers were enriched with either the native GM1 or its fluorescent analog (the acyl chain-BODIPY labeled GM1). These bilayers were simulated as such, as well as in the presence of CTxB.

First, the headgroup exposure to the water phase was analyzed by calculating the solvent accessible surface area (SASA) of the GM1 and bdGM1 molecules. While SASA for the native GM1 was similar in both systems, for bdGM1 a pronounced change of $\sim$0.43 nm^2 per molecule was observed between the L_d and L_o phases (see Fig. 5.2A), indicating higher exposure of the headgroup to water in the L_d phase. To understand the origin of the discovered change, the orientation of the GM1 headgroup was monitored by calculating angles between the membrane normal and the selected vectors of the GM1 headgroup: forefinger, thumb, and wrist (vectors illustrated in Fig. 5.2B). The GM1 forefinger was observed to have a tilted orientation towards the membrane, while the wrist and the thumb were found to point more towards the water phase. Although the angle distributions were somewhat similar regardless of the lipid environment and the presence of the BODIPY label, a few interesting features can be highlighted. First, the BODIPY label oriented the wrist part more towards the water phase (by $\sim5^\circ$) compared to the native GM1. Second, while the thumb tilted towards water in L_d for bdGM1 when compared to the native GM1, it tilted towards the membrane in the L_o phase. These differences are quite minor but evident and may explain the preferential CTxB binding of bdGM1 in the L_d phase in the phase separated systems [4]. Importantly, in the previous study by Lingwood et al. [126], cholesterol was found to tilt the headgroup of GM1 towards the membrane, which we did not observe with the present L_d and L_o membranes. To address this difference, we replaced SSM in the L_o phase by DOPC and simulated the revised system. Interestingly, a significant tilt of the GM1 headgroup towards the membrane was observed, in agreement with the previous study [126], thus showing that the effect of cholesterol on GM1 orientation depends largely on the lipid pool hosting it.

Next, the availability of the GM1 headgroup for CTxB binding was studied. The number of hydrogen bonds between GM1 molecules and CTxB was used as a correlate to the binding affinity. Regardless of the GM1 structure (native or labeled), binding to the L_d phase was recognized to be more prominent based on the higher number of hydrogen bonds compared to the L_o phase (see Fig. 5.3C). However, this is not in

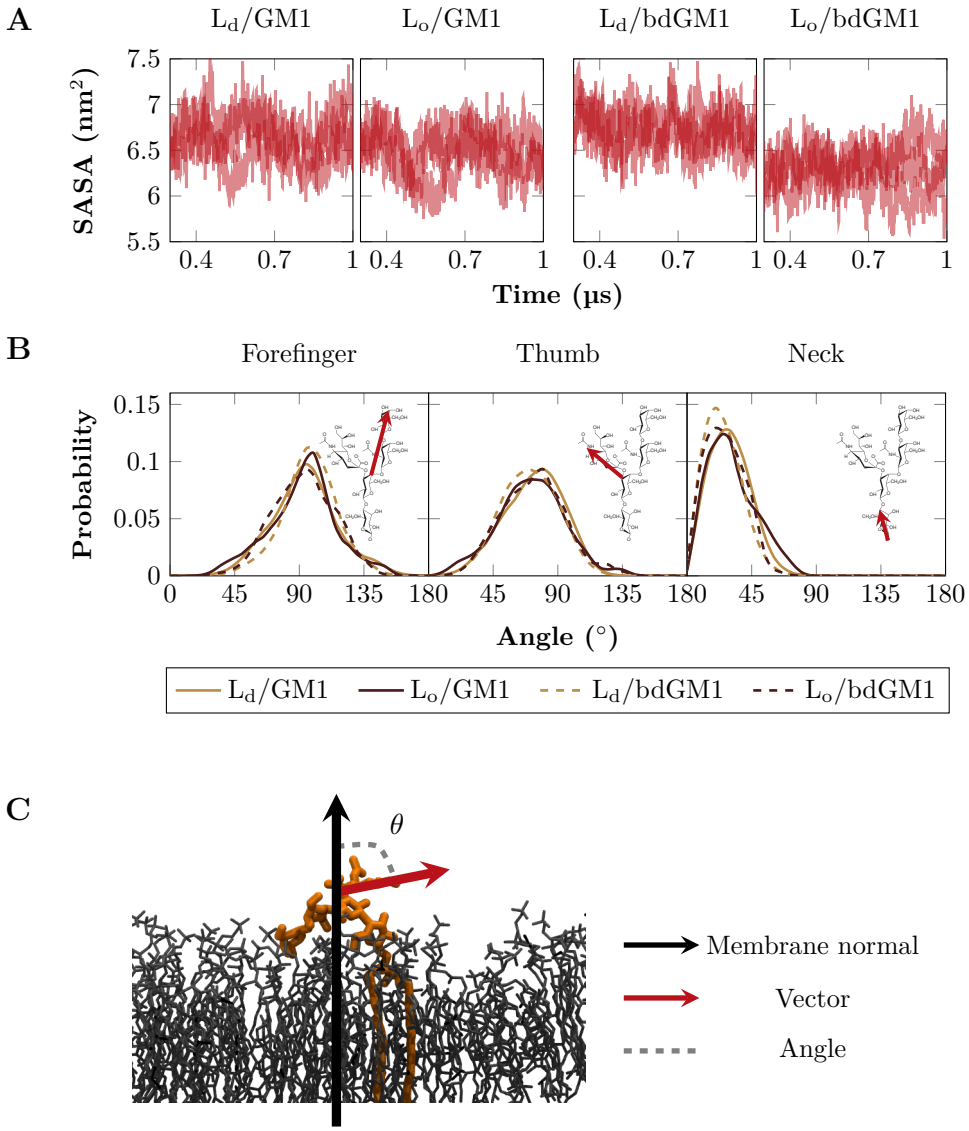

Figure 5.2 *(A) Solvent accessible surface area (SASA) calculated for all the simulated systems. Each replica is shown as a transparent line. In case of bdGM1 (on the right), SASA clearly decreases when moving from the* L_d *to the* L_o *phase, meaning higher exposure of the GM1 headgroup to water in the* L_d *phase. (B) Angle distribution of the three vectors defined in the GM1 headgroup (vectors presented in each plot as a subfigure). Headgroup orientation remains similar in all the simulated systems, regardless of the membrane environment (*L_d *or* L_o *phase) or the presence of the BODIPY tag. The "wrist" vector slightly tilts (*$\sim 5°$*) towards the water phase when GM1 is labeled. This happens both in the* L_d *and* L_o *environments. (C) Figure showing the angle between the membrane normal and a selected vector. Here, "thumb" vector is highlighted as red arrow, showing the orientation approximately at the peak of the angle distribution curve (B). Figure adapted from Ref. [247].*

agreement with the previous knowledge that CTxB is used as a lipid raft (L_o phase) marker. To reveal the enigma, CTxB binding was also measured experimentally (see Article II) using synthetic liposomes. The equilibrium binding affinities were discovered to be similar in all the four systems, in agreement with the MD results. Still, an evident decrease in the maximum binding affinity for the BODIPY labeled GM1 was detected compared to the native GM1 vesicles both in L_d and L_o. The difference was significant, especially in the vesicles mimicking the L_o phase (∼35–40%), suggesting that many bdGM1 molecules remain unbound to CTxB.

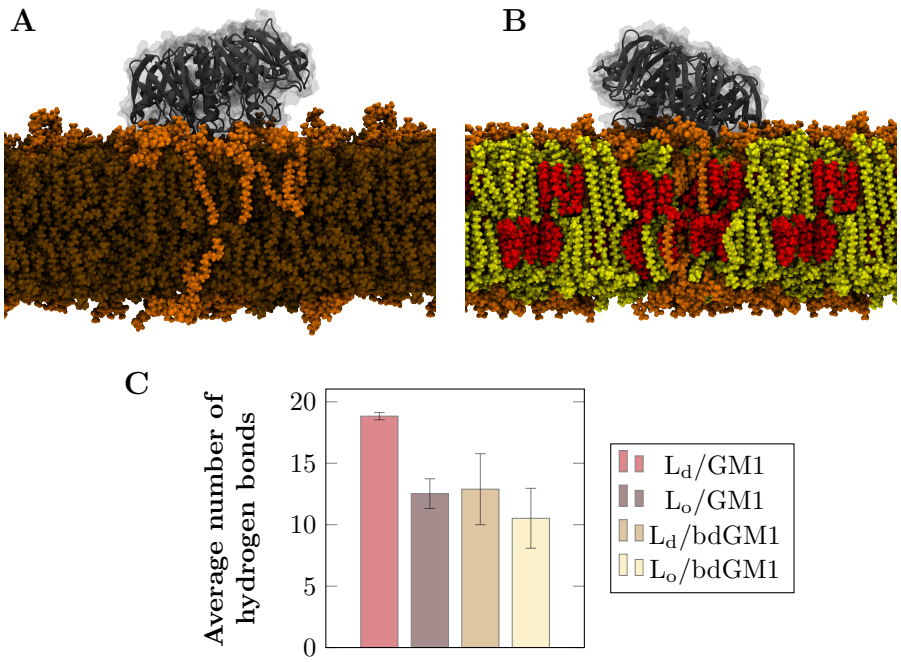

Figure 5.3 *Snapshots of the end structure of the (A) L_d and (B) L_o systems. The CTxB is shown as a gray transparent surface on top of a gray secondary structure. Cholesterol is colored as red, DOPC in brown, SSM in yellow, and GM1 in orange. In (C) the average number of hydrogen bonds between CTxB and GM1 is shown. The mean values are calculated by averaging over all the three replicas and from each replica, the last 700 ns is used for calculation. The error shown is the standard error. Figure adapted from Ref. [247].*

As the CTxB binding to the studied L_d and L_o phases remains merely unchanged, and the molecular details of GM1 receptors in the studied bilayers are not changing dramatically, the following question arises: how CTxB recognizes the native GM1 in L_o, and bdGM1 in the L_d phase, in the phase separated systems? Some other factors that change in the headgroup presentation must be involved, such as ganglioside

oligomerization (also proposed by Shi et al. [248]) or the GM1 phase partitioning. This needs further research, but the key result of this study is that even if the BODIPY label does not strongly affect the GM1 headgroup presentation or ligand binding, the used acyl-chain labeling can change molecules' functional properties significantly. Thus, great care needs to be taken when interpreting data from studies where fluorescent labels are used.

5.3 Article III: Calcium Regulating PI(4,5)P_2 Presentation

Intracellular calcium ions (Ca^{2+}) have diverse roles in cellular functioning, including cell proliferation, cell cycle control, gene expression, autophagy, and cell death [249, 250]. One controlling mechanism for adjusting the calcium levels inside the cell is caused by phospholipase C (PLC) that binds to PI(4,5)P_2 in the plasma membrane and hydrolyzes it to water-soluble inositol 1,4,5-trisphosphate (IP3) and diacylglycerol (DAG). Further, IP3 induces the Ca^{2+} release from the endoplasmic reticulum and thus increases the calcium concentration in the cytosol [6].

PI(4,5)P_2 lipid receptor is enriched in the cytoplasmic (inner) leaflet of the plasma membrane [251, 252] and is there, among the other negatively charged lipids, continuously exposed to divalent ions. Ca^{2+} is proposed to cause acyl chain thickening of the PI(4,5)P_2 molecules [253], and that upon interactions between Ca^{2+} on PI(4,5)P_2, they partially dehydrate each other and further cause electron density to increase in the lipid headgroup region [254]. While the overall effects of Ca^{2+} on PI(4,5)P_2 have been studied extensively, the interactions between Ca^{2+} and PI(4,5)P_2 at the molecular level remain unclear.

In Article III, we unraveled the functional and structural consequences of the interplay between Ca^{2+} and PI(4,5)P_2 through MD simulations bridged to experiments. For the MD simulations, systems of a lipid bilayer with various salts were prepared (for details, see Section 4.3). Systems were repeated with different force fields, all giving (at least qualitatively) similar results. Here, only the results from one force field (here CHARMM36) are presented.

Even the visual comparison of the systems with and without Ca^{2+} revealed a striking difference between the two systems: PI(4,5)P_2 headgroup is more tilted towards the membrane in the presence of Ca^{2+}. To quantitatively determine the tilting, the angle between the membrane normal and the C1–C4 carbon atoms of the PI(4,5)P_2

was monitored (see Fig. 5.4A). The mean value of the angle for the Ca^{2+} system was 69° and for the system without divalent ions 36°, suggesting a strong tilting of the PI(4,5)P_2 headgroup towards a membrane caused by the calcium ions. As a reference, another divalent ion present in the cytosol, Mg^{2+}, was found to induce a mean tilt angle of 49°, showing milder tilting towards the membrane compared to Ca^{2+}. The angle data were complemented by mass density profiles (see Fig. 5.4B) that show the movement of the PI(4,5)P_2 headgroups away from the water towards the membrane, when Ca^{2+} is present. Again, Mg^{2+} also caused penetration of the PI(4,5)P_2 headgroup to the membrane interior, but not as deeply as Ca^{2+} did.

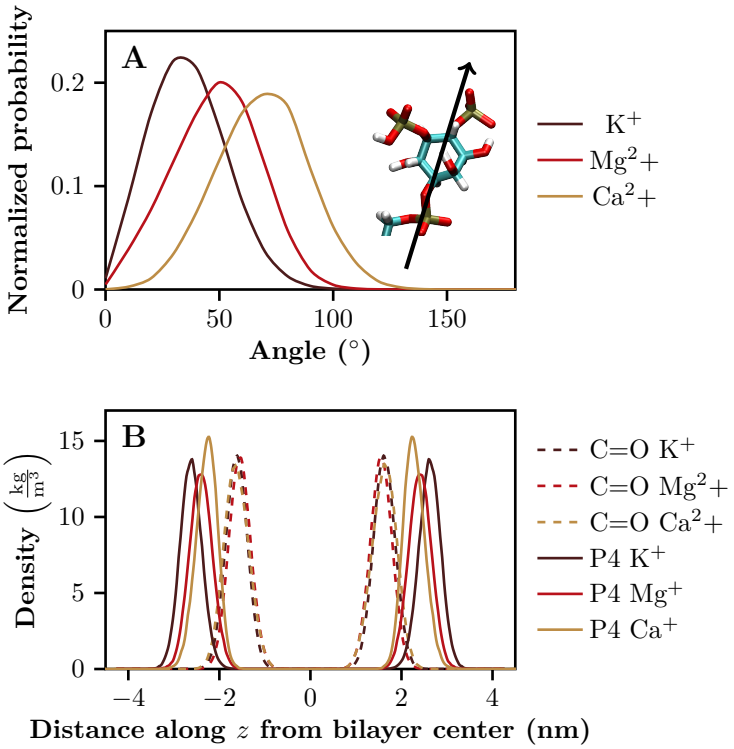

Figure 5.4 *(A) Angle distributions of the angle between the PI(4,5)P_2 headgroup (vector illustrated in the subfigure) and the bilayer normal for the system with calcium in brown, magnesium in red, and without divalent ions in dark red. Simulation time 400–1000 ns was used for analysis. From the distributions, the PI(4,5)P_2 headgroup tilting can be clearly seen when Ca^{2+} is present. (B) Density profiles of phosphorus atoms at position four in the inositol ring (P4) and carbonyl oxygens atoms of the PI(4,5)P_2 molecule. The same coloring scheme is used as in (A), and the dashed line shows the carbonyl oxygens, whereas the solid line represents the P4 phosphorus atoms. From the density profiles, the total movement of the PI(4,5)P_2 headgroups towards the membrane center can be clearly seen. Figure adapted from Ref. [255].*

Next, the ion binding to PI(4,5)P_2 was analyzed in more detail by calculating the

radial distribution function of ions using five different reference points selected from the PI(4,5)P_2 molecule: i–ii) phosphorus atoms in the positions 4 (P4) and 5 (P5) of the inositol ring, iii) the phosphorus in the backbone phosphate (P1), and iv–v) the carbonyl oxygens of both acyl chains (C=O_{sn-1}, C=O_{sn-2}). From the radial distribution profiles (see Fig. 5.5) one can clearly see that Ca^{2+} binds mostly to the phosphate groups at positions 4 and 5, but it also penetrates deeper into the lipid bilayer interacting with the carbonyl groups. The presence of calcium ions was also observed to correlate with other membrane properties, including increasing acyl chain order, slower headgroup rotation, and decreased area per lipid (data not shown). Importantly, using protein–lipid binding assays, the PLC binding to the PI(4,5)P_2 containing liposomes was observed. Nevertheless, when calcium was added, the binding was almost fully inhibited. Also, PLC was not observed to bind to the POPC liposomes, indicating its specificity to PI(4,5)P_2.

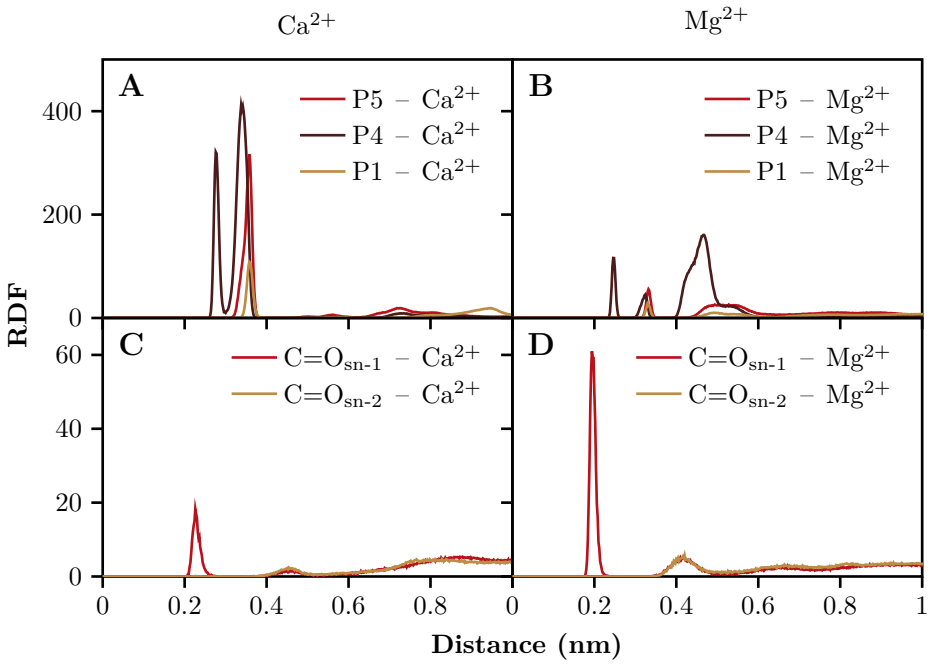

Figure 5.5 *Radial distribution function (RDF) between calcium (left column) or magnesium (right column), and each PI(4,5)P_2 phosphorus atoms (top row) or the carbonyl oxygens (bottom row). Only the results based on the CHARMM36 force field are shown here, as the results of the other force fields are in good agreement with the present results (see Article III). Figure adapted from Ref. [255].*

Altogether, these findings indicate that calcium has the ability to switch PI(4,5)P_2 conformational states that can further serve as a potential cellular mechanism for receptor recognition. Thus, the results present an undiscovered role and mechanism

of Ca^{2+} in cellular signaling. The results are in good agreement with the experiments done by our collaborators. Also, in the previous study by Seo et al. [256], the effect of Mg^{2+} was observed to be weaker than the one induced by Ca^{2+} for different PLCs, suggesting that the divalent ions bind to PI(4,5)P_2 with different binding affinities.

5.4 Cholesterol Plays a Fundamental Role in PI(4,5)P_2 recognition

PI(4,5)P_2 is the most abundant phosphoinositide and is concentrated in the plasma membrane. However, PI(4,5)P_2 is also found in other cell compartments, such as Golgi (reviewed in [7, 8]). Interestingly, it has been shown that certain PI(4,5)P_2 binding ligands recognize their receptor only in the plasma membrane [9]. How the binding is regulated, remains unclear.

Membrane cholesterol concentration increases along the secretory pathway [10, 11] and is highest in the plasma membrane [10, 11]. In the present work, we studied in atomic detail how cholesterol affects the PI(4,5)P_2 binding properties. The employed atomistic MD simulations were bridged to experiments through collaborators.

5.4.1 High Cholesterol Concentration Makes Lipid Headgroups More Exposed to Water without Changing Headgroup Orientation

To study the membrane properties in atomistic detail, MD simulations were employed for membranes with various cholesterol concentrations (for system details, see Section 4.4). In brief, all the simulated atomistic (AT) membranes contained 232 POPC and 24 PI(4,5)P_2 molecules. Depending on the system, 0, 28, 64, or 138 cholesterol molecules were added to the membranes to explore them systematically with various cholesterol concentrations from 0 to 35 mol%.

In the acyl chain region, the effect of cholesterol was clearly seen as increasing order in POPC *sn*-1 carbons, when the cholesterol concentration was increased (see Fig. 5.6A). Moreover, to see the change(s) in the POPC headgroup presentation, the angle between the membrane normal and a vector characterizing the orientation of the POPC headgroup was calculated (see Fig. 5.6B). Interestingly, the tilt angle distribution

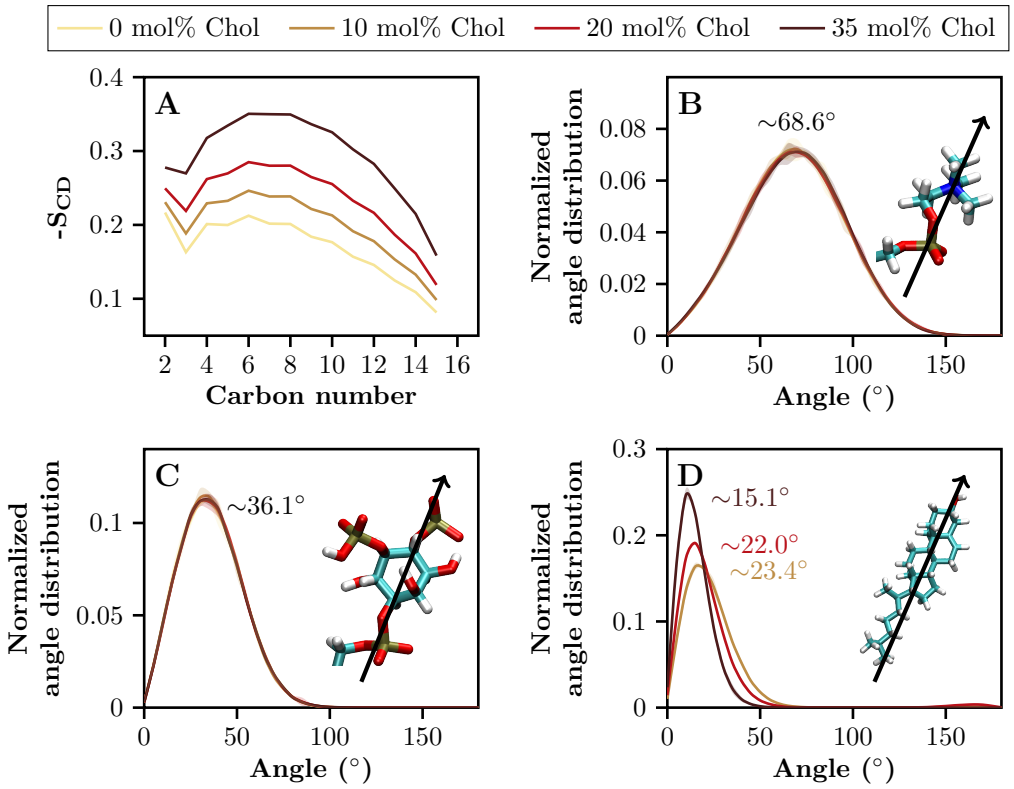

Figure 5.6 *(A) Acyl chain order parameter of the POPC sn-1 chain for atomistic 0 mol% Chol/10 mol% Chol/20 mol% Chol/35 mol% Chol systems. Order parameter is higher for the membranes with high cholesterol concentration, thus showing the ordering effect of cholesterol. Tilt angle distribution of (B) the POPC headgroup, (C) the PI(4,5)P_2 headgroup, and (D) cholesterol. Angle is measured between the membrane normal and the vector shown in the subfigures. The headgroup orientation of neither POPC nor PI(4,5)P_2 is affected by cholesterol. Nevertheless, the tilt angle distribution of cholesterol is shifted towards smaller angles when increasing cholesterol concentration, thus showing more strict orientation of the cholesterol molecules in cholesterol-rich membranes.*

of POPC was found to be essentially independent of cholesterol concentration. A similar finding was made for the headgroup orientation of PI(4,5)P_2 (see Fig. 5.6C), whereas cholesterol molecules oriented more strongly along the membrane normal in a cholesterol-rich bilayer (see Fig. 5.6D). Although the POPC and PI(4,5)P_2 headgroup orientation is not affected by cholesterol, the exposure of the lipid headgroup can be switched, eventually leading to altered access for water and ligands.

To analyze the behavior of the lipid headgroups in more detail, hydrogen bonds between water and the lipid molecules (and their components) were calculated (see Fig. 5.7A,B). At lower cholesterol concentrations (0, 10, and 20 mol%) the number

of hydrogen bonds between water and lipids (PI(4,5)P_2 and POPC) was observed to be rather similar. However, at 35 mol%, the number of hydrogen bonds increased significantly for both lipids, thus indicating the lipids to be more exposed at high cholesterol concentrations. This result is supported by the solvent accessible surface area (SASA) data depicted in Fig. 5.7A,B, which shows a clear change at high cholesterol concentrations.

To further quantify the changes in the lipid bilayers of various cholesterol concentrations, the same analysis (number of hydrogen bonds and SASA) was done by dividing PI(4,5)P_2 and POPC molecules into four components; head, phosphate (PO_4), carbonyl, and tail regions (see Table 5.1). While the acyl chain region gets more compact in the cholesterol-rich membranes (in agreement with the order parameter data), the headgroup and the phosphate were found to have more interactions with water, thus demonstrating a more exposed headgroup presentation. Furthermore, although the carbonyl region has higher SASA and more contacts with water in the case of 35 mol% cholesterol, the number of hydrogen bonds stayed similar, or even decreased, especially with POPC. This may be due to the more packed environment of the acyl chains so that the water molecules do not have enough space to orient properly to form hydrogen bonds with the carbonyl oxygens. Further, the increased number of hydrogen bonds between water and cholesterol molecules and between the carbonyl groups and cholesterol may also disturb the hydrogen bonds from water to the carbonyl groups. Moreover, the deeper penetration of water can be seen as a tiny shift in the density profile of water towards the membrane interior (see Fig. 5.7C).

To conclude, the results show that although the lipid headgroup orientation is largely independent of the amount of cholesterol, with high cholesterol concentrations lipid headgroups are more exposed to water, thus supporting the idea of higher hydration in the headgroup, phosphate (PO_4), and carbonyl regions.

5.4.2 Coarse-Grained Simulations Highlight PLC δ1-PH Binding to Be Rapid, and to Favor Cholesterol-Rich Membranes

To study the binding properties of the PLC δ1-PH-domain to the PI(4,5)P_2 containing membranes in cholesterol-free and cholesterol-rich environments, we performed MD simulations in a multiscale manner (see Section 4.4). In all the systems, the protein

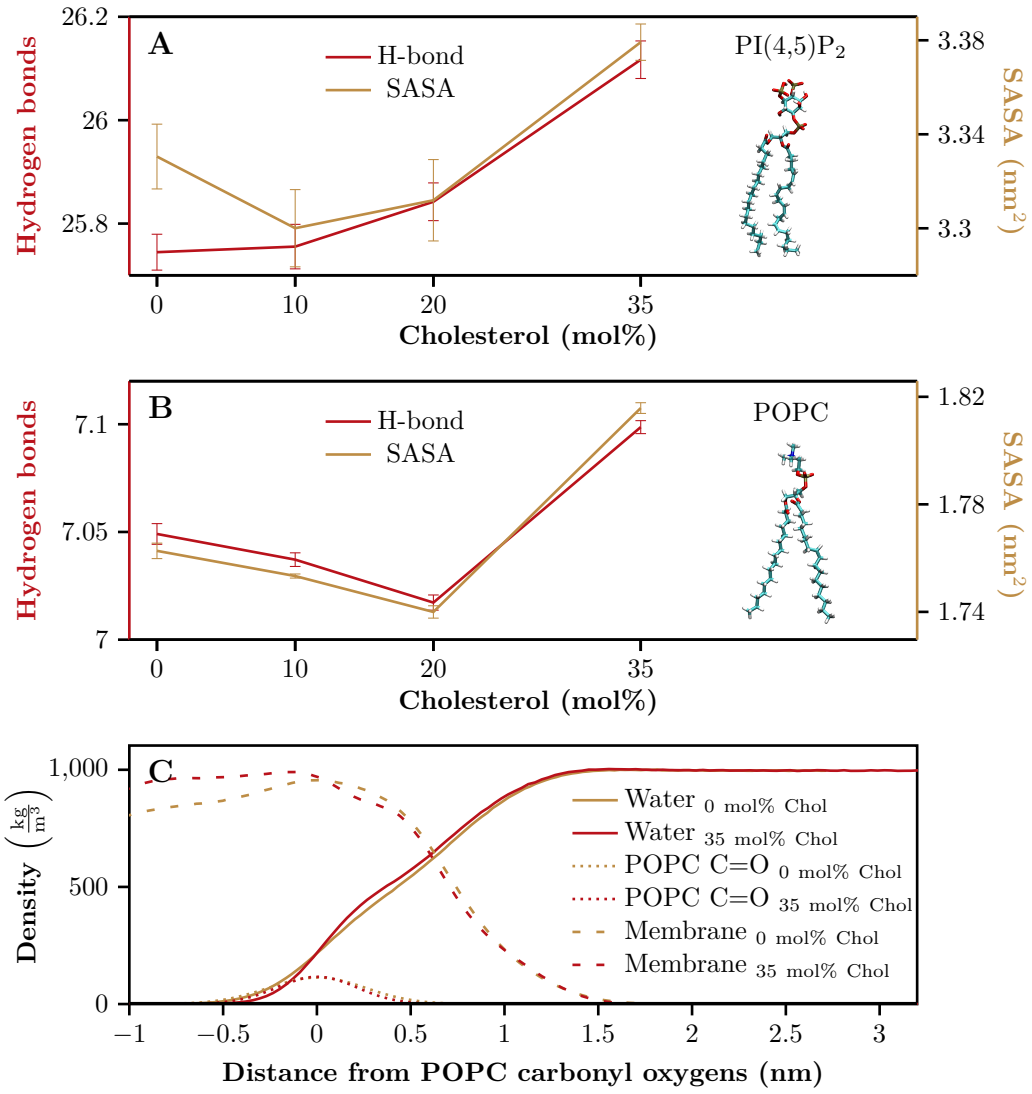

Figure 5.7 *Number of hydrogen bonds (red) between water and (A) PI(4,5)P_2 or (B) POPC as a function of cholesterol concentration. The number given here is per lipid. In the same graph, the solvent accessible surfaces area (SASA, brown) per lipid is shown. While the number of hydrogen bonds and SASA are roughly constant or decrease slightly with low cholesterol concentrations (up to 20 mol%), there is a significant increase in both quantities at high cholesterol concentration (35 mol%). A more detailed analysis (see Table 5.1), reveals that it is the headgroup and the phosphate groups that form more hydrogen bonds, and also the carbonyl region is observed to be more exposed to water in the cholesterol-rich membrane. (C) Density profiles (calculated symmetrically for the bilayer) for the simulated atomistic membranes. The distance is measured along the membrane normal and the zero position is set on the POPC carbonyl oxygens. The negative distance is towards the membrane interior and the positive distance towards the bulk water. Water penetrates deeper into the cholesterol-rich membrane (35 mol% cholesterol) as the density of the membrane decreases in the headgroup region when increasing cholesterol concentration.*

Table 5.1 *Number of hydrogen bonds per molecule between water and different components of the membrane. The first 400 ns of the simulation is considered as equilibrium time. Standard error for all the values is smaller than 0.05 and therefore not shown.*

	Chol concentration			
Component	0 mol%	10 mol%	20 mol%	35 mol%
PI(4,5)P_2	25.7	25.8	25.8	26.1
POPC	7.0	7.0	7.0	7.1
Chol	-	1.6	1.6	1.7
PI(4,5)P_2 head	19.5	19.5	19.6	19.7
PI(4,5)P_2 PO_4	4.3	4.3	4.3	4.5
PI(4,5)P_2 carbonyl	1.9	1.9	1.9	1.9
PI(4,5)P_2 chain	-	-	-	-
POPC head	-	-	-	-
POPC PO_4	5.3	5.3	5.3	5.3
POPC carbonyl	1.8	1.8	1.7	1.8
POPC chain	-	-	-	-

was observed to bind to the membrane during the first 300 ns of the simulation. Moreover, in all the systems a single PI(4,5)P_2 molecule was found to attach to the PLC δ1-PH-domain's PI(4,5)P_2 canonical binding site, which is expressed in the crystal structure [226] and also presented in other studies, such as *in silico* studies by Yamamoto et al. [257]. Thus, the present results are in good agreement with the previous studies. Once PI(4,5)P_2 found the canonical binding site, it did not leave the binding site during the course of the simulations.

To quantify how strong the protein binding is, the free energy of binding was calculated using the umbrella sampling method [227]. When the potential was set to zero in bulk water, the free energy minima for protein binding were obtained to be -76.6 kJ/mol and -87.6 kJ/mol for cholesterol concentrations of 0 and 35 mol%, in respective order (see Fig. 5.8). Furthermore, the position of the free energy minimum was obtained to shift (from 3.65 to 3.35 nm) towards the bilayer center in case of a cholesterol-rich membrane, demonstrating that PLC δ1-PH penetrates deeper into the lipid bilayer with high cholesterol concentrations.

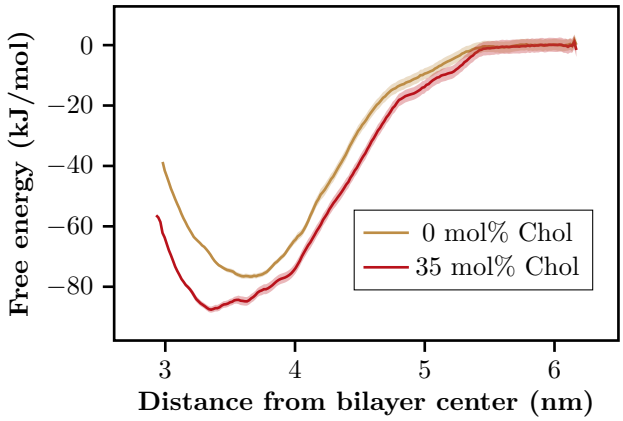

Figure 5.8 *The free energy profile for PLC δ1-PH binding along the membrane normal. The cholesterol-rich membrane presents a deeper free energy minimum, thus supporting the idea of stronger membrane binding with increasing cholesterol concentration.*

5.4.3 PLC Binding Is Enhanced by Interactions with Lipid Phosphate-Groups in Cholesterol-Rich Membranes

To understand the difference in protein binding, five atomistic replicas for each membrane using the CHARMM36 [161, 162] force field were simulated. As a result, PLC δ1-PH was found to remain bound to the membrane in all the fine-grained systems. In the systems where the protein was placed into bulk water, the protein bound quickly (in the first 300 ns) to the membrane surface, independent of the cholesterol concentration.

The probability to have a contact with a membrane, described separately for each protein residue, is depicted in Fig. 5.9. It reveals that the residues involved in the binding are similar in cholesterol-poor and cholesterol-rich systems. This suggests that the orientation of the membrane-bound PLC δ1-PH is not dependent on cholesterol concentration. Moreover, the PI(4,5)P_2 canonical binding site found in the β1/β2 loop is occupied almost all the time in both systems (see Fig. 5.9). As reported in the paper by Yamamoto et al. [257], in addition to the canonical PI(4,5)P_2 binding site, the PLC δ1-PH domain has strong interactions with PI(4,5)P_2 also with the β3/β4 loop that is next to the canonical binding site (see Fig. 5.9). Further, also the α2 unit that has been found to be involved in protein binding in previous solid-state NMR studies [258, 259] formed contacts with the simulated membranes almost all the time during the course of the simulations (the region illustrated in blue in Fig. 5.9). Although all the protein residues forming contacts in the cholesterol-free membrane

are also involved in the protein binding to the cholesterol-rich membrane, the residues 27 and 111 have a higher probability to make contacts with the membrane whose cholesterol concentration is high. Interestingly, these residues are next to each other (see Fig. 5.9). This suggests that there is a new binding mode (a slightly tilted protein orientation) in membranes with a high cholesterol concentration. Notably, the residues in the canonical binding site (β1/β2 loop) and in the β3/β4 loop are still involved in the binding.

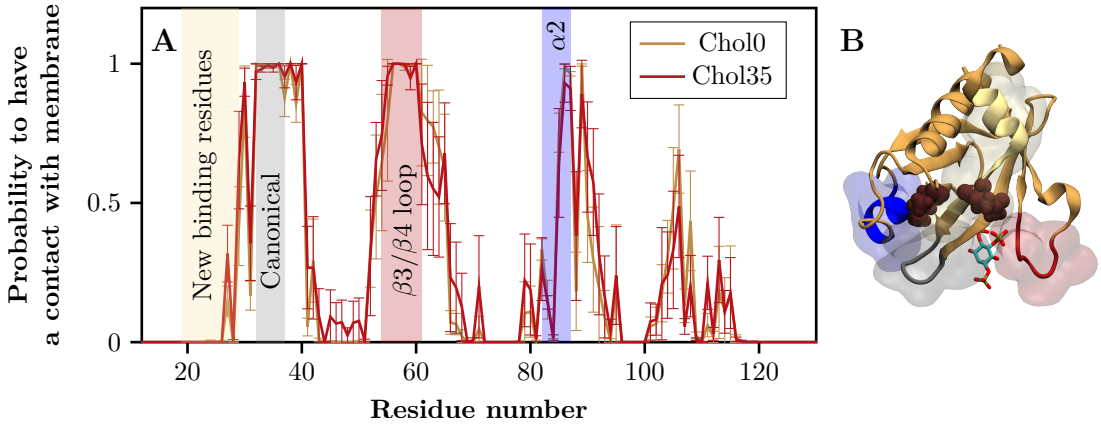

Figure 5.9 *(A) Probability to have a contact with a membrane as a function of the PLC δ1-PH residue number. Brown and red lines show the probability to have a contact with cholesterol-free and cholesterol-rich membranes, respectively. Average values are calculated using the data over a period of 400–1000 ns of all the five replicas, and the error bars given are standard errors. The known PI(4,5)P_2 canonical binding site (β1/β2 loop) is highlighted in gray. The other proposed PI(4,5)P_2 binding site for PLC δ1-PH (β3/β4 loop) is highlighted in red, and the α2-helix is highlighted in blue. (B) Illustrative picture of PLC δ1-PH showing the positions of the highlighted residues with transparent surfaces. The two residues (27 and 111) that have more contacts with a cholesterol-rich membrane are shown as dark-red van der Waals spheres. Moreover, the inositol ring presented in the crystal structure (pdb ID: 1MAI, [226]) is shown in licorice using the standard coloring scheme.*

The number of hydrogen bonds between PLC δ1-PH and the membrane was observed to be 22.6 and 25.3 in cholesterol-free and cholesterol-rich membranes, respectively (see Table. 5.2). The difference of 2.7 hydrogen bonds, favoring binding in membranes with high cholesterol concentration is in good agreement with the CG free energy results, as well as with the binding assay experiments done by our collaborator (data not shown). Interestingly, although the PLC δ1-PH is a known PI(4,5)P_2 lipid sensor, the increased number of H-bonds in a cholesterol-rich membrane was formed mainly by POPC (63%). Moreover, when the lipids were divided into four components (see Table 5.2) and hydrogen bonds between the protein and lipid components were

analyzed, the phosphate group region (PO_4 from both $PI(4,5)P_2$ and POPC) was found to form 2.37 hydrogen bonds more in the cholesterol-rich membrane, thus corresponding to 88% of the total change.

Table 5.2 *Number of hydrogen bonds between PLC δ1-PH and each component of the membrane. Notably, the number of hydrogen bonds increases by 2.7 bonds from a cholesterol-free to a cholesterol-rich membrane and is mainly due to the POPC and PI(4,5)P_2 backbone phosphate groups (88% of the total change). The values given are calculated over all the 5 replicas, using the simulation time 400-1000 ns for analysis. Error shown is standard error.*

Component	0 mol% Chol	35 mol% Chol
Membrane	22.56 ± 0.78	25.27 ± 1.10
$PI(4,5)P_2$	19.22 ± 0.77	20.03 ± 1.36
POPC	3.34 ± 0.64	5.05 ± 1.11
Chol	-	0.18 ± 0.06
$PI(4,5)P_2$ head	18.68 ± 0.59	18.68 ± 1.45
$PI(4,5)P_2$ backbone PO_4	0.52 ± 0.20	1.30 ± 0.68
$PI(4,5)P_2$ carbonyl	0.02 ± 0.01	0.05 ± 0.03
$PI(4,5)P_2$ acyl chains	0	0
POPC head	0	0
POPC PO_4	3.18 ± 0.63	4.77 ± 1.04
POPC carbonyl	0.17 ± 0.02	0.28 ± 0.09
POPC acyl chains	0	0

5.4.4 Conclusions

To conclude, in CG umbrella sampling simulations it was shown that the free energy of binding of PLC δ1-PH to the membrane is about 10 kJ/mol stronger in cholesterol-rich membranes in comparison to cholesterol-free bilayers. In the fine-grained atomistic systems, it was shown that the difference in the free energy of binding is coupled to an increase of 2.7 hydrogen bonds between the lipids and the protein. Interestingly, it is not only $PI(4,5)P_2$ that forms more hydrogen bonds with its lipid sensor PLC δ1-PH, but also POPC. The role of POPC is even more significant in cholesterol-free membranes. Although most of the hydrogen bonds between the protein and the membrane are formed with the $PI(4,5)P_2$ inositol group, the largest contribution to the observed increase in the number of hydrogen bonds in cholesterol-rich membranes in comparison to cholesterol-free bilayers comes from the phosphate (PO_4) group in both $PI(4,5)P_2$ and POPC. Moreover, although some

hydrogen bonds were formed between the protein and the carbonyl groups of the lipids, their number is minor compared to the headgroup and PO_4 components. The larger ability to form hydrogen bonds between PLC δ1-PH and cholesterol-rich bilayer is attributed to the looser packing in the membrane headgroup region. Essentially this leads to more exposed lipid headgroups, deeper penetration of PLC δ1-PH, and a stronger protein binding to the cholesterol-rich membrane.

6. CONCLUSIONS

The structure and the dynamical properties of lipid receptors are challenging to study using experimental methods. This is primarily due to the small size and the dynamic nature of lipid molecules. Molecular dynamics simulations can offer added value to biomolecular experiments by providing atomic-scale explanations for phenomena unreachable by experiments. In this Thesis, MD simulations were employed to study specific lipid–protein interactions and properties of two lipid receptors, GM1 and $PI(4,5)P_2$.

First, the joint action of $PI(4,5)P_2$ and talin in integrin activation was demonstrated. In the presence of talin, integrin stability was impaired by hindering the salt bridge in the inner membrane clasp of the transmembrane receptor. Importantly, $PI(4,5)P_2$ alone was not observed to interfere with integrin stability. Instead, the presence of talin was also required for $PI(4,5)P_2$ molecules to interact directly with the salt bridge and to eventually break it.

GM1 is a default lipid marker for nanoscale liquid-ordered membrane domains [4, 240, 241, 242, 243]. Nevertheless, in the previous study by Sezgin et al. [4], CTxB was found to bind to GM1 exclusively in the liquid-disordered phase of the phase separated system, when the acyl chain-BODIPY labeled analog of GM1 was used. Our objective was to study the molecular details leading to the aforementioned behavior of (bd)GM1 and cholera toxin. Through atomistic simulations, the conformation of the GM1 headgroup was observed to be similar, regardless of the lipid environment or the presence of the fluorescent label. This was further complemented by experimental measurements that showed similar binding affinities of CTxB to the vesicles mimicking L_d and L_o phases. This leads us to conclude that other properties than structural changes, such as clustering and partitioning, play a major role in the binding of CTxB. Nevertheless, the properties of GM1 and bdGM1 were clearly different from each other.

Concerning the natural compounds present in eukaryotic cells, the effects of Ca^{2+} and

cholesterol were explored in lipid bilayers with $PI(4,5)P_2$. Here, we showed in atomic detail the switched conformation of the $PI(4,5)P_2$ headgroup controlled by Ca^{2+} ions, eventually leading to the inhibited $PI(4,5)P_2$ ligand binding. Importantly, these results offer molecular details for the negative feedback loop in cell signaling. Without calcium, PLC binds to $PI(4,5)P_2$, leading to a release of Ca^{2+} to the cytosol. Again, the increased calcium concentration tilts the $PI(4,5)P_2$ headgroup and consequently inhibits new PLC ligand binding. On the other hand, the presence of cholesterol was found to enhance PLC binding to $PI(4,5)P_2$ membranes by increasing the exposure of the phosphate region of lipids to water. Because cholesterol concentration in the plasma membrane is high, these results offer one explanation for the question of why certain proteins bind to $PI(4,5)P_2$ only in the plasma membrane but not in the other cell compartments. These results indicate the sensitive nature of lipid receptors and reveal new insights on the cell signaling regulatory machinery.

To summarize, three key take-home messages can be concluded from the results presented in this Thesis. First, the usage of fluorescent probes in experimental studies can be complicated. The attachment of BODIPY to a GM1 acyl chain can alter functional properties of the GM1 receptor even without significantly changing the lipid orientation. Hence, great care needs to be taken when designing and interpreting results from fluorescent studies. Second, lipid receptors can be extremely sensitive. For instance, $PI(4,5)P_2$ that is present in the inner plasma membrane was found to switch its conformation based on the varying cytosolic Ca^{2+} concentration, also affecting the ligand binding. Third, molecular dynamics simulations have proven to be a useful tool to study biomolecular systems and to complement related experimental findings.

Several ideas for further studies arise from the results. First, the partitioning of GM1 (or bdGM1) to different phases was not studied by atomic-level simulations. This task is challenging but doable. Notably, in phase separated systems the part of the membrane mimicking the liquid-ordered phase is problematic due to slow lipid diffusion that calls for long simulation times to sample the lipid movements adequately. Next, the effect of enhanced receptor binding to cholesterol-rich membranes raises a question of the role of lipid acyl chains. Cholesterol affects the acyl chain region, e.g., by increasing acyl chain order, and therefore different lipid chains could potentially alter the cholesterol-induced effects. This topic remains elusive and requires further investigation. Finally, while using various parameter sets for biomolecular simulations, the development of the force fields is of particular importance. Continually increasing

computer capacity allows longer simulations and larger system sizes, and therefore the importance of accurate models becomes more and more crucial.

REFERENCES

[1] R. Zaidel-Bar, S. Itzkovitz, A. Ma'ayan, R. Iyengar, and B. Geiger, "Functional Atlas of the Integrin Adhesome", *Nature Cell Biology*, vol. 9, no. 8, p. 858, 2007.

[2] D. A. Calderwood, R. Zent, R. Grant, D. J. G. Rees, R. O. Hynes, and M. H. Ginsberg, "The Talin Head Domain Binds to Integrin β Subunit Cytoplasmic Tails and Regulates Integrin Activation", *Journal of Biological Chemistry*, vol. 274, no. 40, pp. 28 071–28 074, 1999.

[3] S. Tadokoro, S. J. Shattil, K. Eto, V. Tai, R. C. Liddington, J. M. de Pereda, M. H. Ginsberg, and D. A. Calderwood, "Talin Binding to Integrin β Tails: A Final Common Step in Integrin Activation", *Science*, vol. 302, no. 5642, pp. 103–106, 2003.

[4] E. Sezgin, I. Levental, M. Grzybek, G. Schwarzmann, V. Mueller, A. Honigmann, V. N. Belov, C. Eggeling, Ü. Coskun, K. Simons, and P. Schwille, "Partitioning, Diffusion, and Ligand Binding of Raft Lipid Analogs in Model and Cellular Plasma Membranes", *Biochimica et Biophysica Acta (BBA)-Biomembranes*, vol. 1818, no. 7, pp. 1777–1784, 2012.

[5] C. Cui, R. Merritt, L. Fu, and Z. Pan, "Targeting Calcium Signaling in Cancer Therapy", *Acta Pharmaceutica Sinica B*, vol. 7, no. 1, pp. 3–17, 2017.

[6] J. W. Putney and T. Tomita, "Phospholipase C Signaling and Calcium Influx", *Advances in Biological Regulation*, vol. 52, no. 1, p. 152, 2012.

[7] M. A. De Matteis, A. Di Campli, and A. Godi, "The Role of the Phosphoinositides at the Golgi Complex", *Biochimica et Biophysica Acta (BBA)-Molecular Cell Research*, vol. 1744, no. 3, pp. 396–405, 2005.

[8] G. Di Paolo and P. De Camilli, "Phosphoinositides in Cell Regulation and Membrane Dynamics", *Nature*, vol. 443, no. 7112, p. 651, 2006.

[9] T. Balla and P. Várnai, "Visualizing Cellular Phosphoinositide Pools With GFP-fused Protein-Modules", *Science's STKE*, vol. 2002, no. 125, pl3–pl3, 2002.

[10] L. Liscum and N. J. Munn, "Intracellular Cholesterol Transport", *Biochimica et Biophysica Acta (BBA)-Molecular and Cell Biology of Lipids*, vol. 1438, no. 1, pp. 19–37, 1999.

[11] L. Kalvodova, J. L. Sampaio, S. Cordo, C. S. Ejsing, A. Shevchenko, and K. Simons, "The Lipidomes of Vesicular Stomatitis Virus, Semliki Forest Virus, and the Host Plasma Membrane Analyzed by Quantitative Shotgun Mass Spectrometry", *Journal of Virology*, vol. 83, no. 16, pp. 7996–8003, 2009.

[12] M. T. Nakamura, B. E. Yudell, and J. J. Loor, "Regulation of Energy Metabolism by Long-Chain Fatty Acids", *Progress in Lipid Research*, vol. 53, pp. 124–144, 2014.

[13] T. Shimizu, "Lipid Mediators in Health and Disease: Enzymes and Receptors as Therapeutic Targets for the Regulation of Immunity and Inflammation", *Annual Review of Pharmacology and Toxicology*, vol. 49, pp. 123–150, 2009.

[14] M. D. Resh, "Fatty Acylation of Proteins: The Long and the Short of It", *Progress in Lipid Research*, vol. 63, pp. 120–131, 2016.

[15] G. Van Meer, D. R. Voelker, and G. W. Feigenson, "Membrane Lipids: Where They Are and How They Behave", *Nature Reviews Molecular Cell Biology*, vol. 9, no. 2, p. 112, 2008.

[16] A.-E. Saliba, I. Vonkova, and A.-C. Gavin, "The Systematic Analysis of Protein–Lipid Interactions Comes of Age", *Nature Reviews Molecular Cell Biology*, vol. 16, no. 12, p. 753, 2015.

[17] O. Quehenberger, A. M. Armando, A. H. Brown, S. B. Milne, D. S. Myers, A. H. Merrill, S. Bandyopadhyay, K. N. Jones, S. Kelly, R. L. Shaner, C. M. Sullards, E. Wang, R. C. Murphy, R. M. Barkley, T. J. Leiker, C. R. H. Raetz, Z. Guan, G. M. Laird, D. A. Six, D. W. Russel, J. G. McDonald, S. Subramaniam, E. Fahy, and E. A. Dennis, "Lipidomics Reveals a Remarkable Diversity of Lipids in Human Plasma", *Journal of Lipid Research*, vol. 51, no. 11, pp. 3299–3305, 2010.

[18] S. Kolay, U. Basu, and P. Raghu, "Control of Diverse Subcellular Processes by a Single Multi-Functional Lipid Phosphatidylinositol 4, 5-bisphosphate [PI(4,5)P2]", *Biochemical Journal*, vol. 473, no. 12, pp. 1681–1692, 2016.

[19] A. Yamashita, Y. Hayashi, Y. Nemoto-Sasaki, M. Ito, S. Oka, T. Tanikawa, K. Waku, and T. Sugiura, "Acyltransferases and Transacylases That Determine the Fatty Acid Composition of Glycerolipids and the Metabolism of Bioactive Lipid Mediators in Mammalian Cells and Model Organisms", *Progress in Lipid Research*, vol. 53, pp. 18–81, 2014.

[20] G. van Meer and Q. Lisman, "Sphingolipid Transport: Rafts and Translocators", *Journal of Biological Chemistry*, vol. 277, no. 29, pp. 25 855–25 858, 2002.

[21] S. Grösch, S. Schiffmann, and G. Geisslinger, "Chain Length-Specific Properties of Ceramides", *Progress in Lipid Research*, vol. 51, no. 1, pp. 50–62, 2012.

[22] S.-T. Yang, A. J. Kreutzberger, J. Lee, V. Kiessling, and L. K. Tamm, "The Role of Cholesterol in Membrane Fusion", *Chemistry and Physics of Lipids*, vol. 199, pp. 136–143, 2016.

[23] F. Maxfield and M. Mondal, "Sterol and Lipid Trafficking in Mammalian Cells", *Biochemical Society Transactions*, vol. 34, no. 3, pp. 335–339, 2006.

[24] D. Marquardt, B. Geier, and G. Pabst, "Asymmetric Lipid Membranes: Towards More Realistic Model Systems", *Membranes*, vol. 5, no. 2, pp. 180–196, 2015.

[25] S.-L. Liu, R. Sheng, J. H. Jung, L. Wang, E. Stec, M. J. O'Connor, S. Song, R. K. Bikkavilli, R. A. Winn, D. Lee, K. Baek, K. Ueda, I. Levitan, K.-P. Kim, and W. Cho, "Orthogonal Lipid Sensors Identify Transbilayer Asymmetry of Plasma Membrane Cholesterol", *Nature Chemical Biology*, vol. 13, no. 3, p. 268, 2017.

[26] W. Humphrey, A. Dalke, and K. Schulten, "VMD: Visual Molecular Dynamics", *Journal of Molecular Graphics*, vol. 14, no. 1, pp. 33–38, 1996.

[27] J. Stone, "An efficient library for parallel ray tracing and animation", Master's thesis, Computer Science Department, University of Missouri-Rolla, Apr. 1998.

[28] B. Payrastre, K. Missy, S. Giuriato, S. Bodin, M. Plantavid, and M.-P. Gratacap, "Phosphoinositides: Key Players in Cell Signalling, in Time and Space", *Cellular Signalling*, vol. 13, no. 6, pp. 377–387, 2001.

[29] S. Desrivières, F. T. Cooke, P. J. Parker, and M. N. Hall, "MSS4, a Phosphatidylinositol-4-phosphate 5-Kinase Required for Organization of the Actin Cytoskeleton in Saccharomyces Cerevisiae", *Journal of Biological Chemistry*, vol. 273, no. 25, pp. 15 787–15 793, 1998.

[30] S. L. Osborne, C. L. Thomas, S. Gschmeissner, and G. Schiavo, "Nuclear PtdIns(4,5)P2 Assembles in a Mitotically Regulated Particle Involved in Pre-mRNA Splicing", *Journal of Cell Science*, vol. 114, no. 13, pp. 2501–2511, 2001.

[31] H. Ishihara, Y. Shibasaki, N. Kizuki, T. Wada, Y. Yazaki, T. Asano, and Y. Oka, "Type I Phosphatidylinositol-4-phosphate 5-Kinases Cloning of the Third Isoform and Deletion/Substitution Analysis of Members of This Novel Lipid Kinase Family", *Journal of Biological Chemistry*, vol. 273, no. 15, pp. 8741–8748, 1998.

[32] M. W. Bunce, I. V. Boronenkov, and R. A. Anderson, "Coordinated Activation of the Nuclear Ubiquitin Ligase Cul3-Spop by the Generation of Phosphatidylinositol 5-Phosphate", *Journal of Biological Chemistry*, vol. 283, no. 13, pp. 8678–8686, 2008.

[33] J. H. Clarke, P. C. Emson, and R. F. Irvine, "Localization of Phosphatidylinositol Phosphate Kinase IIγ in Kidney to a Membrane Trafficking Compartment Within Specialized Cells of the Nephron", *American Journal of Physiology-Renal Physiology*, vol. 295, no. 5, F1422–F1430, 2008.

[34] Y. Liu and V. A. Bankaitis, "Phosphoinositide Phosphatases in Cell Biology and Disease", *Progress in Lipid Research*, vol. 49, no. 3, pp. 201–217, 2010.

[35] T. Harayama and H. Riezman, "Understanding the Diversity of Membrane Lipid Composition", *Nature Reviews Molecular Cell Biology*, vol. 19, pp. 281–296, 2018.

[36] A. J. Marcus, H. L. Ullman, and L. B. Safier, "Lipid Composition of Subcellular Particles of Human Blood Platelets", *Journal of Lipid Research*, vol. 10, no. 1, pp. 108–114, 1969.

[37] T. Itoh and T. Takenawa, "Phosphoinositide-Binding Domains: Functional Units for Temporal and Spatial Regulation of Intracellular Signalling", *Cellular Signalling*, vol. 14, no. 9, pp. 733–743, 2002.

[38] J.-O. De Craene, R. Ripp, O. Lecompte, J. D. Thompson, O. Poch, and S. Friant, "Evolutionary Analysis of the ENTH/ANTH/VHS Protein Superfamily Reveals a Coevolution Between Membrane Trafficking and Metabolism", *BMC Genomics*, vol. 13, no. 1, p. 297, 2012.

[39] M. E. Taylor and K. Drickamer, *Introduction to Glycobiology*. Oxford university press, 2011.

[40] Y. D. Vankar and R. R. Schmidt, "Chemistry of Glycosphingolipids–Carbohydrate Molecules of Biological Significance", *Chemical Society Reviews*, vol. 29, no. 3, pp. 201–216, 2000.

[41] R. W. Ledeen and K. Y. Robert, "Gangliosides: Structure, Isolation, and Analysis", in *Methods in Enzymology*, vol. 83, Elsevier, 1982, pp. 139–191.

[42] R. W. Ledeen, G. Wu, Z.-H. Lu, D. Kozireski-Chuback, and Y. Fang, "The Role of GM1 and Other Gangliosides in Neuronal Differentiation Overview and New Findings", *Annals of the New York Academy of Sciences*, vol. 845, no. 1, pp. 161–175, 1998.

[43] R. L. Schnaar, R. Gerardy-Schahn, and H. Hildebrandt, "Sialic Acids in the Brain: Gangliosides and Polysialic Acid in Nervous System Development, Stability, Disease, and Regeneration", *Physiological Reviews*, vol. 94, no. 2, pp. 461–518, 2014.

[44] A. Leon, L. Facci, G. Toffano, S. Sonnino, and G. Tettamanti, "Activation of (Na+, K+)-ATPase by Nanomolar Concentrations of GM1 Ganglioside", *Journal of Neurochemistry*, vol. 37, no. 2, pp. 350–357, 1981.

[45] G. Wu and R. W. Ledeen, "Stimulation of Neurite Outgrowth in Neuroblastoma Cells by Neuraminidase: Putative Role of GM1 Ganglioside in Differentiation", *Journal of Neurochemistry*, vol. 56, no. 1, pp. 95–104, 1991.

[46] J. Wang, Z.-H. Lu, H.-J. Gabius, C. Rohowsky-Kochan, R. W. Ledeen, and G. Wu, "Cross-Linking of GM1 Ganglioside by Galectin-1 Mediates Regulatory T Cell Activity Involving TRPC5 Channel Activation: Possible Role in Suppressing Experimental Autoimmune Encephalomyelitis", *The Journal of Immunology*, vol. 182, no. 7, pp. 4036–4045, 2009.

[47] G. Wu, Z.-H. Lu, H.-J. Gabius, R. W. Ledeen, and D. Bleich, "Ganglioside GM1 Deficiency in Effector T Cells From NOD Mice Induces Resistance to Regulatory T-Cell Suppression", *Diabetes*, vol. 60, no. 9, pp. 2341–2349, 2011.

[48] S. Sonnino, L. Mauri, V. Chigorno, and A. Prinetti, "Gangliosides as Components of Lipid Membrane Domains", *Glycobiology*, vol. 17, no. 1, 1R–13R, 2006.

[49] R. W. Ledeen and G. Wu, "The Multi-Tasked Life of GM1 Ganglioside, a True Factotum of Nature", *Trends in Biochemical Sciences*, vol. 40, no. 7, pp. 407–418, 2015.

[50] E. A. Merritt, P. Kuhn, S. Sarfaty, J. L. Erbe, R. K. Holmes, and W. G. Hol, "The 1.25 Å Resolution Refinement of the Cholera Toxin B-Pentamer: Evidence of Peptide Backbone Strain at the Receptor-Binding Site", *Journal of Molecular Biology*, vol. 282, no. 5, pp. 1043–1059, 1998.

[51] A. Schoen and E. Freire, "Thermodynamics of Intersubunit Interactions in Cholera Toxin Upon Binding to the Oligosaccharide Portion of Its Cell Surface Receptor, Ganglioside GM1", *Biochemistry*, vol. 28, no. 12, pp. 5019–5024, 1989.

[52] W. B. Turnbull, B. L. Precious, and S. W. Homans, "Dissecting the Cholera Toxin–Ganglioside GM1 Interaction by Isothermal Titration Calorimetry", *Journal of the American Chemical Society*, vol. 126, no. 4, pp. 1047–1054, 2004.

[53] G. Pabst, N. Kučerka, M.-P. Nieh, and J. Katsaras, *Liposomes, Lipid Bilayers and Model Membranes: From Basic Research to Application*. CRC Press, 2014.

[54] J. D. Robertson, "The Ultrastructure of Cell Membranes and Their Derivatives", in *Biochemical Society Symposium*, vol. 16, 1959, p. 3.

[55] J. Lenard and S. Singer, "Protein Conformation in Cell Membrane Preparations as Studied by Optical Rotatory Dispersion and Circular Dichroism", *Proceedings of the National Academy of Sciences*, vol. 56, no. 6, pp. 1828–1835, 1966.

[56] S. J. Singer and G. L. Nicolson, "The Fluid Mosaic Model of the Structure of Cell Membranes", *Science*, vol. 175, no. 4023, pp. 720–731, 1972.

[57] G. L. Nicolson, "The Fluid–Mosaic Model of Membrane Structure: Still Relevant to Understanding the Structure, Function and Dynamics of Biological Membranes After More Than 40 Years", *Biochimica et Biophysica Acta (BBA)-Biomembranes*, vol. 1838, no. 6, pp. 1451–1466, 2014.

[58] K. Simons and E. Ikonen, "Functional Rafts in Cell Membranes", *Nature*, vol. 387, no. 6633, p. 569, 1997.

[59] K. Simons and D. Toomre, "Lipid Rafts and Signal Transduction", *Nature Reviews Molecular Cell Biology*, vol. 1, no. 1, p. 31, 2000.

[60] D. Lingwood and K. Simons, "Lipid Rafts as a Membrane-Organizing Principle", *Science*, vol. 327, no. 5961, pp. 46–50, 2010.

[61] E. Sezgin, I. Levental, S. Mayor, and C. Eggeling, "The Mystery of Membrane Organization: Composition, Regulation and Roles of Lipid Rafts", *Nature Reviews Molecular Cell Biology*, vol. 18, no. 6, p. 361, 2017.

[62] J. T. Hannich, D. Mellal, S. Feng, A. Zumbuehl, and H. Riezman, "Structure and Conserved Function of Iso-Branched Sphingoid Bases From the Nematode Caenorhabditis Elegans", *Chemical Science*, vol. 8, no. 5, pp. 3676–3686, 2017.

[63] T. Harayama, M. Eto, H. Shindou, Y. Kita, E. Otsubo, D. Hishikawa, S. Ishii, K. Sakimura, M. Mishina, and T. Shimizu, "Lysophospholipid Acyltransferases Mediate Phosphatidylcholine Diversification to Achieve the Physical Properties Required in Vivo", *Cell Metabolism*, vol. 20, no. 2, pp. 295–305, 2014.

[64] B. Antonny, S. Vanni, H. Shindou, and T. Ferreira, "From Zero to Six Double Bonds: Phospholipid Unsaturation and Organelle Function", *Trends in Cell Biology*, vol. 25, no. 7, pp. 427–436, 2015.

[65] A. A. Spector and M. A. Yorek, "Membrane Lipid Composition and Cellular Function.", *Journal of Lipid Research*, vol. 26, no. 9, pp. 1015–1035, 1985.

[66] E. Zinser, C. Sperka-Gottlieb, E.-V. Fasch, S. D. Kohlwein, F. Paltauf, and G. Daum, "Phospholipid Synthesis and Lipid Composition of Subcellular Membranes in the Unicellular Eukaryote Saccharomyces Cerevisiae.", *Journal of Bacteriology*, vol. 173, no. 6, pp. 2026–2034, 1991.

[67] F. Lamari, F. Mochel, F. Sedel, and J. Saudubray, "Disorders of Phospholipids, Sphingolipids and Fatty Acids Biosynthesis: Toward a New Category of Inherited Metabolic Diseases", *Journal of Inherited Metabolic Disease*, vol. 36, no. 3, pp. 411–425, 2013.

[68] L. Wigger, C. Cruciani-Guglielmacci, A. Nicolas, J. Denom, N. Fernandez, F. Fumeron, P. Marques-Vidal, A. Ktorza, W. Kramer, A. Schulte, H. L. Stunff, R. Liechti, I. Xenarios, P. Vollenweider, G. Waeber, I. Uphues, R. Roussel, C. Magnan, and B. Thorens, "Plasma Dihydroceramides Are Diabetes Susceptibility Biomarker Candidates in Mice and Humans", *Cell Reports*, vol. 18, no. 9, pp. 2269–2279, 2017.

[69] G. J. Gaspard and C. R. McMaster, "Cardiolipin Metabolism and Its Causal Role in the Etiology of the Inherited Cardiomyopathy Barth Syndrome", *Chemistry and Physics of Lipids*, vol. 193, pp. 1–10, 2015.

[70] C. Bissig and J. Gruenberg, "Lipid Sorting and Multivesicular Endosome Biogenesis", *Cold Spring Harbor Perspectives in Biology*, vol. 5, no. 10, a016816, 2013.

[71] J. Chevallier, Z. Chamoun, G. Jiang, G. Prestwich, N. Sakai, S. Matile, R. G. Parton, and J. Gruenberg, "Lysobisphosphatidic Acid Controls Endosomal Cholesterol Levels", *Journal of Biological Chemistry*, vol. 283, no. 41, pp. 27 871–27 880, 2008.

[72] R. Ernst, C. S. Ejsing, and B. Antonny, "Homeoviscous Adaptation and the Regulation of Membrane Lipids", *Journal of Molecular Biology*, vol. 428, no. 24, pp. 4776–4791, 2016.

[73] A. Pagliuso, C. Valente, L. L. Giordano, A. Filograna, G. Li, D. Circolo, G. Turacchio, V. M. Marzullo, L. Mandrich, M. A. Zhukovsky, F. Fromiggini, R. S. Polishchuk, D. Corda, and A. Luini, "Golgi Membrane Fission Requires the CtBP1-S/BARS-induced Activation of Lysophosphatidic Acid Acyltransferase δ", *Nature Communications*, vol. 7, p. 12 148, 2016.

[74] M. Zick, C. Stroupe, A. Orr, D. Douville, and W. T. Wickner, "Membranes Linked by Trans-Snare Complexes Require Lipids Prone to Non-Bilayer Structure for Progression to Fusion", *eLIFE*, vol. 3, 2014.

[75] J. B. de la Serna, J. Perez-Gil, A. C. Simonsen, and L. A. Bagatolli, "Cholesterol Rules Direct Observation of the Coexistence of Two Fluid Phases in Native Pulmonary Surfactant Membranes at Physiological Temperatures", *Journal of Biological Chemistry*, vol. 279, no. 39, pp. 40 715–40 722, 2004.

[76] T. Baumgart, A. T. Hammond, P. Sengupta, S. T. Hess, D. A. Holowka, B. A. Baird, and W. W. Webb, "Large-Scale Fluid/Fluid Phase Separation of Proteins and Lipids in Giant Plasma Membrane Vesicles", *Proceedings of the National Academy of Sciences*, vol. 104, no. 9, pp. 3165–3170, 2007.

[77] I.-H. Lee, S. Saha, A. Polley, H. Huang, S. Mayor, M. Rao, and J. T. Groves, "Live Cell Plasma Membranes Do Not Exhibit a Miscibility Phase Transition Over a Wide Range of Temperatures", *The Journal of Physical Chemistry B*, vol. 119, no. 12, pp. 4450–4459, 2015.

[78] S. P. Rayermann, G. E. Rayermann, C. E. Cornell, A. J. Merz, and S. L. Keller, "Hallmarks of Reversible Separation of Living, Unperturbed Cell Membranes into Two Liquid Phases", *Biophysical Journal*, vol. 113, no. 11, pp. 2425–2432, 2017.

[79] D. L. Daleke, "Phospholipid Flippases", *Journal of Biological Chemistry*, vol. 282, no. 2, pp. 821–825, 2007.

[80] P. F. Devaux and R. Morris, "Transmembrane Asymmetry and Lateral Domains in Biological Membranes", *Traffic*, vol. 5, no. 4, pp. 241–246, 2004.

[81] J. Suzuki, D. P. Denning, E. Imanishi, H. R. Horvitz, and S. Nagata, "Xk-Related Protein 8 and CED-8 Promote Phosphatidylserine Exposure in Apoptotic Cells", *Science*, vol. 341, no. 6144, pp. 403–406, 2013.

[82] T. C. Anglin, J. Liu, and J. C. Conboy, "Facile Lipid Flip-Flop in a Phospholipid Bilayer Induced by Gramicidin a Measured by Sum-Frequency Vibrational Spectroscopy", *Biophysical Journal*, vol. 92, no. 1, pp. L01–L03, 2007.

[83] A. Papadopulos, S. Vehring, I. López-Montero, L. Kutschenko, M. Stöckl, P. F. Devaux, M. Kozlov, T. Pomorski, and A. Herrmann, "Flippase Activity Detected With Unlabeled Lipids by Shape Changes of Giant Unilamellar Vesicles", *Journal of Biological Chemistry*, vol. 282, no. 21, pp. 15 559–15 568, 2007.

[84] S. J. Marrink, A. H. de Vries, T. A. Harroun, J. Katsaras, and S. R. Wassall, "Cholesterol Shows Preference for the Interior of Polyunsaturated Lipid Membranes", *Journal of the American Chemical Society*, vol. 130, no. 1, pp. 10–11, 2008.

[85] R. Raghupathy, A. A. Anilkumar, A. Polley, P. P. Singh, M. Yadav, C. Johnson, S. Suryawanshi, V. Saikam, S. D. Sawant, A. Panda, Z. Guo, R. A. Vishwakarma, M. Rao, and S. Mayor, "Transbilayer Lipid Interactions Mediate Nanoclustering of Lipid-Anchored Proteins", *Cell*, vol. 161, no. 3, pp. 581–594, 2015.

[86] E. Oldfield and D. Chapman, "Effects of Cholesterol and Cholesterol Derivatives on Hydrocarbon Chain Mobility in Lipids", *Biochemical and Biophysical Research Communications*, vol. 43, no. 3, pp. 610–616, 1971.

[87] R. A. Haberkorn, R. G. Griffin, M. D. Meadows, and E. Oldfield, "Deuterium Nuclear Magnetic Resonance Investigation of the Dipalmitoyl Lecithin-Cholesterol-Water System", *Journal of the American Chemical Society*, vol. 99, no. 22, pp. 7353–7355, 1977.

[88] H. I. Petrache, D. Harries, and V. A. Parsegian, "Alteration of Lipid Membrane Rigidity by Cholesterol and Its Metabolic Precursors", in *Macromolecular Symposia*, Wiley Online Library, vol. 219, 2005, pp. 39–50.

[89] M. El-Sayed, T. Guion, and M. Fayer, "Effect of Cholesterol on Viscoelastic Properties of Dipalmitoylphosphatidylcholine Multibilayers as Measured by a Laser-Induced Ultrasonic Probe", *Biochemistry*, vol. 25, no. 17, pp. 4825–4832, 1986.

[90] R. Bittman, S. Clejan, S. Lund-Katz, and M. C. Phillips, "Influence of Cholesterol on Bilayers of Ester-And Ether-Linked Phospholipids Permeability and 13c-Nuclear Magnetic Resonance Measurements", *Biochimica et Biophysica Acta (BBA)-Biomembranes*, vol. 772, no. 2, pp. 117–126, 1984.

[91] J. Rubenstein, B. A. Smith, and H. M. McConnell, "Lateral Diffusion in Binary Mixtures of Cholesterol and Phosphatidylcholines", *Proceedings of the National Academy of Sciences*, vol. 76, no. 1, pp. 15–18, 1979.

[92] N. Kahya, D. Scherfeld, K. Bacia, B. Poolman, and P. Schwille, "Probing Lipid Mobility of Raft-Exhibiting Model Membranes by Fluorescence Correlation Spectroscopy", *Journal of Biological Chemistry*, vol. 278, no. 30, pp. 28 109–28 115, 2003.

[93] J. M. Crane and L. K. Tamm, "Role of Cholesterol in the Formation and Nature of Lipid Rafts in Planar and Spherical Model Membranes", *Biophysical Journal*, vol. 86, no. 5, pp. 2965–2979, 2004.

[94] Z. Chen and R. Rand, "The Influence of Cholesterol on Phospholipid Membrane Curvature and Bending Elasticity", *Biophysical Journal*, vol. 73, no. 1, pp. 267–276, 1997.

[95] L. Yang and H. W. Huang, "Observation of a Membrane Fusion Intermediate Structure", *Science*, vol. 297, no. 5588, pp. 1877–1879, 2002.

[96] S. Aeffner, T. Reusch, B. Weinhausen, and T. Salditt, "Energetics of Stalk Intermediates in Membrane Fusion Are Controlled by Lipid Composition", *Proceedings of the National Academy of Sciences*, vol. 109, no. 25, E1609–E1618, 2012.

[97] Y. Levine and M. Wilkins, "Structure of Oriented Lipid Bilayers", *Nature New Biology*, vol. 230, no. 11, pp. 69–72, 1971.

[98] J. Pan, T. T. Mills, S. Tristram-Nagle, and J. F. Nagle, "Cholesterol Perturbs Lipid Bilayers Nonuniversally", *Physical Review Letters*, vol. 100, no. 19, p. 198 103, 2008.

[99] H. J. Sharpe, T. J. Stevens, and S. Munro, "A Comprehensive Comparison of Transmembrane Domains Reveals Organelle-Specific Properties", *Cell*, vol. 142, no. 1, pp. 158–169, 2010.

[100] H. Träuble and H. Eibl, "Electrostatic Effects on Lipid Phase Transitions: Membrane Structure and Ionic Environment", *Proceedings of the National Academy of Sciences*, vol. 71, no. 1, pp. 214–219, 1974.

[101] A. Hodgkin and P. Horowicz, "The Influence of Potassium and Chloride Ions on the Membrane Potential of Single Muscle Fibres", *The Journal of Physiology*, vol. 148, no. 1, pp. 127–160, 1959.

[102] J. Song, J. Franck, P. Pincus, M. W. Kim, and S. Han, "Specific Ions Modulate Diffusion Dynamics of Hydration Water on Lipid Membrane Surfaces", *Journal of the American Chemical Society*, vol. 136, no. 6, pp. 2642–2649, 2014.

[103] A. Portis, C. Newton, W. Pangborn, and D. Papahadjopoulos, "Studies on the Mechanism of Membrane Fusion: Evidence for an Intermembrane Calcium (2+) Ion-Phospholipid Complex, Synergism With Magnesium (2+) Ion, and Inhibition by Spectrin", *Biochemistry*, vol. 18, no. 5, pp. 780–790, 1979.

[104] J. Wilschut, N. Duzgunes, R. Fraley, and D. Papahadjopoulos, "Studies on the Mechanism of Membrane Fusion: Kinetics of Calcium Ion Induced Fusion of Phosphatidylserine Vesicles Followed by a New Assay for Mixing of Aqueous Vesicle Contents", *Biochemistry*, vol. 19, no. 26, pp. 6011–6021, 1980.

[105] D. E. Clapham, "Calcium Signaling", *Cell*, vol. 131, no. 6, pp. 1047–1058, 2007.

[106] R. Friedman, "Membrane–Ion Interactions", *The Journal of Membrane Biology*, pp. 1–8, 2018.

[107] G. Pabst, N. Kučerka, M.-P. Nieh, M. Rheinstädter, and J. Katsaras, "Applications of Neutron and X-Ray Scattering to the Study of Biologically Relevant Model Membranes", *Chemistry and Physics of Lipids*, vol. 163, no. 6, pp. 460–479, 2010.

[108] O. Becconi, E. Ahlstrand, A. Salis, and R. Friedman, "Protein-Ion Interactions: Simulations of Bovine Serum Albumin in Physiological Solutions of NaCl, KCl and LiCl", *Israel Journal of Chemistry*, vol. 57, no. 5, pp. 403–412, 2017.

[109] E. Project, E. Nachliel, and M. Gutman, "Parameterization of Ca+ 2–Protein Interactions for Molecular Dynamics Simulations", *Journal of Computational Chemistry*, vol. 29, no. 7, pp. 1163–1169, 2008.

[110] E. Ahlstrand, D. Spångberg, K. Hermansson, and R. Friedman, "Interaction Energies Between Metal Ions (Zn2+ and Cd2+) and Biologically Relevant Ligands", *International Journal of Quantum Chemistry*, vol. 113, no. 23, pp. 2554–2562, 2013.

[111] R. M. Venable, Y. Luo, K. Gawrisch, B. Roux, and R. W. Pastor, "Simulations of Anionic Lipid Membranes: Development of Interaction-Specific Ion Parameters and Validation Using NMR Data", *The Journal of Physical Chemistry B*, vol. 117, no. 35, pp. 10 183–10 192, 2013.

[112] A. D. Dupuy and D. M. Engelman, "Protein Area Occupancy at the Center of the Red Blood Cell Membrane", *Proceedings of the National Academy of Sciences*, vol. 105, no. 8, pp. 2848–2852, 2008.

[113] G. von Heijne, "Membrane-Protein Topology", *Nature Reviews Molecular Cell Biology*, vol. 7, no. 12, p. 909, 2006.

[114] B. Alberts, D. Bray, K. Hopkin, A. Johnson, J. Lewis, M. Raff, K. Roberts, and P. Walter, *Essential Cell Biology*, 3rd edition. Taylor & Francis Group, 2010.

[115] A. G. Lee, "How Lipids Affect the Activities of Integral Membrane Proteins", *Biochimica et Biophysica Acta (BBA)-Biomembranes*, vol. 1666, no. 1, pp. 62–87, 2004.

[116] Ü. Coskun and K. Simons, "Cell Membranes: The Lipid Perspective", *Structure*, vol. 19, no. 11, pp. 1543–1548, 2011.

[117] C. Hunte and S. Richers, "Lipids and Membrane Protein Structures", *Current Opinion in Structural Biology*, vol. 18, no. 4, pp. 406–411, 2008.

[118] H. Palsdottir and C. Hunte, "Lipids in Membrane Protein Structures", *Biochimica et Biophysica Acta (BBA)-Biomembranes*, vol. 1666, no. 1, pp. 2–18, 2004.

[119] F.-X. Contreras, A. M. Ernst, F. Wieland, and B. Brügger, "Specificity of Intramembrane Protein–Lipid Interactions", *Cold Spring Harbor Perspectives in Biology*, vol. 3, no. 6, a004705, 2011.

[120] P. S. Niemelä, M. S. Miettinen, L. Monticelli, H. Hammaren, P. Bjelkmar, T. Murtola, E. Lindahl, and I. Vattulainen, "Membrane Proteins Diffuse as Dynamic Complexes With Lipids", *Journal of the American Chemical Society*, vol. 132, no. 22, pp. 7574–7575, 2010.

[121] F.-X. Contreras, A. M. Ernst, P. Haberkant, P. Björkholm, E. Lindahl, B. Gönen, C. Tischer, A. Elofsson, G. von Heijne, C. Thiele, R. Pepperkok, F. Wieland, and B. Brügger, "Molecular Recognition of a Single Sphingolipid Species by a Protein's Transmembrane Domain", *Nature*, vol. 481, no. 7382, p. 525, 2012.

[122] F. Perrotti, C. Rosa, I. Cicalini, P. Sacchetta, P. Del Boccio, D. Genovesi, and D. Pieragostino, "Advances in Lipidomics for Cancer Biomarkers Discovery", *International Journal of Molecular Sciences*, vol. 17, no. 12, p. 1992, 2016.

[123] R. M. Epand, "Proteins and Cholesterol-Rich Domains", *Biochimica et Biophysica Acta (BBA)-Biomembranes*, vol. 1778, no. 7, pp. 1576–1582, 2008.

[124] J. Fantini, N. Yahi, and N. Garmy, "Cholesterol Accelerates the Binding of Alzheimer's β-Amyloid Peptide to Ganglioside GM1 Through a Universal Hydrogen-Bond-Dependent Sterol Tuning of Glycolipid Conformation", *Frontiers in Physiology*, vol. 4, p. 120, 2013.

[125] T. Róg and I. Vattulainen, "Cholesterol, Sphingolipids, and Glycolipids: What Do We Know About Their Role in Raft-Like Membranes?", *Chemistry and Physics of Lipids*, vol. 184, pp. 82–104, 2014.

[126] D. Lingwood, B. Binnington, T. Róg, I. Vattulainen, M. Grzybek, Ü. Coskun, C. A. Lingwood, and K. Simons, "Cholesterol Modulates Glycolipid Conformation and Receptor Activity", *Nature Chemical Biology*, vol. 7, no. 5, pp. 260–262, 2011.

[127] M. Manna, M. Niemelä, J. Tynkkynen, M. Javanainen, W. Kulig, D. J. Müller, T. Róg, and I. Vattulainen, "Mechanism of Allosteric Regulation of β2-Adrenergic Receptor by Cholesterol", *eLIFE*, vol. 5, 2016.

[128] T. J. Pucadyil and A. Chattopadhyay, "Cholesterol Modulates Ligand Binding and G-Protein Coupling to Serotonin 1A Receptors From Bovine Hippocampus", *Biochimica et Biophysica Acta (BBA)-Biomembranes*, vol. 1663, no. 1, pp. 188–200, 2004.

[129] Ç. Eroglu, B. Brügger, F. Wieland, and I. Sinning, "Glutamate-Binding Affinity of Drosophila Metabotropic Glutamate Receptor Is Modulated by Association With Lipid Rafts", *Proceedings of the National Academy of Sciences*, vol. 100, no. 18, pp. 10 219–10 224, 2003.

[130] M. Bouvier, "Oligomerization of G-Protein-Coupled Transmitter Receptors", *Nature Reviews Neuroscience*, vol. 2, no. 4, p. 274, 2001.

[131] R. O. Hynes, "Integrins: Bidirectional, Allosteric Signaling Machines", *Cell*, vol. 110, no. 6, pp. 673–687, 2002.

[132] J. S. Desgrosellier and D. A. Cheresh, "Integrins in Cancer: Biological Implications and Therapeutic Opportunities", *Nature Reviews Cancer*, vol. 10, no. 1, p. 9, 2010.

[133] J. Takagi, B. M. Petre, T. Walz, and T. A. Springer, "Global Conformational Rearrangements in Integrin Extracellular Domains in Outside-In and Inside-Out Signaling", *Cell*, vol. 110, no. 5, pp. 599–611, 2002.

[134] J. Zhu, B.-H. Luo, P. Barth, J. Schonbrun, D. Baker, and T. A. Springer, "The Structure of a Receptor With Two Associating Transmembrane Domains on the Cell Surface: Integrin αIIbβ3", *Molecular Cell*, vol. 34, no. 2, pp. 234–249, 2009.

[135] T.-L. Lau, C. Kim, M. H. Ginsberg, and T. S. Ulmer, "The Structure of the Integrin αIIbβ3 Transmembrane Complex Explains Integrin Transmembrane Signalling", *The EMBO Journal*, vol. 28, no. 9, pp. 1351–1361, 2009.

[136] T. A. Springer and M. L. Dustin, "Integrin Inside-Out Signaling and the Immunological Synapse", *Current Opinion in Cell Biology*, vol. 24, no. 1, pp. 107–115, 2012.

[137] F. Saltel, E. Mortier, V. P. Hytönen, M.-C. Jacquier, P. Zimmermann, V. Vogel, W. Liu, and B. Wehrle-Haller, "New PI(4,5)P2-and Membrane Proximal Integrin–Binding Motifs in the Talin Head Control β3-Integrin Clustering", *The Journal of Cell Biology*, vol. 187, no. 5, pp. 715–731, 2009.

[138] D. T. Moore, P. Nygren, H. Jo, K. Boesze-Battaglia, J. S. Bennett, and W. F. DeGrado, "Affinity of Talin-1 for the β3-Integrin Cytosolic Domain Is Modulated by Its Phospholipid Bilayer Environment", *Proceedings of the National Academy of Sciences*, vol. 109, no. 3, pp. 793–798, 2012.

[139] V. Martel, C. Racaud-Sultan, S. Dupe, C. Marie, F. Paulhe, A. Galmiche, M. R. Block, and C. Albiges-Rizo, "Conformation, Localization, and Integrin Binding of Talin Depend on Its Interaction With Phosphoinositides", *Journal of Biological Chemistry*, vol. 276, no. 24, pp. 21 217–21 227, 2001.

[140] X. Song, J. Yang, J. Hirbawi, S. Ye, H. D. Perera, E. Goksoy, P. Dwivedi, E. F. Plow, R. Zhang, and J. Qin, "A Novel Membrane-Dependent on/Off Switch Mechanism of Talin FERM Domain at Sites of Cell Adhesion", *Cell Research*, vol. 22, no. 11, p. 1533, 2012.

[141] B. Alder and T. Wainwright, "Phase Transition for a Hard Sphere System", *The Journal of Chemical Physics*, vol. 27, no. 5, pp. 1208–1209, 1957.

[142] A. Rahman, "Correlations in the Motion of Atoms in Liquid Argon", *Physical Review*, vol. 136, no. 2A, A405, 1964.

[143] J. A. McCammon, B. R. Gelin, and M. Karplus, "Dynamics of Folded Proteins", *Nature*, vol. 267, no. 5612, p. 585, 1977.

[144] Y. Duan and P. A. Kollman, "Pathways to a Protein Folding Intermediate Observed in a 1-Microsecond Simulation in Aqueous Solution", *Science*, vol. 282, no. 5389, pp. 740–744, 1998.

[145] E. Tarasova, V. Farafonov, R. Khayat, N. Okimoto, T. S. Komatsu, M. Taiji, and D. Nerukh, "All-Atom Molecular Dynamics Simulations of Entire Virus Capsid Reveal the Role of Ion Distribution in Capsid's Stability", *The Journal of Physical Chemistry Letters*, vol. 8, no. 4, pp. 779–784, 2017.

[146] H. I. Ingólfsson, T. S. Carpenter, H. Bhatia, P.-T. Bremer, S. J. Marrink, and F. C. Lightstone, "Computational Lipidomics of the Neuronal Plasma Membrane", *Biophysical Journal*, vol. 113, no. 10, pp. 2271–2280, 2017.

[147] D. E. Shaw, P. Maragakis, K. Lindorff-Larsen, S. Piana, R. O. Dror, M. P. Eastwood, J. A. Bank, J. M. Jumper, J. K. Salmon, Y. Shan, and W. Wriggers, "Atomic-Level Characterization of the Structural Dynamics of Proteins", *Science*, vol. 330, no. 6002, pp. 341–346, 2010.

[148] T. Schlick, *Molecular Modeling and Simulation: An Interdisciplinary Guide*. Springer Verlag, 2010, vol. 21.

[149] M. Tuckerman, *Statistical Mechanics: Theory and Molecular Simulation*. Oxford University Press, 2010.

[150] M. Abraham, B. Hess, D. van der Spoel, and E. Lindahl, "User Manual Version 5.0.7", *The GROMACS Development Teams at the Royal Institute of Technology and Uppsala University, Sweden*, 2015.

[151] D. Frenkel and B. Smit, *Understanding Molecular Simulation: From Algorithms to Applications*. Academic Press, 2002, vol. 1.

[152] A. R. Leach, *Molecular Modelling: Principles and Applications*. Addison-Wesley Longman Ltd, 2001.

[153] H. Berman, J. Westbrook, Z. Feng, G. Gilliland, T. Bhat, H. Weissig, I. Shindyalov, and P. Bourne, "The Protein Data Bank", *Nucleic Acids Research*, vol. 28, no. 1, pp. 235–242, 2000.

[154] A. C. Van Duin, S. Dasgupta, F. Lorant, and W. A. Goddard, "Reaxff: A Reactive Force Field for Hydrocarbons", *The Journal of Physical Chemistry A*, vol. 105, no. 41, pp. 9396–9409, 2001.

[155] J. B. Marion, *Classical Dynamics of Particles and Systems*. Academic Press, 2013.

[156] W. Qiu-Dong, "The Global Solution of the N-Body Problem", *Celestial Mechanics and Dynamical Astronomy*, vol. 50, no. 1, pp. 73–88, 1990.

[157] R. Hockney, S. Goel, and J. Eastwood, "Quiet High-Resolution Computer Models of a Plasma", *Journal of Computational Physics*, vol. 14, no. 2, pp. 148–158, 1974.

[158] L. Verlet, "Computer" Experiments" on Classical Fluids. I. Thermodynamical Properties of Lennard-Jones Molecules", *Physical Review*, vol. 159, no. 1, p. 98, 1967.

[159] B. Hess, H. Bekker, H. J. C. Berendsen, and J. G. E. M. Fraaije, "LINCS: A Linear Constraint Solver for Molecular Simulations", *Journal of Computational Chemistry*, vol. 18, no. 12, pp. 1463–1472, 1997.

[160] S. Miyamoto and P. A. Kollman, "Settle: An Analytical Version of the SHAKE and RATTLE Algorithm for Rigid Water Models", *Journal of Computational Chemistry*, vol. 13, no. 8, pp. 952–962, 1992.

[161] R. B. Best, X. Zhu, J. Shim, P. E. Lopes, J. Mittal, M. Feig, and A. D. MacKerell Jr, "Optimization of the Additive CHARMM All-Atom Protein Force Field Targeting Improved Sampling of the Backbone Φ, ψ and Side-Chain $\chi 1$ and $\chi 2$ Dihedral Angles", *Journal of Chemical Theory and Computation*, vol. 8, no. 9, pp. 3257–3273, 2012.

[162] J. B. Klauda, R. M. Venable, J. A. Freites, J. W. O'Connor, D. J. Tobias, C. Mondragon-Ramirez, I. Vorobyov, A. D. MacKerell Jr, and R. W. Pastor, "Update of the CHARMM All-Atom Additive Force Field for Lipids: Validation on Six Lipid Types", *The Journal of Physical Chemistry B*, vol. 114, no. 23, pp. 7830–7843, 2010.

[163] K. Hart, N. Foloppe, C. M. Baker, E. J. Denning, L. Nilsson, and A. D. MacKerell Jr, "Optimization of the CHARMM Additive Force Field for DNA: Improved Treatment of the BI/BII Conformational Equilibrium", *Journal of Chemical Theory and Computation*, vol. 8, no. 1, pp. 348–362, 2011.

[164] O. Guvench, S. S. Mallajosyula, E. P. Raman, E. Hatcher, K. Vanommeslaeghe, T. J. Foster, F. W. Jamison, and A. D. MacKerell Jr, "CHARMM Additive All-Atom Force Field for Carbohydrate Derivatives and Its Utility in Polysaccharide and Carbohydrate–Protein Modeling", *Journal of Chemical Theory and Computation*, vol. 7, no. 10, pp. 3162–3180, 2011.

[165] W. L. Jorgensen and J. Tirado-Rives, "The OPLS [Optimized Potentials for Liquid Simulations] Potential Functions for Proteins, Energy Minimizations for Crystals of Cyclic Peptides and Crambin", *Journal of the American Chemical Society*, vol. 110, no. 6, pp. 1657–1666, 1988.

[166] A. Maciejewski, M. Pasenkiewicz-Gierula, O. Cramariuc, I. Vattulainen, and T. Róg, "Refined OPLS All-Atom Force Field for Saturated Phosphatidylcholine Bilayers at Full Hydration", *The Journal of Physical Chemistry B*, vol. 118, no. 17, pp. 4571–4581, 2014.

[167] W. Kulig, M. Pasenkiewicz-Gierula, and T. Róg, "C*is* and *Trans* Unsaturated Phosphatidylcholine Bilayers: A Molecular Dynamics Simulation Study", *Chemistry and Physics of Lipids*, vol. 195, pp. 12–20, 2016.

[168] E. Harder, W. Damm, J. Maple, C. Wu, M. Reboul, J. Y. Xiang, L. Wang, D. Lupyan, M. K. Dahlgren, J. L. Knight, J. W. Kaus, D. S. Cerutti, G. Krilov, W. L. Jorgensen, R. Abel, and R. A. Friesner, "OPLS3: A Force Field Providing Broad Coverage of Drug-Like Small Molecules and Proteins", *Journal of Chemical Theory and Computation*, vol. 12, no. 1, pp. 281–296, 2015.

[169] J. A. Maier, C. Martinez, K. Kasavajhala, L. Wickstrom, K. E. Hauser, and C. Simmerling, "ff14SB: Improving the Accuracy of Protein Side Chain and Backbone Parameters From ff99SB", *Journal of Chemical Theory and Computation*, vol. 11, no. 8, pp. 3696–3713, 2015.

[170] C. J. Dickson, B. D. Madej, Å. A. Skjevik, R. M. Betz, K. Teigen, I. R. Gould, and R. C. Walker, "Lipid14: The AMBER Lipid Force Field", *Journal of Chemical Theory and Computation*, vol. 10, no. 2, pp. 865–879, 2014.

[171] B. D. Madej, I. R. Gould, and R. C. Walker, "A Parameterization of Cholesterol for Mixed Lipid Bilayer Simulation Within the AMBER Lipid14 Force Field", *The Journal of Physical Chemistry B*, vol. 119, no. 38, pp. 12 424–12 435, 2015.

[172] J. P. Jämbeck and A. P. Lyubartsev, "Another Piece of the Membrane Puzzle: Extending Slipids Further", *Journal of Chemical Theory and Computation*, vol. 9, no. 1, pp. 774–784, 2012.

[173] J. P. Jämbeck and A. P. Lyubartsev, "Derivation and Systematic Validation of a Refined All-Atom Force Field for Phosphatidylcholine Lipids", *The Journal of Physical Chemistry B*, vol. 116, no. 10, pp. 3164–3179, 2012.

[174] J. P. Jämbeck and A. P. Lyubartsev, "An Extension and Further Validation of an All-Atomistic Force Field for Biological Membranes", *Journal of Chemical Theory and Computation*, vol. 8, no. 8, pp. 2938–2948, 2012.

[175] M. Javanainen and H. Martinez-Seara, "Efficient Preparation and Analysis of Membrane and Membrane Protein Systems", *Biochimica et Biophysica Acta (BBA)-Biomembranes*, vol. 1858, no. 10, pp. 2468–2482, 2016.

[176] A. Botan, F. Favela-Rosales, P. F. Fuchs, M. Javanainen, M. Kanduč, W. Kulig, A. Lamberg, C. Loison, A. Lyubartsev, M. S. Miettinen, L. Monticelli, J. Määttä, O. H. S. Ollila, M. Retegan, T. Róg, H. Santuz, and J. Tynkkynen, "Toward Atomistic Resolution Structure of Phosphatidylcholine Headgroup and Glycerol Backbone at Different Ambient Conditions", *The Journal of Physical Chemistry B*, vol. 119, no. 49, pp. 15 075–15 088, 2015.

[177] K. Pluhackova and R. A. Böckmann, "Biomembranes in Atomistic and Coarse-Grained Simulations", *Journal of Physics: Condensed Matter*, vol. 27, no. 32, p. 323 103, 2015.

[178] W. D. Cornell, P. Cieplak, C. I. Bayly, I. R. Gould, K. M. Merz, D. M. Ferguson, D. C. Spellmeyer, T. Fox, J. W. Caldwell, and P. A. Kollman, "A Second Generation Force Field for the Simulation of Proteins, Nucleic Acids, and Organic Molecules", *Journal of the American Chemical Society*, vol. 117, no. 19, pp. 5179–5197, 1995.

[179] B. Wang and D. G. Truhlar, "Partial Atomic Charges and Screened Charge Models of the Electrostatic Potential", *Journal of Chemical Theory and Computation*, vol. 8, no. 6, pp. 1989–1998, 2012.

[180] M. Patra, M. Karttunen, M. T. Hyvönen, E. Falck, P. Lindqvist, and I. Vattulainen, "Molecular Dynamics Simulations of Lipid Bilayers: Major Artifacts Due to Truncating Electrostatic Interactions", *Biophysical Journal*, vol. 84, no. 6, pp. 3636–3645, 2003.

[181] P. Ewald, "The Calculation of Optical and Electrostatic Grid Potential", *Annalen Der Physik*, vol. 64, no. 3, pp. 253–87, 1921.

[182] A. Toukmaji and J. Board, "Ewald Summation Techniques in Perspective: A Survey", *Computer Physics Communications*, vol. 95, no. 2, pp. 73–92, 1996.

[183] H. J. C. Berendsen, J. P. M. Postma, W. F. van Gunsteren, A. DiNola, and J. R. Haak, "Molecular Dynamics With Coupling to an External Bath", *The Journal of Chemical Physics*, vol. 81, no. 8, pp. 3684–3690, 1984.

[184] S. Nosé, "A Molecular Dynamics Method for Simulations in the Canonical Ensemble", *Molecular Physics*, vol. 52, no. 2, pp. 255–268, 1984.

[185] W. G. Hoover, "Canonical Dynamics: Equilibrium Phase-Space Distributions", *Physical Review A*, vol. 31, no. 3, p. 1695, 1985.

[186] G. Bussi, D. Donadio, and M. Parrinello, "Canonical Sampling Through Velocity Rescaling", *The Journal of Chemical Physics*, vol. 126, no. 1, p. 014 101, 2007.

[187] P. H. Hünenberger, "Thermostat Algorithms for Molecular Dynamics Simulations", in *Advanced Computer Simulation*, Springer, 2005, pp. 105–149.

[188] M. Parrinello and A. Rahman, "Polymorphic Transitions in Single Crystals: A New Molecular Dynamics Method", *Journal of Applied Physics*, vol. 52, no. 12, pp. 7182–7190, 1981.

[189] S. Nose and M. Klein, "Constant Pressure Molecular Dynamics for Molecular Systems", *Molecular Physics*, vol. 50, no. 5, pp. 1055–1076, 1983.

[190] O. Berger, O. Edholm, and F. Jähnig, "Molecular Dynamics Simulations of a Fluid Bilayer of Dipalmitoylphosphatidylcholine at Full Hydration, Constant Pressure, and Constant Temperature", *Biophysical Journal*, vol. 72, no. 5, pp. 2002–2013, 1997.

[191] S. J. Marrink, A. H. De Vries, and A. E. Mark, "Coarse Grained Model for Semiquantitative Lipid Simulations", *The Journal of Physical Chemistry B*, vol. 108, no. 2, pp. 750–760, 2004.

[192] S. J. Marrink, H. J. Risselada, S. Yefimov, D. P. Tieleman, and A. H. De Vries, "The MARTINI Force Field: Coarse Grained Model for Biomolecular Simulations", *The Journal of Physical Chemistry B*, vol. 111, no. 27, pp. 7812–7824, 2007.

[193] D. H. de Jong, G. Singh, W. D. Bennett, C. Arnarez, T. A. Wassenaar, L. V. Schäfer, X. Periole, D. P. Tieleman, and S. J. Marrink, "Improved Parameters for the MARTINI Coarse-Grained Protein Force Field", *Journal of Chemical Theory and Computation*, vol. 9, no. 1, pp. 687–697, 2012.

[194] J. J. Uusitalo, H. I. Ingólfsson, P. Akhshi, D. P. Tieleman, and S. J. Marrink, "MARTINI Coarse-Grained Force Field: Extension to DNA", *Journal of Chemical Theory and Computation*, vol. 11, no. 8, pp. 3932–3945, 2015.

[195] C. A. López, A. J. Rzepiela, A. H. De Vries, L. Dijkhuizen, P. H. Hünenberger, and S. J. Marrink, "MARTINI Coarse-Grained Force Field: Extension to Carbohydrates", *Journal of Chemical Theory and Computation*, vol. 5, no. 12, pp. 3195–3210, 2009.

[196] S. O. Yesylevskyy, L. V. Schäfer, D. Sengupta, and S. J. Marrink, "Polarizable Water Model for the Coarse-Grained MARTINI Force Field", *PLoS Computational Biology*, vol. 6, no. 6, e1000810, 2010.

[197] C. Arnarez, J. J. Uusitalo, M. F. Masman, H. I. Ingólfsson, D. H. de Jong, M. N. Melo, X. Periole, A. H. de Vries, and S. J. Marrink, "Dry Martini, a Coarse-Grained Force Field for Lipid Membrane Simulations with Implicit Solvent", *Journal of Chemical Theory and Computation*, vol. 11, no. 1, pp. 260–275, 2014.

[198] T. A. Wassenaar, H. I. Ingólfsson, R. A. Böckmann, D. P. Tieleman, and S. J. Marrink, "Computational Lipidomics with insane: A Versatile Tool for Generating Custom Membranes for Molecular Simulations", *Journal of Chemical Theory and Computation*, vol. 11, no. 5, pp. 2144–2155, 2015.

[199] T. A. Wassenaar, K. Pluhackova, R. A. Böckmann, S. J. Marrink, and D. P. Tieleman, "Going Backward: A Flexible Geometric Approach to Reverse Transformation From Coarse Grained to Atomistic Models", *Journal of Chemical Theory and Computation*, vol. 10, no. 2, pp. 676–690, 2014.

[200] X.-Z. Li, B. Walker, and A. Michaelides, "Quantum Nature of the Hydrogen Bond", *Proceedings of the National Academy of Sciences*, vol. 108, no. 16, pp. 6369–6373, 2011.

[201] C. Chen, W. Z. Li, Y. C. Song, L. D. Weng, and N. Zhang, "The Effect of Geometrical Criteria on Hydrogen Bonds Analysis in Aqueous Glycerol Solutions", *Journal of Molecular Imaging and Dynamics*, vol. 1, no. 1, p. 1 000 101, 2011.

[202] F. Eisenhaber, P. Lijnzaad, P. Argos, C. Sander, and M. Scharf, "The Double Cubic Lattice Method: Efficient Approaches to Numerical Integration of Surface Area and Volume and to Dot Surface Contouring of Molecular Assemblies", *Journal of Computational Chemistry*, vol. 16, no. 3, pp. 273–284, 1995.

[203] H. I. Petrache, S. W. Dodd, and M. F. Brown, "Area Per Lipid and Acyl Length Distributions in Fluid Phosphatidylcholines Determined by 2H NMR Spectroscopy", *Biophysical Journal*, vol. 79, no. 6, pp. 3172–3192, 2000.

[204] B. Garcia-Alvarez, J. M. de Pereda, D. A. Calderwood, T. S. Ulmer, D. Critchley, I. D. Campbell, M. H. Ginsberg, and R. C. Liddington, "Structural Determinants of Integrin Recognition by Talin", *Molecular Cell*, vol. 11, no. 1, pp. 49–58, 2003.

[205] P. R. Elliott, B. T. Goult, P. M. Kopp, N. Bate, J. G. Grossmann, G. C. Roberts, D. R. Critchley, and I. L. Barsukov, "The Structure of the Talin Head Reveals a Novel Extended Conformation of the FERM Domain", *Structure*, vol. 18, no. 10, pp. 1289–1299, 2010.

[206] B. T. Goult, M. Bouaouina, P. R. Elliott, N. Bate, B. Patel, A. R. Gingras, J. G. Grossmann, G. C. Roberts, D. A. Calderwood, D. R. Critchley, *et al.*, "Structure of a Double Ubiquitin-Like Domain in the Talin Head: A Role in Integrin Activation", *The EMBO Journal*, vol. 29, no. 6, pp. 1069–1080, 2010.

[207] J. Yang, Y.-Q. Ma, R. C. Page, S. Misra, E. F. Plow, and J. Qin, "Structure of an Integrin αIIbβ3 Transmembrane-Cytoplasmic Heterocomplex Provides Insight into Integrin Activation", *Proceedings of the National Academy of Sciences*, vol. 106, no. 42, pp. 17 729–17 734, 2009.

[208] D. G. Metcalf, D. T. Moore, Y. Wu, J. M. Kielec, K. Molnar, K. G. Valentine, A. J. Wand, J. S. Bennett, and W. F. DeGrado, "NMR Analysis of the αIIbβ3 Cytoplasmic Interaction Suggests a Mechanism for Integrin Regulation", *Proceedings of the National Academy of Sciences*, vol. 107, no. 52, pp. 22 481–22 486, 2010.

[209] N. J. Anthis, K. L. Wegener, F. Ye, C. Kim, B. T. Goult, E. D. Lowe, I. Vakonakis, N. Bate, D. R. Critchley, M. H. Ginsberg, *et al.*, "The Structure of an Integrin/Talin Complex Reveals the Basis of Inside-Out Signal Transduction", *The EMBO Journal*, vol. 28, no. 22, pp. 3623–3632, 2009.

[210] A. Šali and T. L. Blundell, "Comparative Protein Modelling by Satisfaction of Spatial Restraints", *Journal of Molecular Biology*, vol. 234, no. 3, pp. 779–815, 1993.

[211] W. L. Jorgensen, J. Chandrasekhar, J. D. Madura, R. W. Impey, and M. L. Klein, "Comparison of Simple Potential Functions for Simulating Liquid Water", *The Journal of Chemical Physics*, vol. 79, no. 2, pp. 926–935, 1983.

[212] R. Faller, "Molecular Modeling of Lipid Probes and Their Influence on the Membrane", *Biochimica et Biophysica Acta (BBA)-Biomembranes*, vol. 1858, no. 10, pp. 2353–2361, 2016.

[213] E. Mobarak, M. Javanainen, W. Kulig, A. Honigmann, E. Sezgin, N. Aho, C. Eggeling, T. Rog, and I. Vattulainen, "How to Minimize Dye-Induced Perturbations While Studying Biomembrane Structure and Dynamics: PEG Linkers as a Rational Alternative", *Biochimica et Biophysica Acta (BBA)-Biomembranes*, 2018.

[214] M. Hölttä-Vuori, R.-L. Uronen, J. Repakova, E. Salonen, I. Vattulainen, P. Panula, Z. Li, R. Bittman, and E. Ikonen, "BODIPY-Cholesterol: A New Tool to Visualize Sterol Trafficking in Living Cells and Organisms", *Traffic*, vol. 9, no. 11, pp. 1839–1849, 2008.

[215] L. M. Loura, A. M. M. do Canto, and J. Martins, "Sensing Hydration and Behavior of Pyrene in POPC and POPC/Cholesterol Bilayers: A Molecular Dynamics Study", *Biochimica et Biophysica Acta (BBA)-Biomembranes*, vol. 1828, no. 3, pp. 1094–1101, 2013.

[216] M. Javanainen, "Universal Method for Embedding Proteins into Complex Lipid Bilayers for Molecular Dynamics Simulations", *Journal of Chemical Theory and Computation*, vol. 10, no. 6, pp. 2577–2582, 2014.

[217] J. C. Pickens, D. D. Mitchell, J. Liu, X. Tan, Z. Zhang, C. L. Verlinde, W. G. Hol, and E. Fan, "Nonspanning Bivalent Ligands as Improved Surface Receptor Binding Inhibitors of the Cholera Toxin B Pentamer", *Chemistry & Biology*, vol. 11, no. 9, pp. 1205–1215, 2004.

[218] A. D. Becke, "Becke's Three Parameter Hybrid Method Using the LYP Correlation Functional", *The Journal of Chemical Physics*, vol. 98, pp. 5648–5652, 1993.

[219] M. J. Frisch, G. W. Trucks, H. B. Schlegel, G. E. Scuseria, M. A. Robb, J. R. Cheeseman, G. Scalmani, V. Barone, G. A. Petersson, H. Nakatsuji, X. Li, M. Caricato, A. V. Marenich, J. Bloino, B. G. Janesko, R. Gomperts, B. Mennucci, H. P. Hratchian, J. V. Ortiz, A. F. Izmaylov, J. L. Sonnenberg, D. Williams-Young, F. Ding, F. Lipparini, F. Egidi, J. Goings, B. Peng, A. Petrone, T. Henderson, D. Ranasinghe, V. G. Zakrzewski, J. Gao, N. Rega, G. Zheng, W. Liang, M. Hada, M. Ehara, K. Toyota, R. Fukuda, J. Hasegawa, M. Ishida, T. Nakajima, Y. Honda, O. Kitao, H. Nakai, T. Vreven, K. Throssell, J. A. Montgomery Jr., J. E. Peralta, F. Ogliaro, M. J. Bearpark, J. J. Heyd,

E. N. Brothers, K. N. Kudin, V. N. Staroverov, T. A. Keith, R. Kobayashi, J. Normand, K. Raghavachari, A. P. Rendell, J. C. Burant, S. S. Iyengar, J. Tomasi, M. Cossi, J. M. Millam, M. Klene, C. Adamo, R. Cammi, J. W. Ochterski, R. L. Martin, K. Morokuma, O. Farkas, J. B. Foresman, and D. J. Fox, *Gaussian16 Revision A.03*, Gaussian Inc. Wallingford CT, 2016.

[220] C. M. Breneman and K. B. Wiberg, "Determining Atom-Centered Monopoles From Molecular Electrostatic Potentials. The Need for High Sampling Density in Formamide Conformational Analysis", *Journal of Computational Chemistry*, vol. 11, no. 3, pp. 361–373, 1990.

[221] B. R. Brooks, C. L. Brooks, A. D. MacKerell, L. Nilsson, R. J. Petrella, B. Roux, Y. Won, G. Archontis, C. Bartels, S. Boresch, A. Caflisch, L. Caves, Q. Cui, A. R. Dinner, M. Feig, S. Fischer, J. Gao, M. Hodoscek, W. Im, K. Kuczera, T. Lazaridis, J. Ma, V. Ovchinnikov, E. Paci, R. W. Pastor, C. B. Post, J. Z. Pu, M. Schaefer, B. Tidor, R. M. Venable, H. L. Woodcock, X. Wu, W. Yang, D. M. York, and M. Karplus, "CHARMM: The Biomolecular Simulation Program", *Journal of Computational Chemistry*, vol. 30, no. 10, pp. 1545–1614, 2009.

[222] J. Lee, X. Cheng, J. M. Swails, M. S. Yeom, P. K. Eastman, J. A. Lemkul, S. Wei, J. Buckner, J. C. Jeong, Y. Qi, S. Jo, V. S. Pande, D. A. Case, C. L. Brooks, A. D. MacKerell Jr., J. B. Klauda, and W. Im, "CHARMM-GUI Input Generator for NAMD, GROMACS, AMBER, OpenMM, and CHARMM/OpenMM Simulations Using the CHARMM36 Additive Force Field", *Journal of Chemical Theory and Computation*, vol. 12, no. 1, pp. 405–413, 2016.

[223] M. Kohagen, E. Pluharova, P. E. Mason, and P. Jungwirth, "Exploring Ion–Ion Interactions in Aqueous Solutions by a Combination of Molecular Dynamics and Neutron Scattering", *The Journal of Physical Chemistry Letters*, vol. 6, no. 9, pp. 1563–1567, 2015.

[224] A. D. MacKerell Jr, D. Bashford, M. Bellott, R. L. Dunbrack Jr, J. D. Evanseck, M. J. Field, S. Fischer, J. Gao, H. Guo, S. Ha, J. McCarthy, L. Kuchnir, K. Kuczera, F. T. K. Lau, C. Mattos, S. Michnick, T. Ngo, D. T. Nguyen, B. Prodhom, W. E. Reiher, B. Roux, M. Schlenkrich, J. C. Smith, R. Stote, J. Straub, M. Watanabe, J. Wiorkiewicz-Kuczera, D. Yin, and M. Karplus, "All-Atom Empirical Potential for Molecular Modeling and Dynamics Studies

of Proteins", *The Journal of Physical Chemistry B*, vol. 102, no. 18, pp. 3586–3616, 1998.

[225] Y. Qi, H. I. Ingólfsson, X. Cheng, J. Lee, S. J. Marrink, and W. Im, "CHARMM-GUI MARTINI Maker for Coarse-Grained Simulations With the MARTINI Force Field", *Journal of Chemical Theory and Computation*, vol. 11, no. 9, pp. 4486–4494, 2015.

[226] K. M. Ferguson, M. A. Lemmon, J. Schlessinger, and P. B. Sigler, "Structure of the High Affinity Complex of Inositol Trisphosphate With a Phospholipase C Pleckstrin Homology Domain", *Cell*, vol. 83, no. 6, pp. 1037–1046, 1995.

[227] J. Kästner, "Umbrella Sampling", *Wiley Interdisciplinary Reviews: Computational Molecular Science*, vol. 1, no. 6, pp. 932–942, 2011.

[228] S. Nosé, "A Unified Formulation of the Constant Temperature Molecular Dynamics Methods", *The Journal of Chemical Physics*, vol. 81, no. 1, pp. 511–519, 1984.

[229] S. Páll and B. Hess, "A Flexible Algorithm for Calculating Pair Interactions on SIMD Architectures", *Computer Physics Communications*, vol. 184, no. 12, pp. 2641–2650, 2013.

[230] U. Essmann, L. Perera, M. L. Berkowitz, T. Darden, H. Lee, and L. G. Pedersen, "A Smooth Particle Mesh Ewald Method", *The Journal of Chemical Physics*, vol. 103, no. 19, pp. 8577–8593, 1995.

[231] P. J. Steinbach and B. R. Brooks, "New Spherical-Cutoff Methods for Long-Range Forces in Macromolecular Simulation", *Journal of Computational Chemistry*, vol. 15, no. 7, pp. 667–683, 1994.

[232] B. Hess, "P-LINCS: A Parallel Linear Constraint Solver for Molecular Simulation", *Journal of Chemical Theory and Computation*, vol. 4, no. 1, pp. 116–122, 2008.

[233] P. E. Hughes, F. Diaz-Gonzalez, L. Leong, C. Wu, J. A. McDonald, S. J. Shattil, and M. H. Ginsberg, "Breaking the Integrin Hinge a Defined Structural Constraint Regulates Integrin Signaling", *Journal of Biological Chemistry*, vol. 271, no. 12, pp. 6571–6574, 1996.

[234] A. Orłowski, S. Kukkurainen, A. Pöyry, S. Rissanen, I. Vattulainen, V. P. Hytönen, and T. Róg, "PIP2 and Talin Join Forces to Activate Integrin", *The Journal of Physical Chemistry B*, vol. 119, no. 38, pp. 12 381–12 389, 2015.

[235] N. J. Anthis and I. D. Campbell, "The Tail of Integrin Activation", *Trends in Biochemical Sciences*, vol. 36, no. 4, pp. 191–198, 2011.

[236] C. Kim, T.-L. Lau, T. S. Ulmer, and M. H. Ginsberg, "Interactions of Platelet Integrin αIIb and β3 Transmembrane Domains in Mammalian Cell Membranes and Their Role in Integrin Activation", *Blood*, vol. 113, no. 19, pp. 4747–4753, 2009.

[237] K. Simons and M. J. Gerl, "Revitalizing Membrane Rafts: New Tools and Insights", *Nature Reviews Molecular Cell Biology*, vol. 11, no. 10, nrm2977, 2010.

[238] K.-A. Karlsson, "Animal Glycosphingolipids as Membrane Attachment Sites for Bacteria", *Annual Review of Biochemistry*, vol. 58, no. 1, pp. 309–350, 1989.

[239] E. A. Miljan and E. G. Bremer, "Regulation of Growth Factor Receptors by Gangliosides", *Science Signaling*, vol. 2002, no. 160, re15–re15, 2002.

[240] H. Ewers, W. Römer, A. E. Smith, K. Bacia, S. Dmitrieff, W. Chai, R. Mancini, J. Kartenbeck, V. Chambon, L. Berland, A. Oppenheim, G. Schwarzmann, T. Feizi, P. Schwille, P. Sens, A. Helenius, and L. Johannes, "GM1 Structure Determines SV40-induced Membrane Invagination and Infection", *Nature Cell Biology*, vol. 12, no. 1, p. 11, 2010.

[241] T. Harder, P. Scheiffele, P. Verkade, and K. Simons, "Lipid Domain Structure of the Plasma Membrane Revealed by Patching of Membrane Components", *The Journal of Cell Biology*, vol. 141, no. 4, pp. 929–942, 1998.

[242] K. Bacia, P. Schwille, and T. Kurzchalia, "Sterol Structure Determines the Separation of Phases and the Curvature of the Liquid-Ordered Phase in Model Membranes", *Proceedings of the National Academy of Sciences of the United States of America*, vol. 102, no. 9, pp. 3272–3277, 2005.

[243] E. Sezgin, H.-J. Kaiser, T. Baumgart, P. Schwille, K. Simons, and I. Levental, "Elucidating Membrane Structure and Protein Behavior Using Giant Plasma Membrane Vesicles", *Nature Protocols*, vol. 7, no. 6, p. 1042, 2012.

[244] T. Baumgart, G. Hunt, E. R. Farkas, W. W. Webb, and G. W. Feigenson, "Fluorescence Probe Partitioning Between Lo/Ld Phases in Lipid Membranes", *Biochimica et Biophysica Acta (BBA)-Biomembranes*, vol. 1768, no. 9, pp. 2182–2194, 2007.

[245] I. Basu and C. Mukhopadhyay, "Insights into Binding of Cholera Toxin to GM1 Containing Membrane", *Langmuir*, vol. 30, no. 50, pp. 15 244–15 252, 2014.

[246] W. Pezeshkian, L. J. Nåbo, and J. H. Ipsen, "Cholera Toxin B Subunit Induces Local Curvature on Lipid Bilayers", *FEBS Open Bio*, vol. 7, no. 11, pp. 1638–1645, 2017.

[247] S. Rissanen, M. Grzybek, A. Orłowski, T. Róg, O. Cramariuc, I. Levental, C. Eggeling, E. Sezgin, and I. Vattulainen, "Phase Partitioning of GM1 and Its Bodipy-Labeled Analog Determine Their Different Binding to Cholera Toxin", *Frontiers in Physiology*, vol. 8, p. 252, 2017.

[248] J. Shi, T. Yang, S. Kataoka, Y. Zhang, A. J. Diaz, and P. S. Cremer, "GM1 Clustering Inhibits Cholera Toxin Binding in Supported Phospholipid Membranes", *Journal of the American Chemical Society*, vol. 129, no. 18, pp. 5954–5961, 2007.

[249] M. J. Berridge, P. Lipp, and M. D. Bootman, "The Versatility and Universality of Calcium Signalling", *Nature Reviews Molecular Cell Biology*, vol. 1, no. 1, p. 11, 2000.

[250] K. Machaca, "Ca2+ Signaling, Genes and the Cell Cycle", *Cell Calcium*, vol. 49, no. 5, pp. 323–330, 2011.

[251] G. van den Bogaart, K. Meyenberg, U. Diederichsen, and R. Jahn, "Phosphatidylinositol 4, 5-bisphosphate Increases Ca2+ Affinity of Synaptotagmin-1 by 40-Fold", *Journal of Biological Chemistry*, vol. 287, no. 20, pp. 16 447–16 453, 2012.

[252] S. McLaughlin, J. Wang, A. Gambhir, and D. Murray, "PIP2 and Proteins: Interactions, Organization, and Information Flow", *Annual Review of Biophysics and Biomolecular Structure*, vol. 31, no. 1, pp. 151–175, 2002.

[253] Z. Graber, W. Wang, G. Singh, I. Kuzmenko, D. Vaknin, and E. Kooijman, "Competitive Cation Binding to Phosphatidylinositol-4, 5-bisphosphate Domains Revealed by X-Ray Fluorescence", *Rsc Advances*, vol. 5, no. 129, pp. 106 536–106 542, 2015.

[254] Y.-H. Wang, A. Collins, L. Guo, K. B. Smith-Dupont, F. Gai, T. Svitkina, and P. A. Janmey, "Divalent Cation-Induced Cluster Formation by Polyphosphoinositides in Model Membranes", *Journal of the American Chemical Society*, vol. 134, no. 7, pp. 3387–3395, 2012.

[255] E. Bilkova, R. Pleskot, S. Rissanen, S. Sun, A. Czogalla, L. Cwiklik, T. Róg, I. Vattulainen, P. S. Cremer, P. Jungwirth, and Ü. Coskun, "Calcium Directly Regulates Phosphatidylinositol 4,5-Bisphosphate Headgroup Conformation and Recognition", *Journal of the American Chemical Society*, vol. 139, no. 11, pp. 4019–4024, 2017.

[256] J. B. Seo, S.-R. Jung, W. Huang, Q. Zhang, and D.-S. Koh, "Charge Shielding of PIP2 by Cations Regulates Enzyme Activity of Phospholipase C", *PLoS One*, vol. 10, no. 12, e0144432, 2015.

[257] E. Yamamoto, A. C. Kalli, K. Yasuoka, and M. S. Sansom, "Interactions of Pleckstrin Homology Domains With Membranes: Adding Back the Bilayer via High-Throughput Molecular Dynamics", *Structure*, vol. 24, no. 8, pp. 1421–1431, 2016.

[258] M. Tanio and K. Nishimura, "Intramolecular Allosteric Interaction in the Phospholipase C-δ1 Pleckstrin Homology Domain", *Biochimica et Biophysica Acta (BBA)-Proteins and Proteomics*, vol. 1834, no. 6, pp. 1034–1043, 2013.

[259] N. Uekama, T. Sugita, M. Okada, H. Yagisawa, and S. Tuzi, "Phosphatidylserine Induces Functional and Structural Alterations of the Membrane-Associated Pleckstrin Homology Domain of Phospholipase C-δ1", *The FEBS Journal*, vol. 274, no. 1, pp. 177–187, 2007.

ORIGINAL PUBLICATIONS

I

PIP2 and Talin Join Forces to Activate Integrin

by

A. Orłowski, S. Kukkurainen, A. Pöyry, S. Rissanen, I. Vattulainen, V. Hytönen & T. Róg.

The Journal of Physical Chemistry B, vol 119, 12381–12389, 2015.

THE JOURNAL OF PHYSICAL CHEMISTRY B

Article

pubs.acs.org/JPCB

PIP2 and Talin Join Forces to Activate Integrin

Adam Orłowski,[†,#] Sampo Kukkurainen,[‡,∥,#] Annika Pöyry,[†] Sami Rissanen,[†] Ilpo Vattulainen,[†,§] Vesa P. Hytönen,[‡,∥] and Tomasz Róg*[,†]

[†]Department of Physics, Tampere University of Technology, P.O. Box 692, FI-33101 Tampere, Finland

[‡]BioMediTech, University of Tampere, FI-33520 Tampere, Finland

[∥]Fimlab Laboratories Ltd., FI-33520 Tampere, Finland

[§]Department of Physics and Chemistry, MEMPHYS−Center for Biomembrane Physics, University of Southern Denmark, Campusvej 55, DK-5230 Odense M, Denmark

Supporting Information

ABSTRACT: Integrins are major players in cell adhesion and migration, and malfunctions in controlling their activity are associated with various diseases. Nevertheless, the details of integrin activation are not completely understood, and the role of lipids in the process is largely unknown. Herein, we show using atomistic molecular dynamics simulations that the interplay of phosphatidylinositol 4,5-bisphosphate (PIP2) and talin may directly alter the conformation of integrin αIIbβ3. Our results provide a new perspective on the role of PIP2 in integrin activation and indicate that the charged PIP2 lipid headgroup can perturb a clasp at the cytoplasmic face of the integrin heterodimer.

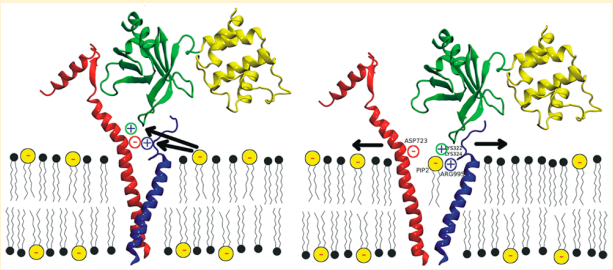

1. INTRODUCTION

Multicellular organisms provide well-defined and tightly controlled mechanisms for cell−cell and cell−extracellular matrix interactions. The group of receptors called integrins plays a central role in these mechanisms. Integrins and integrin-mediated processes are essential for normal cell functions such as signaling, cell migration, adhesion to the local extracellular environment, and leukocyte function. Moreover, integrins play a role in cancer progression and metastasis, and certain tumor types have been found to exhibit higher levels of specific integrins. This makes the integrin-associated signal complex an important spot for cancer therapy development.[1]

Integrins are heterodimeric transmembrane receptors that in mammals are composed of 18 different α and 8 β subunits.[2,3] These proteins respond to both extracellular (outside-in) and intracellular (inside-out) stimuli, connect the extracellular matrix to the cytoskeleton, and pass signals across the plasma membrane in both directions.[3] This requires a properly controlled integrin activation mechanism that involves conformational changes within the integrin heterodimer. In the case of the inside-out signaling, the changes eventually lead to an extended integrin conformation with a high affinity for extracellular ligands.[2,4] Proper control of integrin activation and thus cellular communication with the external environment is crucial for many physiologically relevant processes. Perturbation of this equilibrium can lead to constitutive activation of the integrin[5] and result in bleeding disorders.[3,6−8]

Talin, a 2541-residue-long cytoplasmic protein,[9−11] is one of the triggers that binds to integrin and activates it (inside-out) in the first stages of cell attachment.[12,13] Importantly, the conformational changes induced by talin in the transmembrane part of the integrin $\alpha\beta$ complex are crucial for the inside-out activation process.[14] More specifically, the N-terminal FERM domain of talin binds to the NPxY motif of the integrin β tail, induces a reorganization of the integrin heterodimer, and contributes to integrin activation.[11,15−18] Attachment of talin to a membrane is enhanced by a lipid known as phosphatidylinositol 4,5-bisphosphate (PIP2),[19,20] which can enforce talin to undergo conformational changes that expose the integrin β-tail binding site in its head domain.[11,21−23]

The role of PIP2 in integrin activation is intriguing given that PIP2 is a major phosphoinositide of the inner plasma membrane.[24,25] Moreover, talin itself binds and activates phosphatidylinositol phosphate kinase type Iγ[26,27] and may thereby regulate the local concentration of PIP2 in the membrane. PIP2 is able to regulate many important cellular processes including vesicular trafficking, platelet activation, and organization of the cytoskeleton,[28−30] and it may control several steps in focal adhesion.[19,20,31] PIP2 can also affect protein conformation,[32−35] target cytoplasmic proteins to the membrane, and stabilize protein oligomers.[31,36]

In this article, we focus on clarifying the importance of lipid membrane composition in the conformational modulation of integrins. In particular, we focus on the role of PIP2 in the

Received: July 6, 2015
Revised: August 21, 2015
Published: August 26, 2015

DOI: 10.1021/acs.jpcb.5b06457
J. Phys. Chem. B 2015, 119, 12381−12389

Table 1. Composition of the Simulated Systems[a]

system	integrin	talin (F0−F3)	talin (F2−F3)	DOPC	PIP2	water	K^+	Cl^-	simulation time (μs)
PIP_{F0-F3}	1	1	-	844	96	113310	703	319	0.5
PIP_{F2F3-A}	1	-	1	440	50	60559	365	169	0.5
PIP_{F2F3-B}	1	-	1	440	50	60559	365	169	0.5
NO-PIP_{F0-F3}	1	1	-	950	0	114470	320	320	0.5
NO-PIP_{F2F3-A}	1	-	1	439	0	56631	158	162	0.5
NO-PIP_{F2F3-B}	1	-	1	439	0	56631	158	162	0.5
$PIP_{CONTROL-A}$	1	-	-	420	50	56182	358	155	0.75
$PIP_{CONTROL-B}$	1	-	-	420	50	56182	358	155	0.75

[a]F0−F3 and F2−F3 correspond to the talin domains included in the systems. The abbreviation PIP refers to systems with PIP2 (and DOPC) lipids, while NO-PIP refers to systems without PIP2 lipids. The subscripts A and B stand for two independent runs of the same system. The control systems with PIP2 but without talin are represented by $PIP_{CONTROL}$.

complex integrin activation process. Despite very well documented earlier studies that showed the role of talin−PIP2 interactions in the integrin activation,[19,22] and the fact that single lipid species have recently been found to regulate the conformation and function of several membrane proteins,[37−39] it is striking that the effects of direct integrin−PIP2 interactions have not received attention until now.

Here, by using extensive atomistic molecular dynamics (MD) simulations, we show that PIP2 can interfere with the integrin heterodimer and therefore have implications for the integrin activation process. We discuss the possible joint action of PIP2 with talin, and define regions in all talin head subdomains F0−F3 that are able to interact with phosphatidylcholine and PIP2 lipids in the studied membranes. Altogether, our results give new insight into integrin−talin interactions with an emphasis on PIP2 and its role in integrin activation.

2. MATERIALS AND METHODS

2.1. Molecular Modeling of the Integrin−Talin Complex. Short and long versions of the mouse talin-1 head domain were prepared using Modeler v 9.9 and 9.10, respectively.[40] The crystal structure of talin-1 subdomains F2−F3 in a complex with β3-integrin (PDB ID: 1MK7)[15] was used as a template for the short talins containing the residues 209−400. Missing residues were added to the talin-1 head domain structure (PDB ID: 3IVF)[41] using the NMR structure of the talin head subdomains F0−F1 (PDB ID: 2KMA)[42] to yield a talin-1 head domain with the residues 2−398 (Δ139−168). Talin−integrin contacts were modeled using two talin−integrin structures (PDB IDs: 1MK7[15] and 3G9W).[43] The transmembrane domains of the integrin $\alpha\beta$ dimer and the free β3 tail were modeled using NMR structures of the αIIbβ3 integrin as templates (PDB IDs: 2K9J,[44] 2KNC,[45] and 2KV9[46]).

2.2. Atomistic Molecular Dynamics Simulations. Extensive atomistic molecular dynamics simulations were performed for the integrin αIIbβ3 and the integrin−talin complex together with a lipid bilayer comprising either pure 1,2-dioleoyl-*sn*-glycero-3-phosphocholine (DOPC) or a 9:1 molar mixture of DOPC and phosphatidylinositol-4,5-bisphosphate (PIP2) (Figure S1; see Supporting Information (SI)). We simulated systems of the integrin heterodimer consisting of transmembrane and cytoplasmic domains of αIIbβ3 in a complex with talin. Talin was present in two different configurations (either with the talin head domain (F0−F3) or with a fragment of talin head (F2−F3)), and for the purpose of having controls, systems consisting of the integrin heterodimer without talin were also studied. All these configurations, except for integrin without talin, were simulated in both membrane compositions. Some of the simulations were repeated for improved sampling. This resulted in a total of eight simulated systems (Table 1), each of which was simulated for 500 or 750 ns, altogether generating 4.5 μs of simulation results. The simulations were performed at a physiological salt concentration of 150 mM KCl. Counter ions were included to neutralize the total charge of the system. To control that the simulations are long enough, we calculated the mean square displacement of the center of mass of lipid molecules in the membrane plane (Figure S2; SI). The data obtained indicate that during the simulation time lipids diffuse on average 4−5 nm, which is 5−6 times the diameter of the lipids in the membrane plane.

The OPLS all-atom force field was used to describe the interactions for all molecules except for lipids.[47] For lipids, a compatible lipid-refined version of the OPLS all-atom force field was applied.[48,49] For water, the TIP3P model that is compatible with the OPLS parametrization was employed.[50] The system setup used in this study is identical to that employed in previous simulations of lipid bilayers with the OPLS all-atom parametrization by the authors.[51,52] Periodic boundary conditions with the minimum image convention were employed in all three dimensions. The length of each hydrogen atom covalent bond was preserved by the LINCS algorithm.[53] The integration time step was set to 2 fs and the simulations were carried out at constant pressure (1 bar) and temperature (310 K). The temperature and pressure were controlled by the v-rescale and Parrinello−Rahman methods, respectively.[54,55] The temperatures of the solute and solvent were coupled separately. For pressure, a semi-isotropic scaling was employed. The Lennard-Jones interactions were cut off at 1.0 nm. For electrostatic interactions, the particle mesh Ewald method was employed with a real space cutoff of 1.0 nm, B-spline interpolation (6th order), and a direct sum tolerance of 10^{-6}.[56] The simulations were performed with the GROMACS 4.5.5 simulation package.[57]

3. RESULTS AND DISCUSSION

3.1. PIP2 Acting on the Integrin Dimer Can Break the Arg995-Asp723 Salt Bridge. The transmembrane domain of integrin possesses two interaction interfaces that stabilize the inactive conformation of the dimer.[14] One is formed between the highly conserved (GFFKR) motif of αIIb integrin and the hydrophobic residues Trp715 and Ile719 of β3 integrin within the membrane core, stabilized by a cytoplasmic salt bridge between Arg995 in αIIb and Asp723 in β3 integrin. These interactions are referred to as the inner membrane clasp (IMC).

DOI: 10.1021/acs.jpcb.5b06457
J. Phys. Chem. B 2015, 119, 12381−12389

Further away from the cytoplasm, the interaction of the β3 residue Gly708 with the αIIb G972xxxG976 motif establishes the outer membrane clasp (OMC). Importantly, mutations of residues in either of these interaction sites (IMC and OMC) result in perturbed interactions of the transmembrane (TM) helices that can lead to a constantly active integrin.[14,44] In this respect, our particular interest is the salt bridge Arg995-Asp723 of the IMC.

By using atomistic molecular dynamics simulations, we investigated the interactions between PIP2 and the talin−integrin complex. The number of hydrogen bonds between PIP2 and each of the protein domains in the complex (integrin αIIb, β3, and talin) are shown in Table 2. A more detailed overview of the interactions between the integrin complex residues and PIP2 lipids is shown in Figure 1 and Table S1 and Table S2, where the number of contacts between the atoms of integrin αIIb and β3 and atoms of PIP2 during the last 300 ns of the simulations are reported. Two residues were defined as being in contact when two heavy atoms of different molecules were located at a distance of 0.35 nm or less. Some residues in both αIIb and β3 integrin show a very high affinity toward PIP2. This applies to residues that are already outside the transmembrane helix in the water phase, such as Lys994, Arg995, and Arg997 in integrin αIIb, and His722, Arg724, Lys725, Lys729, and Arg736 in integrin β3. Interestingly, both from visual inspection (see Figure 2) and from the analyses of the number of hydrogen bonds between the residue Arg995 and PIP2 in time (Table 2), one can conclude that the PIP2 headgroup can find its way to the positively charged residue Arg995 and establish a bond with it through negatively charged phosphate groups. This interaction led to the breakage of the Arg995-Asp723 salt bridge (Figure 2B−C, Figure 3), and it took place spontaneously after less than 300 ns of the simulation time in two out of three simulations, where PIP2 was present. It has been shown that this salt bridge is crucial for the stability of the integrin αIIbβ3 dimer, and once it is broken, integrin activation can take place.[2,5,58] The local concentration of PIP2 might thus translate to integrin activation.

Table 2. Average Number of Hydrogen Bonds between Integrin, Talin, or the αIIb Residue Arg995, and PIP2 Lipids[a]

system	Integrin αIIb − PIP2	Integrin β3 − PIP2	Talin − PIP2	Arg995 − PIP2
PIP_{F0-F3}	3.50	6.28	25.30	1.68
PIP_{F2F3-A}	3.17	4.66	17.67	3.00
PIP_{F2F3-B}	2.85	4.53	17.46	0
$PIP_{CONTROL-A}$	8.68	8.10	—	0
$PIP_{CONTROL-B}$	11.99	4.66	—	0

[a]The data were calculated over the last 300 ns of the simulation time, regardless of the total simulation length. Errors are 0.2 or less. A hydrogen bond was judged to be formed when the acceptor−donor distance is ≤0.325 nm and the angle between the acceptor−donor vector and the covalent bond donor−hydrogen is ≤35°.[59]

3.2. Opening of the Arg995-Asp723 Salt Bridge—Step toward Integrin Activation? Having observed the breakage of the Arg995-Asp723 salt bridge, we were tempted to ask whether in the simulations, where PIP2 breaks the Arg995-Asp723 salt bridge, one can see any signs of the initial steps of the integrin activation process. In order to characterize the integrin activation mechanism in more detail, we analyzed a number of parameters suggested to be associated with the activation process.[61,62] Specifically, opening of the integrin dimer at the IMC and OMC and tilting of the transmembrane domain have been proposed to take place in the integrin activation process,[16,18,43−45] although recent simulation studies are not conclusive on the mechanism of activation.[61−65] We therefore analyzed the integrin conformation by measuring the helix−helix distance through the distance of Cα atoms of chosen residues at the bottom and at the top of the helices (Figure S3, Table S3), and the tilt angle of the β3-helix in reference to the bilayer normal, representing the helix as a vector between the center of mass of the residues at the bottom and the corresponding center of mass of the residues at the top of the helix (Figure S4, Table S4).

The distance between helices is expected to increase at the IMC and OMC interfaces when the interactions are disrupted.[61] In our analyses, we assume that the distance between the Cα atoms of the residues Val700 and Gly972 measures the stability of OMC, and similarly between Lys716 and Phe993 of IMC. Time evolutions of these distances are shown in Figure S3, and the average values over the last 300 ns of the simulations are depicted in Table S3. The OMC distances remained in the same range whether or not Arg995 and Asp723 were in contact, with the exception of the system $PIP_{CONTROL-A}$. In $PIP_{CONTROL-A}$, a DOPC lipid tail entered between Val700 and Gly972 during the first 30 ns of the simulation, possibly suggesting that the OMC contact is not very tight. Separation of the IMC was observed for PIP_{F0-F3}, but its distance remained shorter than in the system NO-PIP_{F2F3-A}. Therefore, we observe no clear correlation between the existence of the Arg995-Asp723 salt bridge (Figure 3) and the separation of the integrin transmembrane helices.

Another potential indicator of integrin activation is the tilt angle of the integrin β3 helix, which in the nonactive state has been shown to be ∼25° and is stabilized by the residue Lys716, which keeps the helix in a certain orientation by snorkeling with NH_3^+ toward the phosphate headgroup region.[66] Time evolution (Figure S4) and average over the last 300 ns of the simulations (Table S4) show that, in three of the cases, the tilt angle is approximately 25°. In the systems NO-PIP_{F2F3-A} and NO-PIP_{F2F3-B}, it is higher (33.37° and 29.43°, respectively); while in the systems PIP_{F2F3-A}, NO-PIP_{F0-F3}, and $PIP_{CONTROL-A}$, it is lower (18.12°, 18.00°, and 22.22°, respectively). However, these differences in tilt angle are small,[61,65] and it is difficult to associate the changes in tilt angle with the existence of the Arg995-Asp723 salt bridge.

Experimental and computational data have been reported to be in favor of the view that talin-induced breakage of the Arg995-Asp723 salt bridge is involved in integrin activation.[14,64] Meanwhile, a recent simulation study questioned the paradigm as to the separation of integrin TM helices upon activation.[65] The authors speculated on the insignificance of the Arg995-Asp723 interaction in talin-mediated integrin activation. Our simulations indicate that this interaction can be disrupted in the presence of ionic lipids such as PIP2, which were not present in any of the previous MD simulation studies of integrin activation by talin.[61−65,67] The models we simulated in this work contain only a small part of the integrin, and there are many factors causing stress to the αIIbβ3 interface, including conformational changes of the integrin extracellular domain and its interactions with extracellular proteins. Overall, although we can claim the connection between PIP2 and the initialization of inside-out integrin activation process, the data is not sufficient to clarify

DOI: 10.1021/acs.jpcb.5b06457
J. Phys. Chem. B 2015, 119, 12381−12389

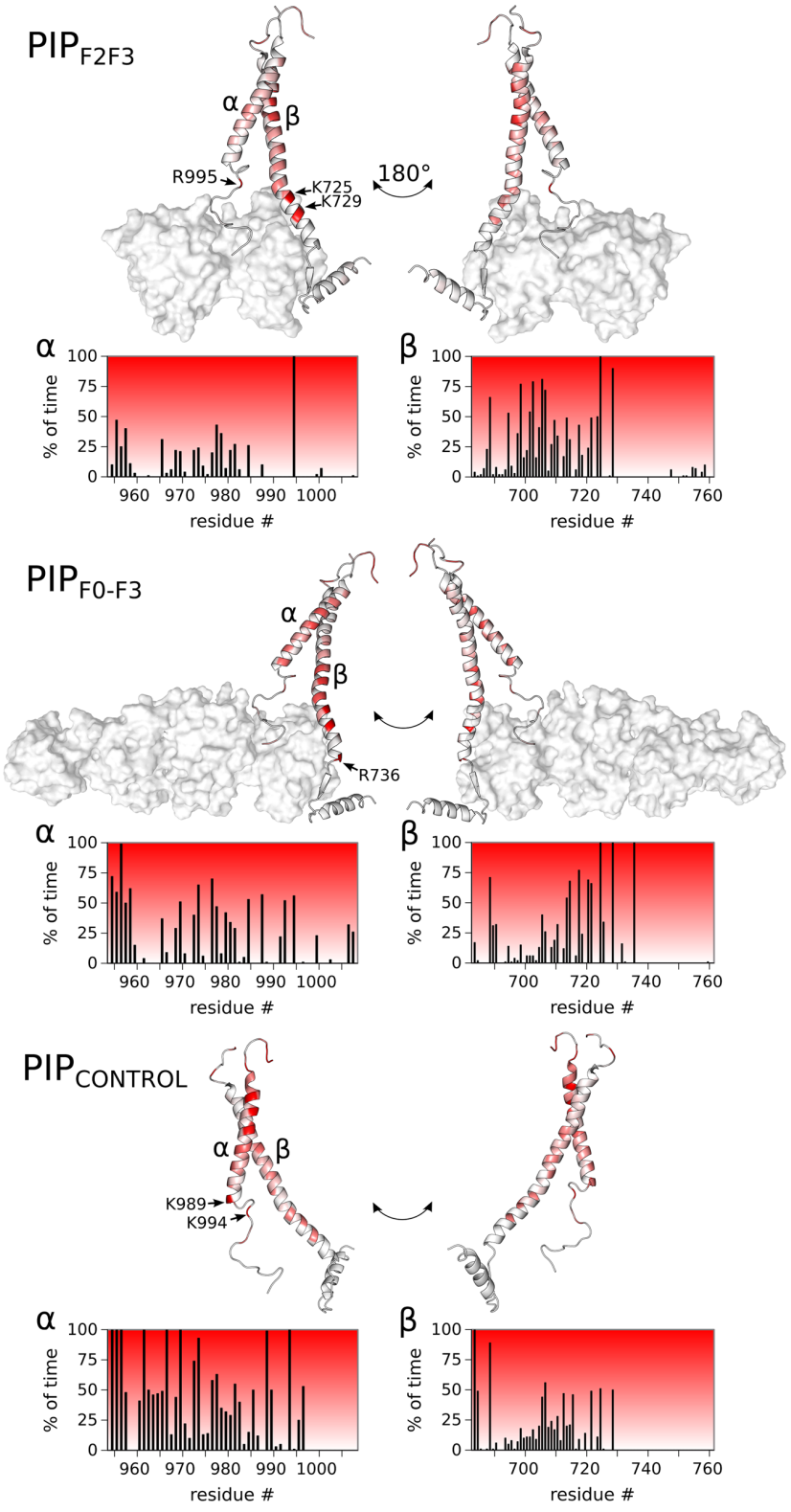

Figure 1. Interactions between integrin and PIP2 lipids. Lipid contact occupancies are mapped on integrin structures in PyMOL (Schrödinger) and presented in separate histograms for the α and β integrins. Occupancy was defined as the percentage of time (during the last 300 ns of the simulation time) when the integrin residue formed contacts with PIP2. Two residues were defined as being in contact when two heavy atoms of different molecules were located at a distance of 0.35 nm or less. The results for PIP_{F2F3} and $PIP_{CONTROL}$ are averages over the two independent simulations (A, B).

DOI: 10.1021/acs.jpcb.5b06457
J. Phys. Chem. B 2015, 119, 12381−12389

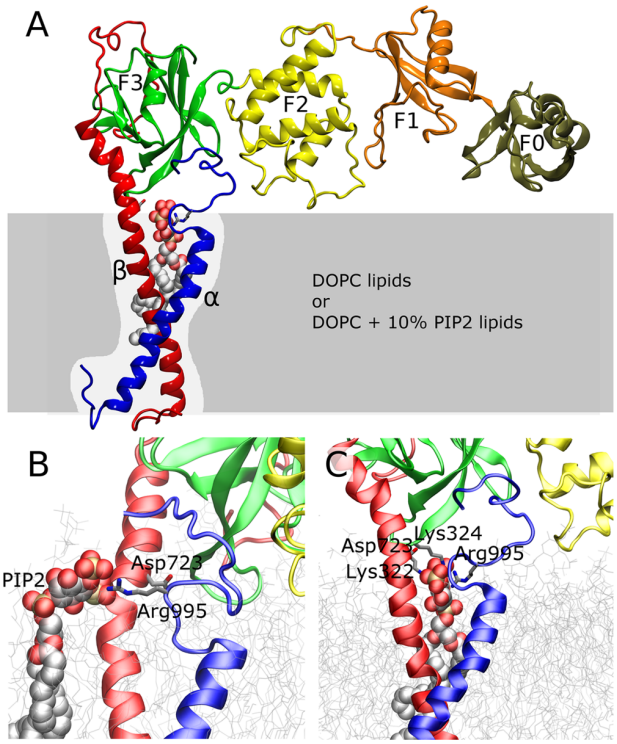

Figure 2. Schematic picture of the simulated system and central findings. (A) Schematic picture of the talin head domain in complex with the integrin αIIbβ3 transmembrane and cytoplasmic domains. Integrin αIIb (blue) and β3 (red) chains are embedded in a lipid bilayer (gray). Talin head subdomains F3 (green), F2 (yellow), F1 (orange), and F0 (olive green) bind the cytoplasmic tail of integrin β3. PIP2 is shown in the van der Waals (vdW) sphere representation. (B) Snapshot of the Arg995-PIP2 contact from the simulation system PIP_{F2F3-A}. The PIP2 lipid interfering with the Asp723-Arg995 interaction is shown in vdW spheres, and other lipids in gray transparent lines. (C) Snapshot of the Arg995-Asp723 salt bridge that is broken by the PIP2−Arg995 interaction from the simulation system PIP_{F0-F3}. Snapshots were made using the VMD package.[60]

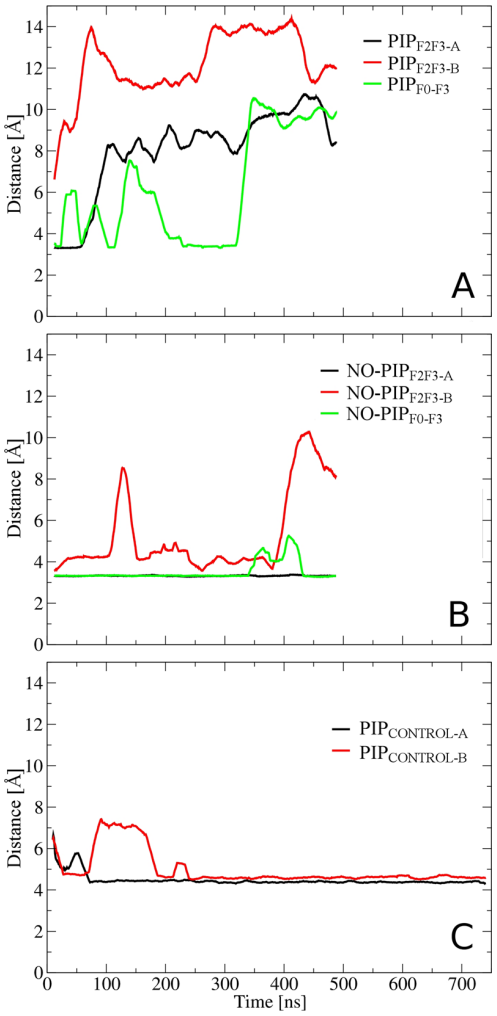

Figure 3. Presence of the Arg995-Asp723 salt bridge. The results show the distance between the Arg995 and Asp723 charged groups. (A) Systems with a membrane containing PIP2 and DOPC lipids. (B) Systems with a membrane containing only DOPC. (C) Systems with a membrane containing PIP2 and DOPC but without talin included in the protein complex. The results shown here were smoothened using a running average over 50 points from a single frame.

the impact of the PIP2-induced breakage of the Arg995-Asp723 salt bridge on integrin activation.

3.3. Role of Talin in PIP2-Mediated Integrin Activation—Joint Action of Talin and PIP2? Interactions of talin with lipids have been shown to be an important factor in integrin activation,[19] but some of the related mechanisms are still not clear. To shed light on this matter, in our simulations we included different talin configurations, containing domains F2−F3 (residues 209−400) and F0−F3 (residues 2−398 Δ139−168), to characterize the interactions that occur between talin and a lipid membrane. Similarly to previous analyses of the contacts between integrin tails and PIP2, we carried out contact and hydrogen bond analyses for talin and PIP2/DOPC (Figures 4 and S5; Tables S5, S6).

Our data show that there are PIP2 binding spots present in the F0 subdomain: the residues Lys15-Met17, Arg35, and Asp55-Lys58 can bind strongly to PIP2. Subdomains F2 and F3 seem to be very well characterized regarding their affinity toward negatively charged lipids, and[20] indeed, our results show that there are regions within this area that interact very strongly with PIP2, including the residues Glu252-Lys284, Lys318-Arg328, Arg339, Lys343, Ile348, and Lys364. Similar regions tend to bind to DOPC (Figure 4), which is in line with recent studies on the talin−integrin in different lipid bilayer compositions.[62,67] The simulated structure in our study only contained a truncated form of the large loop in the F1 domain; however, this truncated F1 domain loop was found to reside near the membrane, in accordance with previous studies.[42,62] An integrin activation mechanism involving a hydrophobic membrane anchor in the F2 domain of talin was recently predicted in a simulation study.[67] One of the reportedly membrane-inserting phenylalanines was found to reside near the membrane in our simulations (see Phe259 and Phe280 in Figure 4 and Table S5 and Table S6), but no anchoring by phenylalanines was observed.

In the simulation of the system PIP_{F0-F3}, the joint action of talin and PIP2 was distinguished. The residues Lys322 and Lys324 in talin F3 domain established hydrogen bond interactions with one of the PIP2 lipids near the integrin helices to further bring it into contact with the residue Arg995 from integrin αIIb. As a result, the important Arg995-Asp723 salt bridge was broken through an interaction between Arg995

DOI: 10.1021/acs.jpcb.5b06457
J. Phys. Chem. B 2015, 119, 12381−12389

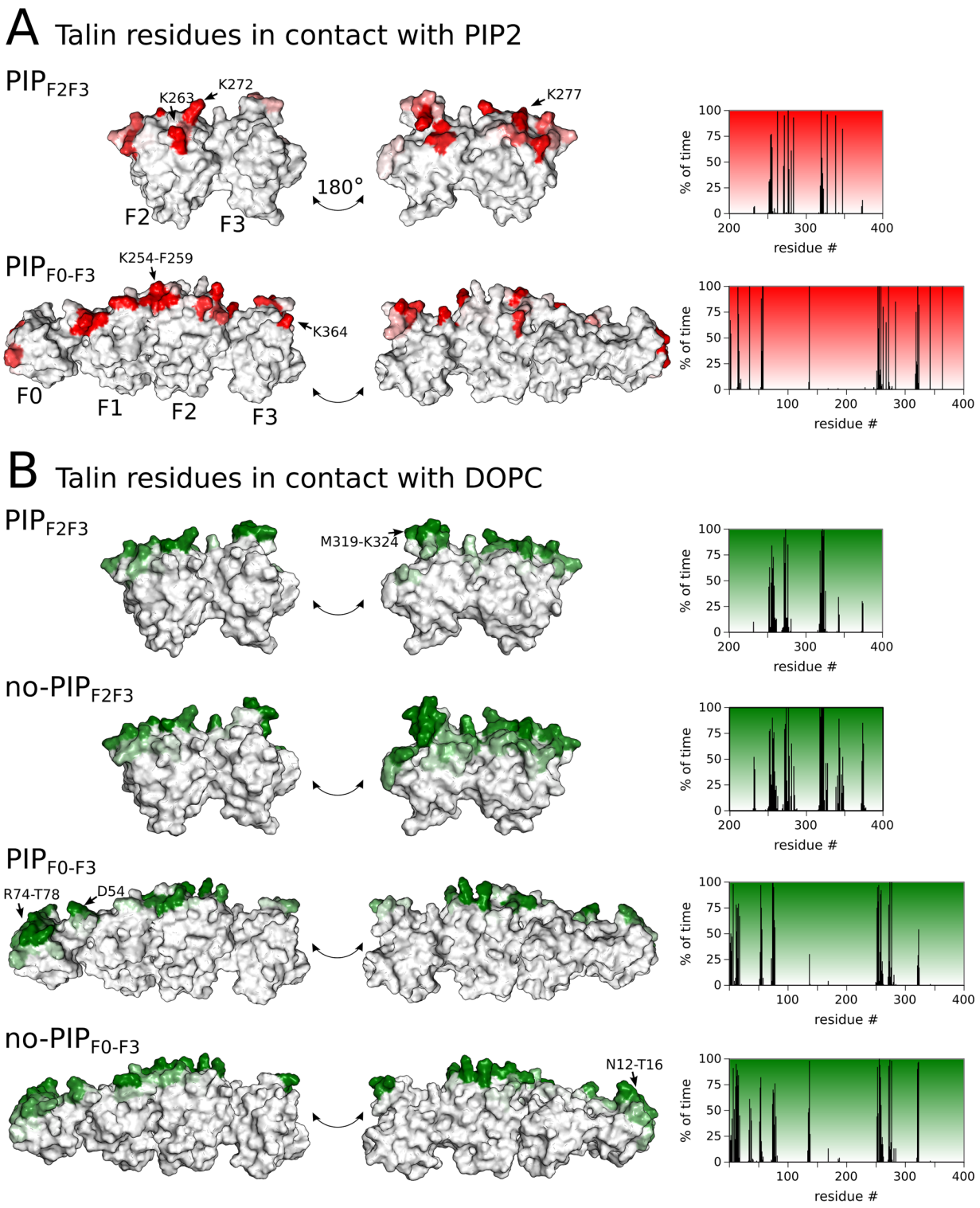

Figure 4. Interactions between talin and (A) PIP2 or (B) DOPC lipids. Lipid contact occupancies are mapped on talin structures in PyMOL (Schrödinger), and presented in histograms. Occupancy was defined as the percentage of time (during the last 300 ns of the simulation time) when the talin residue formed contacts with a lipid. Two residues were defined as being in contact when two heavy atoms of different molecules were located at a distance of 0.35 nm or less. The results for PIP_{F2F3}, $NO\text{-}PIP_{F2F3}$, and $PIP_{CONTROL}$ are averages over the two independent simulation repeats.

and PIP2 lipid headgroup phosphates (see Figure 2C). In the second case where we observed the breakage of the salt bridge mediated by PIP2 (system $PIP_{F2F3\text{–}A}$), talin was not in contact with the PIP2 lipid (for details see Figure 2B). This raises a question whether talin only indirectly facilitates the opening of the IMC by bringing PIP2 lipids into contact with integrin, or

DOI: 10.1021/acs.jpcb.5b06457
J. Phys. Chem. B 2015, 119, 12381−12389

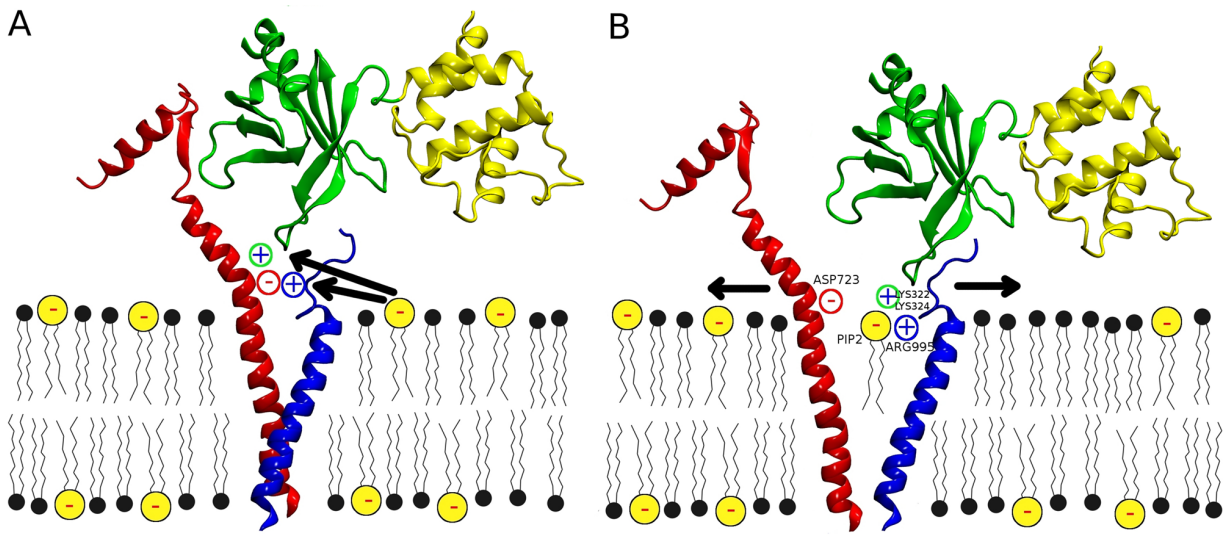

Figure 5. Schematic representation of (A) the suggested PIP2-talin-integrin interaction, and (B) the suggested activation of the integrin complex mediated by PIP2 and talin. DOPC is depicted with a black and PIP2 with a yellow headgroup. Arrows in the panels A and B indicate the direction of PIP2 movement and possible helix dissociation caused by the breaking of the Arg995-Asp723 salt bridge.

whether it has an active role in the process. In the simulations without talin, Arg995 in integrin αIIb did not form contacts to PIP2 lipids, yet its neighboring residue Lys994 was constantly in contact with a PIP2 lipid (Figure 1 and Table S1). This suggests that talin is not required for PIP2 lipids to localize near the integrin dimer and the Arg995-Asp723 salt bridge. However, the binding of talin to β3 integrin may expose the Arg995-Asp723 salt bridge to an attack by PIP2.

4. CONCLUSIONS

Schematic representation of our main results is shown in Figure 5. We propose that PIP2 can have an impact on integrin activation through interaction with talin and Arg995, in a manner which leads to a breakage of the Arg995-Asp723 salt bridge. Our simulations did not show other clear signs of structural changes in the interaction between the αIIb and β3 chains after the breakdown of the ionic bond.

The integrin activation process involves multiple cytoplasmic proteins, and it is possible that the system simulated here is too simplified for the evaluation of further dissociation of the integrin tails and integrin activation. Nevertheless, the fact that experimentally it has been well established that the lack of this salt bridge leads to integrin activation renders our considerations reasonable. Moreover, we recognized other regions of integrin involved in the interactions with PIP2 that might be of high importance in the conformational changes of integrin complexes.

■ ASSOCIATED CONTENT

Supporting Information

The Supporting Information is available free of charge on the ACS Publications website at DOI: 10.1021/acs.jpcb.5b06457.

Structures of the lipids considered and additional data (PDF)

■ AUTHOR INFORMATION

Corresponding Author

*E-mail: tomasz.rog@gmail.com. Tel.: +358 40 198 1010. Fax: +358 3 3115 3015.

Author Contributions

#The two leading authors contributed equally to this work.

Notes

The authors declare no competing financial interest.

■ ACKNOWLEDGMENTS

This work was supported by the Academy of Finland (Center of Excellence program, project no. 272130 (IV); grants 136288 and 273192 (VPH)), the European Research Council (Advanced Grant CROWDED-PRO-LIPIDS (IV)), the Competitive Research Funding of the Tampere University Hospital (VH), and the Sigrid Juselius Foundation (IV). CSC−IT Center for Science (Espoo, Finland) is acknowledged for computational resources. Additionally, the Tampere Graduate Program in Biomedicine and Biotechnology (S.K.) and the Graduate School program of Tampere University of Technology (S.R.) are thanked for financial support. This work was granted access to the HPC resources of EPCC made available within the Distributed European Computing Initiative by the PRACE-2IP, receiving funding from the European Community's Seventh Framework Programme (FP7/2007−2013) under grand agreement no. RI-283493.

■ REFERENCES

(1) Desgrosellier, J. S.; Cheresh, D. A. Integrins in Cancer: Biological Implications and Therapeutic Opportunities. *Nat. Rev. Cancer* **2010**, *10*, 9−22.

(2) Anthis, N. J.; Campbell, I. D. The Tail of Integrin Activation. *Trends Biochem. Sci.* **2011**, *36*, 191−198.

(3) Hynes, R. O. Integrins: Bidirectional, Allosteric Signaling Machines. *Cell* **2002**, *110*, 673−687.

(4) Shattil, S. J.; Kim, C.; Ginsberg, M. H. The Final Steps of Integrin Activation: The End Game. *Nat. Rev. Mol. Cell Biol.* **2010**, *11*, 288−300.

DOI: 10.1021/acs.jpcb.5b06457
J. Phys. Chem. B 2015, 119, 12381−12389

(5) Hughes, P. E.; Diaz-Gonzalez, F.; Leong, L.; Wu, C.; McDonald, J. A.; Shattil, S. J.; Ginsberg, M. H. Breaking the Integrin Hinge. A Defined Structural Constraint Regulates Integrin Signaling. *J. Biol. Chem.* **1996**, *271*, 6571−6574.
(6) Ghevaert, C.; Salsmann, A.; Watkins, N. A.; Schaffner-Reckinger, E.; Rankin, A.; Garner, S. F.; Stephens, J.; Smith, G. A.; Debili, N.; Vainchenker, W.; de Groot, P. G.; Huntington, J. A.; Laffan, M.; Kieffer, N.; Ouwehand, W. H. A Nonsynonymous SNP in the ITGB3 Gene Disrupts the Conserved Membrane-Proximal Cytoplasmic Salt Bridge in the AlphaIIb/beta3 Integrin and Cosegregates Dominantly with Abnormal Proplatelet Formation and Macrothrombocytopenia. *Blood* **2008**, *111*, 3407−3414.
(7) Nurden, A. T.; Pillois, X.; Wilcox, D. A. Glanzmann Thrombasthenia: State of the Art and Future Directions. *Semin. Thromb. Hemostasis* **2013**, *39*, 642−655.
(8) Guan, S.; Tan, S.-M.; Li, Y.; Torres, J.; Uzel, G.; Xiang, L.; Law, S. K. A. Characterization of Single Amino Acid Substitutions in the β2 Integrin Subunit of Patients with Leukocyte Adhesion Deficiency (LAD)-1. *Blood Cells, Mol., Dis.* **2015**, *54*, 177−182.
(9) Burridge, K.; Connell, L. A New Protein of Adhesion Plaques and Ruffling Membranes. *J. Cell Biol.* **1983**, *97*, 359−367.
(10) Moser, M.; Legate, K. R.; Zent, R.; Fässler, R. The Tail of Integrins, Talin, and Kindlins. *Science* **2009**, *324*, 895−899.
(11) Critchley, D. R. Biochemical and Structural Properties of the Integrin-Associated Cytoskeletal Protein Talin. *Annu. Rev. Biophys.* **2009**, *38*, 235−254.
(12) Calderwood, D. A.; Zent, R.; Grant, R.; Rees, D. J. G.; Hynes, R. O.; Ginsberg, M. H. The Talin Head Domain Binds to Integrin β Subunit Cytoplasmic Tails and Regulates Integrin Activation. *J. Biol. Chem.* **1999**, *274*, 28071−28074.
(13) Tadokoro, S.; Shattil, S. J.; Eto, K.; Tai, V.; Liddington, R. C.; de Pereda, J. M.; Ginsberg, M. H.; Calderwood, D. A. Talin Binding to Integrin ß Tails: a Final Common Step in Integrin Activation. *Science* **2003**, *302*, 103−106.
(14) Ye, F.; Snider, A. K.; Ginsberg, M. H. Talin and Kindlin: the One-Two Punch in Integrin Activation. *Frontiers Med.* **2014**, *8*, 6−16.
(15) García-Alvarez, B.; de Pereda, J. M.; Calderwood, D. A.; Ulmer, T. S.; Critchley, D.; Campbell, I. D.; Ginsberg, M. H.; Liddington, R. C. Structural Determinants of Integrin Recognition by Talin. *Mol. Cell* **2003**, *11*, 49−58.
(16) Wegener, K. L.; Partridge, A. W.; Han, J.; Pickford, A. R.; Liddington, R. C.; Ginsberg, M. H.; Campbell, I. D. Structural Basis of Integrin Activation by Talin. *Cell* **2007**, *128*, 171−182.
(17) Kim, C.; Ye, F.; Hu, X.; Ginsberg, M. H. Talin Activates Integrins by Altering the Topology of the β Transmembrane Domain. *J. Cell Biol.* **2012**, *197*, 605−611.
(18) Vinogradova, O.; Velyvis, A.; Velyviene, A.; Hu, B.; Haas, T. A.; Plow, E. F.; Qin, J. A. Structural Mechanism of Integrin αIIbβ3 "Inside-Out" Activation as Regulated by Its Cytoplasmic Face. *Cell* **2002**, *110*, 587−597.
(19) Saltel, F.; Mortier, E.; Hytönen, V. P.; Jacquier, M.-C.; Zimmermann, P.; Vogel, V.; Liu, W.; Wehrle-Haller, B. New PI(4,5)P2- and Membrane Proximal Integrin-Binding Motifs in the Talin Head Control Beta3-Integrin Clustering. *J. Cell Biol.* **2009**, *187*, 715−731.
(20) Moore, D. T.; Nygren, P.; Jo, H.; Boesze-Battaglia, K.; Bennett, J. S.; DeGrado, W. F. Affinity of Talin-1 for the β3-Integrin Cytosolic Domain is Modulated by Its Phospholipid Bilayer Environment. *Proc. Natl. Acad. Sci. U. S. A.* **2012**, *109*, 793−798.
(21) Martel, V.; Racaud-Sultan, C.; Dupe, S.; Marie, C.; Paulhe, F.; Galmiche, A.; Block, M. R.; Albiges-Rizo, C. Conformation, Localization, and Integrin Binding of Talin Depend on Its Interaction with Phosphoinositides. *J. Biol. Chem.* **2001**, *276*, 21217−21227.
(22) Goksoy, E.; Ma, Y.-Q.; Wang, X.; Kong, X.; Perera, D.; Plow, E. F.; Qin, J. Structural Basis for the Autoinhibition of Talin in Regulating Integrin Activation. *Mol. Cell* **2008**, *31*, 124−133.
(23) Song, X.; Yang, J.; Hirbawi, J.; Ye, S.; Perera, H. D.; Goksoy, E.; Dwivedi, P.; Plow, E. F.; Zhang, R.; Qin, J. A Novel Membrane-Dependent on/off Switch Mechanism of Talin FERM Domain at Sites of Cell Adhesion. *Cell Res.* **2012**, *22*, 1533−1545.
(24) McLaughlin, S.; Wang, J.; Gambhir, A.; Murray, D. PIP(2) and Proteins: Interactions, Organization, and Information Flow. *Annu. Rev. Biophys. Biomol. Struct.* **2002**, *31*, 151−175.
(25) Xu, C.; Watras, J.; Loew, L. M. Kinetic Analysis of Receptor-Activated Phosphoinositide Turnover. *J. Cell Biol.* **2003**, *161*, 779−791.
(26) Ling, K.; Doughman, R. L.; Firestone, A. J.; Bunce, M. W.; Anderson, R. A. Type Iγ Phosphatidylinositol Phosphate Kinase Targets and Regulates Focal Adhesions. *Nature* **2002**, *420*, 89−93.
(27) Di Paolo, G.; Pellegrini, L.; Letinic, K.; Cestra, G.; Zoncu, R.; Voronov, S.; Chang, S.; Guo, J.; Wenk, M. R.; De Camilli, P. Recruitment and Regulation of Phosphatidylinositol Phosphate Kinase Type 1 Gamma by the FERM Domain of Talin. *Nature* **2002**, *420*, 85−89.
(28) Sun, Y.; Thapa, N.; Hedman, A. C.; Anderson, R. A. Phosphatidylinositol 4,5-Bisphosphate: Targeted Production and Signaling. *BioEssays* **2013**, *35*, 513−522.
(29) Kwiatkowska, K. One Lipid, Multiple Functions: How Various Pools of PI(4,5)P2 Are Created in the Plasma Membrane. *Cell. Mol. Life Sci.* **2010**, *67*, 3927−3946.
(30) van den Bout, I.; Divecha, N. PIP5K-Driven PtdIns(4,5)P2 Synthesis: Regulation and Cellular Functions. *J. Cell Sci.* **2009**, *122*, 3837−3850.
(31) Chinthalapudi, K.; Rangarajan, E. S.; Patil, D. N.; George, E. M.; Brown, D. T.; Izard, T. Lipid Binding Promotes Oligomerization and Focal Adhesion Activity of Vinculin. *J. Cell Biol.* **2014**, *207*, 643−656.
(32) Raghunathan, V.; Mowery, P.; Rozycki, M.; Lindberg, U.; Schutt, C. Structural Changes in Profilin Accompany its Binding to Phosphatidylinositol, 4,5-Bisphosphate. *FEBS Lett.* **1992**, *297*, 46−50.
(33) Hirao, M.; Sato, N.; Kondo, T.; Yonemura, S.; Monden, M.; Sasaki, T.; Takai, Y.; Tsukita, S.; Tsukita, S. Regulation Mechanism of ERM (Ezrin/Radixin/Moesin) Protein/Plasma Membrane Association: Possible Involvement of Phosphatidylinositol Turnover and Rho-Dependent Signaling Pathway. *J. Cell Biol.* **1996**, *135*, 37−51.
(34) Li, L.; Shi, X.; Guo, X.; Li, H.; Xu, C. Ionic Protein-Lipid Interaction at the Plasma Membrane: What Can the Charge Do? *Trends Biochem. Sci.* **2014**, *39*, 130−140.
(35) Kuo, W.; Herrick, D. Z.; Cafiso, D. S. Phosphatidylinositol 4,5 Bisphosphate Alters Synaptotagmin 2 Membrane Docking and Drives Opposing Bilayers Closer Together. *Biochemistry* **2011**, *50*, 2633−2641.
(36) Steringer, J. P.; Bleicken, S.; Andreas, H.; Zacherl, S.; Laussmann, M.; Temmerman, K.; Contreras, F. X.; Bharat, T. A.; Lechner, J.; Müller, H. M.; Briggs, J. A.; García-Sáez, A. J.; Nickel, W. Phosphatidylinositol 4,5-Bisphosphate (PI(4,5)P2)-Dependent Oligomerization Offibroblast Growth Factor 2 (FGF2) Triggers the Formation of a Lipidic Membrane Pore Implicated in Unconventional Secretion. *J. Biol. Chem.* **2012**, *287*, 27659−27669.
(37) Coskun, Ü.; Grzybek, M.; Drechsel, D.; Simons, K. Regulation of Human EGF Receptor by Lipids. *Proc. Natl. Acad. Sci. U. S. A.* **2011**, *108*, 9044−9048.
(38) Coskun, U.; Simons, K. Cell Membranes: the Lipid Perspective. *Structure* **2011**, *19*, 1543−1548.
(39) Pöyry, S.; Cramariuc, O.; Postila, P. A.; Kaszuba, K.; Sarewicz, M.; Osyczka, A.; Vattulainen, I.; Róg, T. Atomistic Simulations Indicate Cardiolipin to Have an Integral Role in the Structure of the Cytochrome bc1 Complex. *Biochim. Biophys. Acta, Bioenerg.* **2013**, *1827*, 769−778.
(40) Sali, A.; Blundell, T. L. Comparative Protein Modelling by Satisfaction of Spatial Restraints. *J. Mol. Biol.* **1993**, *234*, 779−815.
(41) Elliott, P. R.; Goult, B. T.; Kopp, P. M.; Bate, N.; Grossmann, J. G.; Roberts, G. C. K.; Critchley, D. R.; Barsukov, I. L. The Structure of the Talin Head Reveals a Novel Extended Conformation of the FERM Domain. *Structure* **2010**, *18*, 1289−1299.
(42) Goult, B. T.; Bouaouina, M.; Elliott, P. R.; Bate, N.; Patel, B.; Gingras, A. R.; Grossmann, J. G.; Roberts, G. C. K.; Calderwood, D. A.; Critchley, D. R.; Barsukov, I. L. Structure of a Double Ubiquitin-

DOI: 10.1021/acs.jpcb.5b06457
J. Phys. Chem. B 2015, 119, 12381−12389

Like Domain in the Talin Head: a Role in Integrin Activation. *EMBO J.* **2010**, *29*, 1069−1080.
(43) Anthis, N. J.; Wegener, K. L.; Ye, F.; Kim, C.; Goult, B. T.; Lowe, E. D.; Vakonakis, I.; Bate, N.; Critchley, D. R.; Ginsberg, M. H.; Campbell, I. D. The Structure of an Integrin/Talin Complex Reveals the Basis of Inside-Out Signal Transduction. *EMBO J.* **2009**, *28*, 3623−3632.
(44) Lau, T.-L.; Kim, C.; Ginsberg, M. H.; Ulmer, T. S. The Structure of the Integrin αIIbβ3 Transmembrane Complex Explains Integrin Transmembrane Signalling. *EMBO J.* **2009**, *28*, 1351−1361.
(45) Yang, J.; Ma, Y.-Q.; Page, R. C.; Misra, S.; Plow, E. F.; Qin, J. Structure of an Integrin αIIbβ3 Transmembrane-Cytoplasmic Heterocomplex Provides Insight into Integrin Activation. *Proc. Natl. Acad. Sci. U. S. A.* **2009**, *106*, 17729−17734.
(46) Metcalf, D. G.; Moore, D. T.; Wu, Y.; Kielec, J. M.; Molnar, K.; Valentine, K. G.; Wand, A. J.; Bennett, J. S.; DeGrado, W. F. NMR Analysis of the αIIbβ3 Cytoplasmic Interaction Suggests a Mechanism for Integrin Regulation. *Proc. Natl. Acad. Sci. U. S. A.* **2010**, *107*, 22481−22486.
(47) Jorgensen, W. L.; Tirado-Rives, J. The OPLS [Optimized Potentials for Liquid Simulations] Potential Functions for Proteins, Energy Minimizations for Crystals of Cyclic Peptides and Crambin. *J. Am. Chem. Soc.* **1988**, *110*, 1657−1666.
(48) Maciejewski, A.; Pasenkiewicz-Gierula, M.; Cramariuc, O.; Vattulainen, I.; Rog, T. Refined OPLS All-Atom Force Field for Saturated Phosphatidylcholine Bilayers at Full Hydration. *J. Phys. Chem. B* **2014**, *118*, 4571−4581.
(49) Kulig, W.; Pasenkiewicz-Gierula, M.; Róg, T. Cholesterol Interactions with *Cis* and *Trans* Unsaturated Phosphatidylcholines. Molecular Dynamics Simulation Study. *Chem. Phys. Lipids* **2015**, DOI: 10.1016/j.chemphyslip.2015.07.002.
(50) Jorgensen, W. L.; Chandrasekhar, J.; Madura, J. D.; Impey, R. W.; Klein, M. L. Comparison of Simple Potential Functions for Simulating Liquid Water. *J. Chem. Phys.* **1983**, *79*, 926−935.
(51) Kaiser, H.-J.; Orłowski, A.; Róg, T.; Nyholm, T. K. M.; Chai, W.; Feizi, T.; Lingwood, D.; Vattulainen, I.; Simons, K. Lateral Sorting in Model Membranes by Cholesterol-Mediated Hydrophobic Matching. *Proc. Natl. Acad. Sci. U. S. A.* **2011**, *108*, 16628−16633.
(52) Orłowski, A.; St-Pierre, J.-F.; Magarkar, A.; Bunker, A.; Pasenkiewicz-Gierula, M.; Vattulainen, I.; Róg, T. Properties of the Membrane Binding Component of Catechol-O-Methyltransferase Revealed by Atomistic Molecular Dynamics Simulations. *J. Phys. Chem. B* **2011**, *115*, 13541−13550.
(53) Hess, B.; Bekker, H.; Berendsen, H. J. C.; Fraaije, J. G. E. M. LINCS: a Linear Constraint Solver for Molecular Simulations. *J. Comput. Chem.* **1997**, *18*, 1463−1472.
(54) Parrinello, M.; Rahman, A. Polymorphic Transitions in Single Crystals: a New Molecular Dynamics Method. *J. Appl. Phys.* **1981**, *52*, 7182−7190.
(55) Bussi, G.; Donadio, D.; Parrinello, M. Canonical Sampling through Velocity Rescaling. *J. Chem. Phys.* **2007**, *126*, 014101.
(56) Essmann, U.; Perera, L.; Berkowitz, M. L.; Darden, T.; Lee, H.; Pedersen, L. G. A Smooth Particle Mesh Ewald Method. *J. Chem. Phys.* **1995**, *103*, 8577−8593.
(57) Hess, B.; Kutzner, C.; van der Spoel, D.; Lindahl, E. GROMACS 4: Algorithms for Highly Efficient, Load-Balanced, and Scalable Molecular Simulation. *J. Chem. Theory Comput.* **2008**, *4*, 435−447.
(58) Kim, C.; Lau, T.-L.; Ulmer, T. S.; Ginsberg, M. H. Interactions of Platelet Integrin αIIb and β3 Transmembrane Domains in Mammalian Cell Membranes and Their Role in Integrin Activation. *Blood* **2009**, *113*, 4747−4753.
(59) Murzyn, K.; Róg, T.; Jezierski, G.; Kitamura, K.; Pasenkiewicz-Gierula, M. Effects of Phospholipid Unsaturation on the Membrane/Water Interface: A Molecular Simulation Study. *Biophys. J.* **2001**, *81*, 170−183.
(60) Humphrey, W.; Dalke, A.; Schulten, K. VMD: visual molecular dynamics. *J. Mol. Graphics* **1996**, *14*, 33−38.
(61) Kalli, A. C.; Campbell, I. D.; Sansom, M. S. P. Multiscale Simulations Suggest a Mechanism for Integrin Inside-Out Activation. *Proc. Natl. Acad. Sci. U. S. A.* **2011**, *108*, 11890−11895.
(62) Kalli, A. C.; Campbell, I. D.; Sansom, M. S. P. Conformational Changes in Talin on Binding to Anionic Phospholipid Membranes Facilitate Signaling by Integrin Transmembrane Helices. *PLoS Comput. Biol.* **2013**, *9*, e1003316.
(63) Kalli, A. C.; Wegener, K. L.; Goult, B. T.; Anthis, N. J.; Campbell, I. D.; Sansom, M. S. P. The Structure of the Talin/Integrin Complex at a Lipid Bilayer: an NMR and MD Simulation Study. *Structure* **2010**, *18*, 1280−1288.
(64) Mehrbod, M.; Trisno, S.; Mofrad, M. R. K. On the Activation of Integrin αIIbβ3: Outside-In and Inside-Out Pathways. *Biophys. J.* **2013**, *105*, 1304−1315.
(65) Provasi, D.; Negri, A.; Coller, B. S.; Filizola, M. Talin-Driven Inside-Out Activation Mechanism of Platelet αIIbβ3 Integrin Probed by Multi-Microsecond, All-Atom Molecular Dynamics Simulations. *Proteins: Struct., Funct., Genet.* **2014**, *82*, 3231−3240.
(66) Kim, C.; Schmidt, T.; Cho, E.-G.; Ye, F.; Ulmer, T. S.; Ginsberg, M. H. Basic amino-acid side chains regulate transmembrane integrin signalling. *Nature* **2011**, *481*, 209−213.
(67) Arcario, M. J.; Tajkhorshid, E. Membrane-Induced Structural Rearrangement and Identification of a Novel Membrane Anchor in Talin F2F3. *Biophys. J.* **2014**, *107*, 2059−2069.

DOI: 10.1021/acs.jpcb.5b06457
J. Phys. Chem. B 2015, 119, 12381−12389

II

Phase Partitioning of GM1 and Its Bodipy-Labeled Analog Determine Their Different Binding to Cholera Toxin

by
S. Rissanen[‡], M. Grzybek[‡], A. Orłowski, T. Róg, O. Cramariuc, I. Levental, C. Eggeling, E. Sezgin & I. Vattulainen.
Frontiers in Physiology, vol 8, no. 252, 2017.

frontiers in Physiology

ORIGINAL RESEARCH
published: 09 May 2017
doi: 10.3389/fphys.2017.00252

Phase Partitioning of GM1 and Its Bodipy-Labeled Analog Determine Their Different Binding to Cholera Toxin

Sami Rissanen[1†], Michal Grzybek[2,3†], Adam Orłowski[1,4], Tomasz Róg[1,5], Oana Cramariuc[1], Ilya Levental[6], Christian Eggeling[7], Erdinc Sezgin[7] and Ilpo Vattulainen[1,5,8*]*

[1] Department of Physics, Tampere University of Technology, Tampere, Finland, [2] Paul Langerhans Institute Dresden of the Helmholtz Centre Munich at the University Clinic Carl Gustav Carus, TU Dresden, Dresden, Germany, [3] German Center for Diabetes Research, Neuherberg, Germany, [4] Department of Physics and Energy, University of Limerick, Limerick, Ireland, [5] Department of Physics, University of Helsinki, Helsinki, Finland, [6] Department of Integrative Biology and Pharmacology, University of Texas Health Science Center, Houston, TX, USA, [7] MRC Human Immunology Unit, Weatherall Institute of Molecular Medicine, University of Oxford, Oxford, UK, [8] MEMPHYS–Center for Biomembrane Physics, University of Southern Denmark, Odense, Denmark

Driven by interactions between lipids and proteins, biological membranes display lateral heterogeneity that manifests itself in a mosaic of liquid-ordered (Lo) or raft, and liquid-disordered (Ld) or non-raft domains with a wide range of different properties and compositions. In giant plasma membrane vesicles and giant unilamellar vesicles, specific binding of Cholera Toxin (CTxB) to GM1 glycolipids is a commonly used strategy to label raft domains or Lo membrane environments. However, these studies often use acyl-chain labeled bodipy-GM1 (bdGM1), whose headgroup accessibility and membrane order or phase partitioning may differ from those of GM1, rendering the interpretation of CTxB binding data quite problematic. To unravel the molecular basis of CTxB binding to GM1 and bdGM1, we explored the partitioning and the headgroup presentation of these gangliosides in the Lo and Ld phases using atomistic molecular dynamics simulations complemented by CTxB binding experiments. The conformation of both GM1 and bdGM1 was shown to be largely similar in the Lo and Ld phases. However, bdGM1 showed reduction in receptor availability when reconstituted into synthetic bilayer mixtures, highlighting that membrane phase partitioning of the gangliosides plays a considerable role in CTxB binding. Our results suggest that the CTxB binding is predominately modulated by the partitioning of the receptor to an appropriate membrane phase. Further, given that the Lo and Ld partitioning of bdGM1 differs from those of GM1, usage of bdGM1 for studying GM1 behavior in cells can lead to invalid interpretation of experimental data.

Keywords: GM1, ganglioside, cholera toxin, membrane domains, molecular dynamics simulations, model membranes

OPEN ACCESS

Edited by:
Rainer A Böckmann, University of Erlangen-Nuremberg, Germany

Reviewed by:
Birgit Strodel, Juelich Research Centre, Germany
Rumiana Dimova, Max Planck Institute of Colloids and Interfaces, Germany

***Correspondence:**
Erdinc Sezgin
erdinc.sezgin@rdm.ox.ac.uk
Ilpo Vattulainen
ilpo.vattulainen@helsinki.fi

† These authors have contributed equally to this work.

Specialty section:
This article was submitted to Membrane Physiology and Membrane Biophysics, a section of the journal Frontiers in Physiology

Received: *01 November 2016*
Accepted: *10 April 2017*
Published: *09 May 2017*

Citation:
Rissanen S, Grzybek M, Orłowski A, Róg T, Cramariuc O, Levental I, Eggeling C, Sezgin E and Vattulainen I (2017) Phase Partitioning of GM1 and Its Bodipy-Labeled Analog Determine Their Different Binding to Cholera Toxin. Front. Physiol. 8:252. doi: 10.3389/fphys.2017.00252

INTRODUCTION

Glycosphingolipids (GSLs) are important constituents of cell membranes, participating in a wide range of biological processes such as recognition of hormones, function of bacterial and viral toxins, cell growth/differentiation, and cell-cell interaction (Karlsson, 1989; Miljan and Bremer, 2002; Ewers et al., 2009). The key to understanding GSL function is the conformational behavior of GSL headgroups. Molecular dynamics (MD) simulations and structural data for the GM1 headgroup-lectin interactions have suggested GSL headgroups to undergo differential conformational selection (Lingwood et al., 2011; Blaum et al., 2016). Interestingly, GSLs are often referred to as being "cryptic," which stems from the observation that their recognition is regulated by the physicochemical properties of the proximal membrane environment, such as membrane fluidity influenced by, e.g., cholesterol concentration and protein content (Shichijo and Alving, 1985; Lampio et al., 1986; Stewart and Boggs, 1993; Kiarash et al., 1994; Mahfoud et al., 2010; Sezgin et al., 2012b). These findings suggest that the conformational landscape of the GSL headgroup is subject to various physical factors such as spatial and electrostatic effects imposed by the headgroup's chemical structure and its molecular interactions. Differential ligand recognition of discrete pools of GSLs in native membrane environments has also been suggested to play an important role in triggering specific signaling pathways (Haselhorst et al., 2001; Blaum et al., 2016). Therefore, it is important to understand the molecular mechanism of how membranes and their physicochemical properties modulate GSL headgroup presentation and availability.

Among the many GSLs, GM1 (**Figure 1A**) is used as a default lipid marker for the nanoscopic cholesterol/sphingomyelin (Chol/SM) enriched, liquid-ordered (Lo) membrane domains usually referred to as "membrane rafts," opposing liquid-disordered (Ld) environments (Harder et al., 1998; Bacia et al., 2005; Ewers et al., 2009; Sezgin et al., 2012a,b). In cell membranes, cell-derived giant plasma membrane vesicles (GPMVs), and synthetic giant unilamellar vesicles (GUVs), GM1 detection by fluorescently labeled Cholera Toxin (CTxB) is a well-established tool for monitoring Lo membrane domains. Alternative and more direct reporters of GM1 are fluorescent analogs such as the acyl chain-bodipy labeled GM1 (bdGM1, **Figure 1A**). However, these GM1 analogs are not identical to native GM1 in terms of their biochemical and biophysical behavior, and it is not clear whether the conformational distributions of GM1 and bdGM1 headgroups are alike, as they should be if bdGM1 were used to consider CTxB binding with GM1. Further, bdGM1 is excluded from Lo domains in GUVs, while it is equally distributed in GPMVs (Sezgin et al., 2012a,b). Toxin binding, however, occurs in both systems exclusively in the Ld phase, which gives rise to a question of the importance of membrane phase in CTxB binding. Given the importance of GM1-CTxB binding in initiation of specific signaling pathways at cell surfaces, determination of the principles guiding the binding of CTxB to GM1 and bdGM1 is called for.

Here, we used extensive atomistic MD simulations supported with CTxB binding experiments to investigate how the binding of CTxB to its receptor (GM1, bdGM1) is modulated by the receptor's membrane phase partitioning. The results highlight the importance of ganglioside partitioning in CTxB binding and the great care needed in interpreting results based on the use of labeled ganglioside receptors.

RESULTS

Atomistic Simulations Highlight Subtle Differences between GM1 and bdGM1 Headgroup Conformations

CTxB is a pentameric protein with five GM1 binding sites (Merritt et al., 1994). Therefore, geometrical compatibility between CTxB and GM1 molecules in the plane of a membrane is essential for efficient binding (Ewers et al., 2009). Given this, any structural modifications or GM1 reorganization in the membrane plane could compromise the binding. This would likely take place if a fluorophore were attached to GM1, which is the case with bdGM1, or if the state of liquid ordering of the surrounding lipid matrix would change, which is the case if CTxB binding would take place in Ld instead of Lo. To explore the consequences of these scenarios, we performed all-atom molecular dynamics (MD) simulations on GM1 and bdGM1 (**Figure 1A**) in both Lo (N-stearoyl-D-erythro-sphingosylphosphorylcholine/cholesterol (SSM/Chol)) and Ld (1,2-dioleoyl-sn-glycero-3-phosphocholine (DOPC)) membranes. Lo membranes were composed of ∼46 mol% Chol, ∼46 mol% SSM, and ∼8 mol% GM1 (or bdGM1). Ld membranes were comprised of ∼92 mol% DOPC with about 8 mol% GM1 (or bdGM1). Both Lo and Ld membranes were studied both with and without CTxB (see Table S1, see Supplementary Information (SI)). The key microsecond-simulations were carried out in three replicas. Details of the simulation models, simulations, and experimental methods and materials are discussed in SI.

First we analyzed how the GM1 headgroups are localized and oriented. We therefore calculated the mass density profiles of atoms from the GM1 headgroup and its components subdivided in thumb, forefinger, and wrist subunits (**Figures 1B,C** and Figures S1, S2). No significant differences between the Lo and Ld environments were observed in the localization of the GM1 headgroups for either GM1 or bdGM1, except for a minor shift toward the membrane core for bdGM1 in the Lo phase (**Figure 1**). This effect was strongest for the thumb and the forefinger rings of the bdGM1 headgroup (Figure S2). The results for the mass density profiles were confirmed by data for the solvent accessible surface area (SASA), which is the molecule's surface area that is accessible to solvent (in this case, water) (for the definition of SASA, see SI). SASA provides an estimate for the exposure of the GM1 headgroup to the water phase above the bilayer core and therefore indirectly indicates to what extent the headgroup is oriented toward the water phase. Only for bdGM1 a pronounced SASA change of ∼0.43 nm^2 per molecule between Ld and Lo was observed, indicating a higher exposure of the bdGM1 headgroup in Ld (**Figure 1D** and Table S2). The difference in SASA for bdGM1 was mainly caused by a change in the orientation of the thumb region (Figure S3). Overall, these

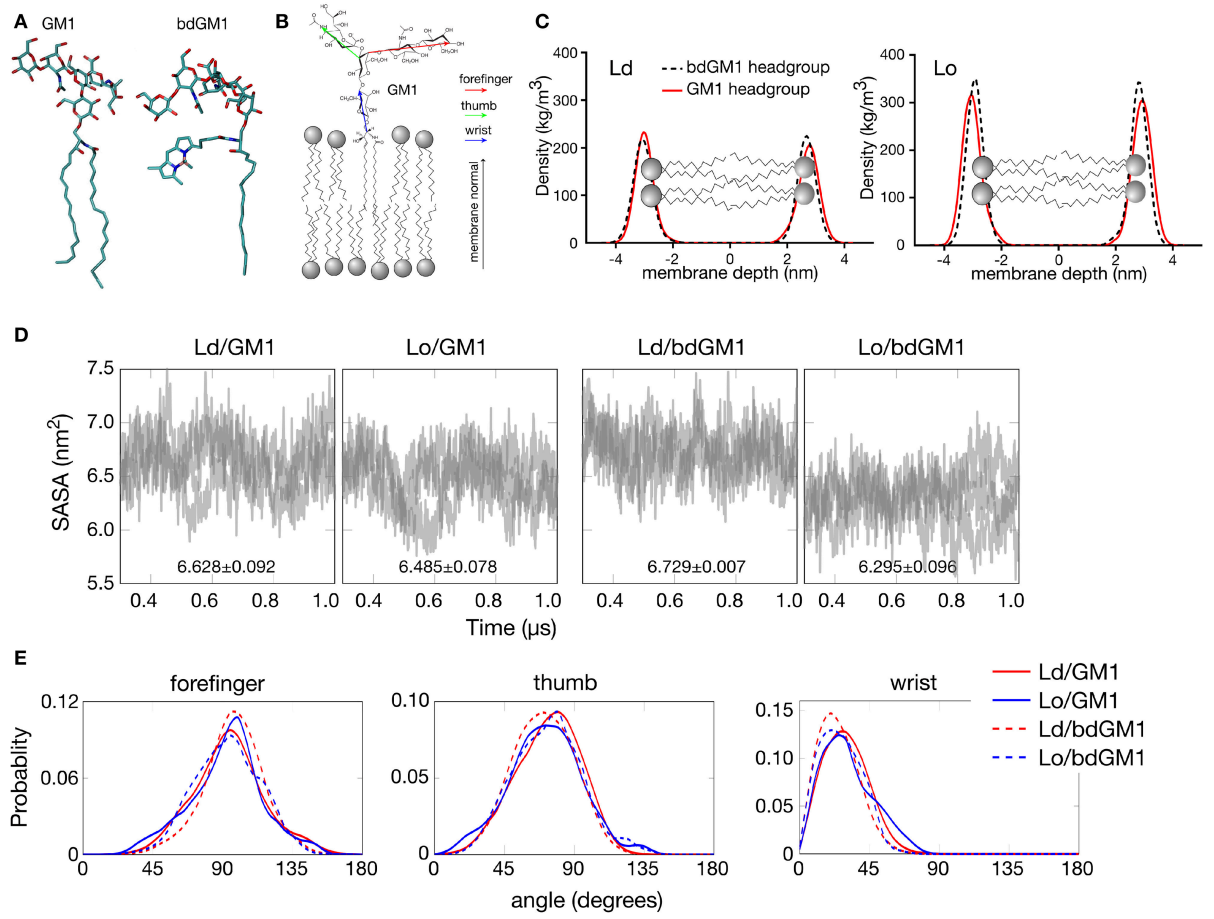

FIGURE 1 | Headgroup geometry of GM1 and bdGM1 in the Lo and Ld phases. (A) Snapshot of GM1 and bdGM1 taken from the atomistic MD simulations. **(B)** Illustration of the vectors representing the different GM1 headgroup subunits. **(C)** Density profiles of atoms from GM1 headgroups in membranes that are in the Ld and Lo phases (in systems 5–8, Table S1 without CTxB). Here, a value of zero in membrane depth corresponds to the bilayer center. The differences in the absolute density values for the GM1 headgroups are attributed to the presence of cholesterol, which is significantly smaller than the other surrounding lipids, thus reducing the dimensions of the simulation box in the Lo system. **(D)** Results for the solvent accessible surface area (SASA) calculated per molecule for GM1 and bdGM1 headgroups (see also Figure S3). In each graph, the results of three replicas are shown by means of gray transparent lines. **(E)** Angle distributions in Ld and Lo for the different subunits of GM1 and bdGM1. The angle is defined with respect to the membrane normal, thus a value of zero corresponds to a situation where the vector stands upright along membrane normal, and an angle of 90° describes a vector lying along the membrane surface. **(D,E)** are based on data with CTxB, but the results have been computed from the leaflet not bound to CTxB.

observations may partially explain the preferential CTxB binding of bdGM1 in the Ld phase of phase separated model membranes (Sezgin et al., 2012b).

To quantitatively determine whether these differences stem from altered headgroup conformations, we calculated the angles between membrane normal and vectors of the respective GM1 headgroup components. Here, we found that for both GM1 and bdGM1 the conformation of the headgroup is very similar—the forefinger is tilted toward the membrane, while the thumb and the wrist subunits are more exposed to water (**Figure 1E** and Table S3)—largely regardless of the molecular structure and membrane environment. However, while the overall changes between the four systems are relatively small (**Figure 1E** and Table S3), there are a few interesting features that may be involved in the altered GM1-CTxB binding and thus need to be highlighted. First, the bodipy label orients the ganglioside wrist subunit toward the water phase by ∼5°, and this result holds in both lipid environments when compared to unlabeled GM1. Second, if the bodipy marker is attached to GM1, the thumb part of the GM1 headgroup is tilted slightly (by ∼3°) toward the water phase in Ld, but (by ∼2°) toward the membrane in Lo, which largely explains the difference observed in the mass density profile in the Lo phase (**Figure 1C**). The forefinger subunit of bdGM1 is oriented slightly more toward the membrane than the forefinger of GM1. In the case of bdGM1, this orientation in favor of the membrane surface is larger in Ld than in Lo. In

the case of GM1, the forefinger in Lo tilts to some extent more toward the membrane surface than in Ld. These differences are not substantial but anyhow evident. The majority of the change in the forefinger orientation is caused by the terminal sugar residue (β-galactose; Figure S4, and Table S4).

The results in **Figure 1E** suggest that the conformation of GM1 with respect to the membrane plane is not dependent on cholesterol. Meanwhile, recent MD simulations on POPC/cholesterol/GM1 membranes (with a ratio of 75/20/5) and experiments are in favor of the opposite view (Lingwood et al., 2011). We therefore explored this matter by considering the conformation of GM1 in a DOPC/cholesterol/GM1 membrane with ∼46 mol% DOPC, ∼46 mol% cholesterol, and about 8 mol% GM1, where the relative amounts of these lipid types match those used in the present Lo bilayers with SSM, cholesterol, and GM1. The results (Figure S5) show that in the DOPC/cholesterol/GM1 membrane the headgroup of GM1 is strongly tilted against the membrane, in agreement with ref. (Lingwood et al., 2011), the tilt angle of the GM1 headgroup in this case being much larger than in SSM/cholesterol/GM1 membranes. Clearly, the GM1 headgroup orients in a cholesterol-dependent manner, however the significance of cholesterol depends on the lipid pool hosting cholesterol.

The observed conformational differences prompted us to follow the availability of the headgroup for ligand binding. We therefore simulated the actual binding of CTxB to both GM1 and bdGM1 in Ld and Lo environments (snapshots taken from simulations shown in **Figure 2A**). As **Figure 2B** illustrates, the binding of CTxB to the membranes took place rapidly in about 20-100 ns. The number of hydrogen bonds established between the protein and the respective GM1 molecules was used as a correlate for the binding affinity (**Figures 2B,C** and Table S5). For GM1, this analysis revealed a greater number of CTxB-GM1 hydrogen bonds in the Ld phase, suggesting a slight preference for CTxB binding to the Ld phase (**Figure 2C**, and Tables S5). For bdGM1, the effect was similar but quite a bit weaker. These conclusions are supported by consideration of contacts between CTxB and GM1 (or bdGM1), (Table S6), using 0.35 nm as the maximum distance for a contact. This analysis revealed that the number of GM1/bdGM1 bound to CTxB was 8.9 ± 0.7 (GM1 in Ld), 6.8 ± 1.0 (GM1 in Lo), 5.6 ± 1.4 (bdGM1 in Ld), and 6.9 ± 0.9 (bdGM1 in Lo).

Experiments Point to Differences in Membrane Phase Partitioning

The high specificity of CTxB binding to GM1 is commonly used to detect the presence of raft or Lo domains in cellular and synthetic membranes, respectively. However, based on our MD simulation data, slightly more efficient binding of CTxB to GM1 in the Ld environment is expected. One possible explanation for the discrepancy is that CTxB would bind GM1 preferentially in an Ld domain, but then the complex would move into an Lo domain, as suggested previously (Bacia et al., 2005). To test this possibility, we followed the binding of Alexa-labeled CTxB to GM1-containing GUVs and GPMVs immediately after addition of CTxB. In both model membranes, CTxB bound rapidly and largely to the Lo phase without obvious initial binding to the Ld phase (**Figures 3A,B** and Supplementary Movies 1, 2). Thus, it is unlikely that the experimentally observed binding to the Lo phase is a result of initial/stronger recognition of the GM1 molecules in the Ld phase by CTxB and subsequent partitioning of the GM1-CTxB complex into the Lo phase.

An alternative explanation for the observed discrepancy is that CTxB binds its lipid receptor GM1 preferentially in Lo

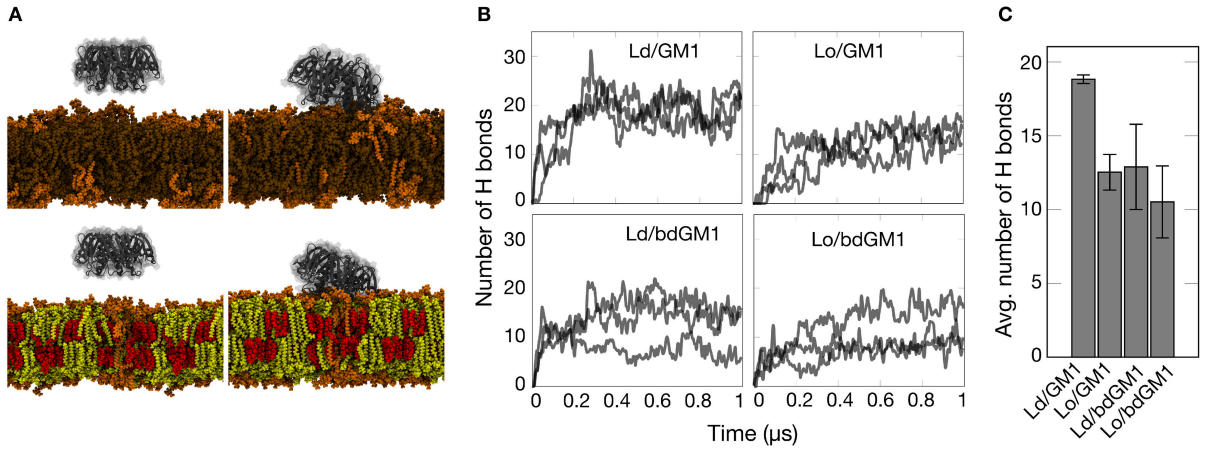

FIGURE 2 | Simulation results gauging the dependence of GM1-CTxB binding on membrane environment in simulations of systems with CTxB. (A) Snapshots of simulated membrane systems at 0 (left) and 500 ns (right) in Ld (upper) and Lo (lower) phases (Lo composition: 46 mol% Chol, 46 mol% SSM, and 8 mol% GM1 (or bdGM1); Ld composition: 92 mol% DOPC and 8 mol% GM1 (or bdGM1)). DOPC is depicted in brown, cholesterol in red, SSM in yellow, and GM1 in orange. Water molecules are not shown for clarity. **(B)** Time course of the number of hydrogen bonds established between GM1 species and CTxB. Each case was simulated three times. **(C)** Average number of hydrogen bonds (H bonds) established between GM1 species and CTxB between 300 and 1,000 ns. The error bar represents the standard error.

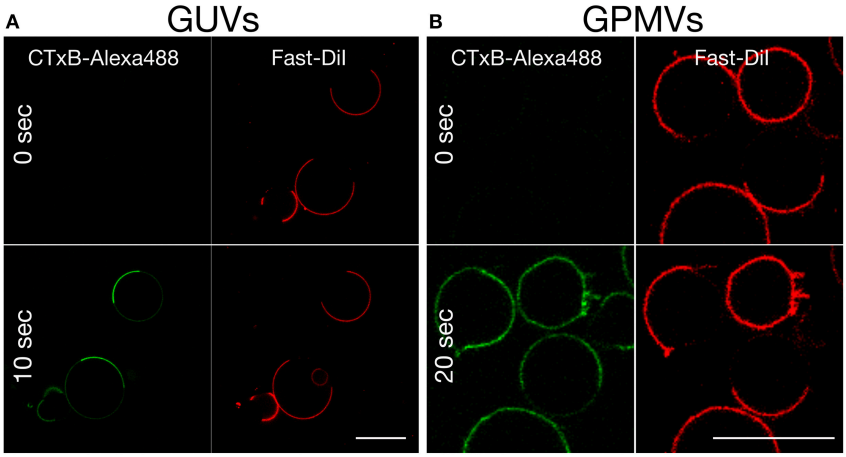

FIGURE 3 | Time-lapse confocal imaging of the equatorial plane of (A) phase separated GUVs (DOPC:SSM:Chol:GM1 = 40:40:20:0.1) and **(B)** phase separated GPMVs prepared from RBL cells (labeled with the Ld marker Fast-DiI, red), following the addition (at time 0) and rapid binding of Alexa 488-labeled CTxB (green) to GM1. Binding occurs right after CTxB addition in the Lo phase. Scale bar 10 μm. Experiments were done at 10°C. Miscibility temperature for GPMVs is around 15°C.

domains, once coexisting Ld/Lo phases are available. In order to selectively monitor CTxB binding to its lipid receptor in pure Ld or Lo membrane only, we used synthetic liposomes consisting of either DOPC (Ld) or SM/Chol (Lo) and 0.1 mol% of either GM1 or bdGM1. These liposomes were then used as capture specimen in electrochemiluminescence ELISA assays to quantitatively evaluate CTxB binding (Kolondra et al., 2010; Lingwood et al., 2011). Equal GSL content in liposomes was validated by thin-layer chromatography (TLC) analysis (Figure S6). In all systems we observed similar equilibrium binding affinities of ∼15 nM, independent of lipid composition or GM1 acyl bodipy modification (**Figure 4**, and **Table 1**). However, we observed obvious differences in Bmax (maximum binding capacity) values. In Ld liposomes, bdGM1 showed Bmax to decrease ∼20% compared to native GM1. In Lo domains, the decrease was ∼35–40%. In our experimental conditions this means that less CTxB were bound to the bdGM1 vesicles than to those containing GM1. Since in all the studied systems the GM1 amounts were similar, the decreased Bmax values suggest that in the respective systems, a number of bdGM1 molecules remain hidden from CTxB. Although these observations are consistent with the trends predicted by atomistic MD simulations (**Figures 2B,C**), there is reason to keep in mind that the headgroup angle distribution and SASA of GM1 and bdGM1 showed only slight differences, and therefore the results suggest that other factors, e.g., ganglioside oligomerization may be involved (Shi et al., 2007).

Our simulations and experimental measurements document that, although GM1 headgroup conformation is slightly modulated by the surrounding lipid environment, it is not the discriminating factor for the differences in CTxB binding to GM1 and its fluorescent analog. CTxB binding to GM1 shows a clear preference for the Lo phase in both GUVs and GPMVs

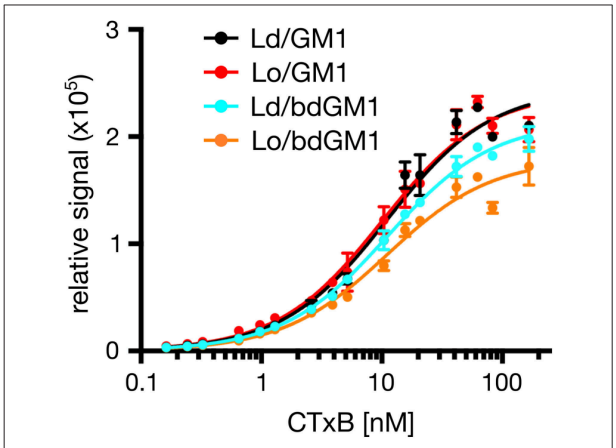

FIGURE 4 | Representative plot showing binding of Alexa 594-labeled CTxB to liposomes containing 0.1 mol % GM1 or bdGM1.

TABLE 1 | Results for characteristics of Alexa594-labeled CTxB binding to liposomes containing 0.1 mol% GM1 or bdGM1 ($n = 3$).

CTxB-Alexa594	Kd [nM]	Bmax
Ld+GM1	16.56 ± 6.11	97.95% ± 1.93
Lo+GM1	15.59 ± 5.80	100%
Ld+bdGM1	13.48 ± 5.34	79.76% ± 7.23
Lo+bdGM1	14.85 ± 4.06	63.76% ± 10.52

The Bmax was normalized to the highest value in each experiment.

(**Figure 3**), which in respect to slight headgroup conformation changes and comparable CTxB binding affinities to these molecules can only be explained by the enrichment of the GM1

lipids in the ordered phases (Morrow et al., 1995; Simons and Ikonen, 1997).

DISCUSSION AND CONCLUDING REMARKS

Our atomistic MD simulation data confirmed that GM1 headgroup localization and geometry is sensitive to membrane environment (**Figures 1**, **2**). Surprisingly, the presence of the bodipy-label at the acyl chain of GM1 caused a deeper penetration of bdGM1 into the membrane in the Lo domains (**Figures 1C,E**), demonstrated by decreased SASA and the density distribution of the forefinger structure (**Figures 1B–E** and Figures S2, S4, S5). The overall changes could thus render the bdGM1 headgroup partially inaccessible to CTxB. Our observations are consistent with previously reported NMR analysis in synthetic membranes, which showed that conformation and motional order of the complex ganglioside headgroups is influenced by factors such as natural variation in the glycolipid hydrocarbon chains, membrane fluidity, temperature, or the presence of cholesterol (Barber et al., 1994; Morrow et al., 1995; Singh et al., 1995). Interestingly, as presented by our simulations, the observed changes in GM1 headgroup conformation indicate a preference for CTxB binding to GM1 in the Ld environment rather than Lo (**Figure 2**). This result is in line with previously published atomistic MD simulations of GM1 in POPC or POPC/Chol membranes, which showed that GM1 headgroup adopts a tilted conformation in the presence of cholesterol, resulting in decreased recognition by CTxB (Lingwood et al., 2011). However, the effect of membrane phase on CTxB-GM1 interaction was weak in the present simulations, and this lack of a strong effect was validated experimentally by measuring binding of CTxB to synthetic liposomes in various phases (**Table 1** and **Figure 4**). The binding data showed that the overall binding of CTxB to bdGM1 was reduced in comparison to GM1 especially in the Lo liposomes (**Figure 4**). Our data therefore confirm at the molecular level that the presence of the fluorophore on the acyl chain, rather than changing the headgroup geometry, largely excludes the bdGM1 molecules from the Lo membrane environments, where native GM1 molecules seemed to be enriched (Komura et al., 2016). Therefore, CTxB binding to GM1 occurs more in the ordered membranes, while binding to bdGM1 takes place preferably, if not exclusively, in the disordered domains (Sezgin et al., 2012b, 2015). The conclusion that the partitioning of bdGM1 does not properly represent the phase partitioning of GM1 is consistent with recent findings by Fricke and Dimova (Fricke and Dimova, 2016) published during the review of this paper.

Our experiments reveal that the recognition of bdGM1 by CTxB is decreased in comparison to native GM1 (**Figure 4**). Meanwhile, the MD simulations do not suggest strong structural changes within the headgroup region of the studied GM1 molecules. Therefore, it seems evident that the observed differences in CTxB recognition do not stem primarily from differences in headgroup conformation but rather from other factors such as clustering of GM1 lipids (Shi et al., 2007; Sachl et al., 2015). Consideration of such dynamical processes based on slow lateral diffusion through atom-scale MD simulations remains to be done in future work.

Gangliosides are important receptors at the cell surface, and the use of fluorescently labeled analogs is a common tool to study their cellular functions (Ewers et al., 2009; Sachl et al., 2015; Sezgin et al., 2015; Fricke and Dimova, 2016; Komura et al., 2016). However, the data presented here and in our previous work (Sezgin et al., 2012b) reveal that the presence of the fluorophore affects the behavior of the host lipid molecules. We have shown that acyl-chain labeling of GM1 changes its phase partitioning without strongly affecting ligand binding (here, CTxB). These effects should be considered for proper interpretation of cellular studies employing these and other fluorescent lipid analogs.

AUTHOR CONTRIBUTIONS

All authors designed the experiments. SR, AO, TR, and OC performed the simulations. ES and MG performed the experiments. All authors contributed to the preparation of the manuscript.

FUNDING

ES is supported by EMBO Long Term and Marie Curie Intra-European Fellowships (MEMBRANE DYNAMICS). MG and UC have been funded by the German Federal Ministry of Education and Research (BMBF) grant to the German Center for Diabetes Research (DZD e.V.). IV, TR, and SR acknowledge the Academy of Finland (Center of Excellence program) and the European Research Council (Advanced Grant CROWDED-PRO-LIPIDS) for financial support. SR thanks FEBS for the Short-Term Fellowship, the Graduate School program of Tampere University of Technology, and Alfred Kordelin Foundation for financial support. CE and ES are supported by the Wolfson Foundation (ref. 18272), the Medical Research Council (MRC, grant number MC_UU_12010/unit programmes G0902418 and MC_UU_12025), MRC/BBSRC/ESPRC (grant number MR/K01577X/1), and the Wellcome Trust (grant ref. 104924/14/Z/14).

ACKNOWLEDGMENTS

The authors thank Ünal Coskun for excellent comments and support. CSC – IT Centre for Science (Espoo, Finland) and the HPC Unit at TU Dresden are acknowledged for computing resources.

SUPPLEMENTARY MATERIAL

The Supplementary Material for this article can be found online at: http://journal.frontiersin.org/article/10.3389/fphys.2017.00252/full#supplementary-material

REFERENCES

Bacia, K., Schwille, P., and Kurzchalia, T. (2005). Sterol structure determines the separation of phases and the curvature of the liquid-ordered phase in model membranes. *Proc. Natl. Acad. Sci. U.S.A.* 102, 3272–3277. doi: 10.1073/pnas.0408215102

Barber, K. R., Hamilton, K. S., Rigby, A. C., and Grant, C. W. (1994). Behaviour of complex oligosaccharides at a bilayer membrane surface: probed by 2H-NMR. *Biochim. Biophys. Acta* 1190, 376–384. doi: 10.1016/0005-2736(94)90097-3

Blaum, B. S., Frank, M., Walker, R. C., Neu, U., and Stehle, T. (2016). Complement Factor H and Simian Virus 40 bind the GM1 ganglioside in distinct conformations. *Glycobiology* 26, 532–539. doi: 10.1093/glycob/cwv170

Ewers, H., Römer, W., Smith, A. E., Bacia, K., Dmitrieff, S., Chai, W., et al. (2009). GM1 structure determines SV40-induced membrane invagination and infection. *Nat. Cell Biol.* 12, 11–18. doi: 10.1038/ncb1999

Fricke, N., and Dimova, R. (2016). GM1 softens POPC membranes and induces the formation of micron-sized domains. *Biophys. J.* 111, 1935–1945. doi: 10.1016/j.bpj.2016.09.028

Harder, T., Scheiffele, P., Verkade, P., and Simons, K. (1998). Lipid domain structure of the plasma membrane revealed by patching of membrane components. *J. Cell Biol.* 141, 929–942. doi: 10.1083/jcb.141.4.929

Haselhorst, T., Weimar, T., and Peters, T. (2001). Molecular recognition of sialyl Lewis(x) and related saccharides by two lectins. *J. Am. Chem. Soc.* 123, 10705–10714. doi: 10.1021/ja011156h

Karlsson, K. A. (1989). Animal glycosphingolipids as membrane attachment sites for bacteria. *Annu. Rev. Biochem.* 58, 309–350. doi: 10.1146/annurev.bi.58.070189.001521

Kiarash, A., Boyd, B., and Lingwood, C. A. (1994). Glycosphingolipid receptor function is modified by fatty acid content. Verotoxin 1 and verotoxin 2c preferentially recognize different globotriaosyl ceramide fatty acid homologues. *J. Biol. Chem.* 269, 11138–11146.

Kolondra, A., Lenoir, M., Wolny, M., Czogalla, A., Overduin, M., Sikorski, A. F., et al. (2010). The role of hydrophobic interactions in ankyrin-spectrin complex formation. *Biochim. Biophys. Acta* 1798, 2084–2089. doi: 10.1016/j.bbamem.2010.07.024

Komura, N., Suzuki, K. G., Ando, H., Konishi, M., Koikeda, M., Imamura, A., et al. (2016). Raft-based interactions of gangliosides with a GPI-anchored receptor. *Nat. Chem. Biol.* 12, 402–410. doi: 10.1038/nchembio.2059

Lampio, A., Rauvala, H., and Gahmberg, C. G. (1986). Exposure of major neutral glycolipids in red cells to galactose oxidase. Effect of neuraminidase. *Eur. J. Biochem.* 157, 611–616. doi: 10.1111/j.1432-1033.1986.tb09709.x

Lingwood, D., Binnington, B., Róg, T., Vattulainen, I., Grzybek, M., Coskun, U., et al. (2011). Cholesterol modulates glycolipid conformation and receptor activity. *Nat. Chem. Biol.* 7, 260–262. doi: 10.1038/nchembio.551

Mahfoud, R., Manis, A., Binnington, B., Ackerley, C., and Lingwood, C. A. (2010). A major fraction of glycosphingolipids in model and cellular cholesterol-containing membranes is undetectable by their binding proteins. *J. Biol. Chem.* 285, 36049–36059. doi: 10.1074/jbc.M110.110189

Merritt, E. A., Sarfaty, S., van den Akker, F., L'Hoir, C., Martial, J. A., Hol, W. G., et al. (1994). Crystal structure of cholera toxin B-pentamer bound to receptor GM1 pentasaccharide. *Protein Sci.* 3, 166–175. doi: 10.1002/pro.5560030202

Miljan, E. A., and Bremer, E. G. (2002). Regulation of growth factor receptors by gangliosides. *Science* 2002, 10. doi: 10.1126/stke.2002.160.re15

Morrow, M. R., Singh, D. M., and Grant, C. W. (1995). Glycosphingolipid headgroup orientation in fluid phospholipid/cholesterol membranes: similarity for a range of glycolipid fatty acids. *Biophys. J.* 69, 955–964. doi: 10.1016/S0006-3495(95)79969-6

Sachl, R., Amaro, M., Aydogan, G., Koukalová, A., Mikhalyov, I. I., Boldyrev, I. A., et al. (2015). On multivalent receptor activity of GM1 in cholesterol containing membranes. *Biochim. Biophys. Acta* 1853, 850–857. doi: 10.1016/j.bbamcr.2014.07.016

Sezgin, E., Gutmann, T., Buhl, T., Dirkx, R., Grzybek, M., Coskun, Ü., et al. (2015). Adaptive lipid packing and bioactivity in membrane domains. *PLoS ONE* 10:e0123930. doi: 10.1371/journal.pone.0123930

Sezgin, E., Kaiser, H. J., Baumgart, T., Schwille, P., Simons, K., and Levental, I. (2012a). Elucidating membrane structure and protein behavior using giant plasma membrane vesicles. *Nat. Protoc.* 7, 1042–1051. doi: 10.1038/nprot.2012.059

Sezgin, E., Levental, I., Grzybek, M., Schwarzmann, G., Mueller, V., Honigmann, A., et al. (2012b). Partitioning, diffusion, and ligand binding of raft lipid analogs in model and cellular plasma membranes. *Biochim. Biophys. Acta* 1818, 1777–1784. doi: 10.1016/j.bbamem.2012.03.007

Shi, J., Yang, T., Kataoka, S., Zhang, Y., Diaz, A. J., Cremer, P. S., et al. (2007). GM1 clustering inhibits cholera toxin binding in supported phospholipid membranes. *J. Am. Chem. Soc.* 129, 5954–5961. doi: 10.1021/ja069375w

Shichijo, S., and Alving, C. R. (1985). Influence of glycolipids on immune reactions of phospholipid antigens in liposomes. *Biochim. Biophys. Acta* 820, 289–294. doi: 10.1016/0005-2736(85)90123-3

Simons, K., and Ikonen, E. (1997). Functional rafts in cell membranes. *Nature* 387, 569–572. doi: 10.1038/42408

Singh, D. M., Shan, X., Davis, J. H., Jones, D. H., and Grant, C. W. (1995). Oligosaccharide behavior of complex natural glycosphingolipids in multicomponent model membranes. *Biochemistry* 34, 451–463. doi: 10.1021/bi00002a009

Stewart, R. J., and Boggs, J. M. (1993). Exposure of galactosylceramide to galactose oxidase in liposomes: dependence on lipid environment and ceramide composition. *Biochemistry* 32, 5605–5614. doi: 10.1021/bi00072a016

Conflict of Interest Statement: The authors declare that the research was conducted in the absence of any commercial or financial relationships that could be construed as a potential conflict of interest.

III

Calcium Directly Regulates Phosphatidylinositol 4,5-Bisphosphate Headgroup Conformation and Recognition

by
E. Bilkova[‡], R. Pleskot[‡], S. Rissanen[‡], S. Sun[‡], A. Czogalla, L. Cwiklik, T. Róg, I. Vattulainen, P. S. Cremer, P. Jungwirth & Ü. Coskun.
Journal of the American Chemical Society, vol 139, 4019–4024, 2017.

JACS
JOURNAL OF THE AMERICAN CHEMICAL SOCIETY
Article
pubs.acs.org/JACS

Calcium Directly Regulates Phosphatidylinositol 4,5-Bisphosphate Headgroup Conformation and Recognition

Eva Bilkova,[†,‡,¶] Roman Pleskot,[§,∥,¶] Sami Rissanen,[⊥,¶] Simou Sun,[#,⊗,¶] Aleksander Czogalla,[†,▽] Lukasz Cwiklik,[&,§] Tomasz Róg,[⊥,○] Ilpo Vattulainen,[⊥,○,◆] Paul S. Cremer,[*,#,⊗] Pavel Jungwirth,[*,§,⊥] and Ünal Coskun[*,†,‡]

[†]Paul Langerhans Institute Dresden of the Helmholtz Zentrum München at the University Hospital and Faculty of Medicine Carl Gustav Carus of TU Dresden, Technische Universität Dresden, Fetscher Strasse 74, 01307 Dresden, Germany

[‡]German Center for Diabetes Research (DZD e.V.), Ingolstädter Landstraße 1, 85764 Neuherberg, Germany

[§]Institute of Organic Chemistry and Biochemistry, Academy of Sciences of the Czech Republic, Flemingovo náměstí 2, 16610 Prague 6, Czech Republic

[∥]Institute of Experimental Botany, Academy of Sciences of the Czech Republic, v.v.i., Rozvojová 263, 16502 Prague 6, Czech Republic

[⊥]Department of Physics, Tampere University of Technology, P.O. Box 692, FI-33101 Tampere, Finland

[#]Department of Chemistry and [⊗]Department of Biochemistry and Molecular Biology, Penn State University, University Park, Pennsylvania 16801, United States

[▽]Laboratory of Cytobiochemistry, Faculty of Biotechnology, University of Wrocław, Joliot-Curie 14a, 50-383 Wrocław, Poland

[&]J. Heyrovský Institute of Physical Chemistry, Academy of Sciences of the Czech Republic, v.v.i., Dolejskova 3, 18223 Prague 8, Czech Republic

[○]Department of Physics, University of Helsinki, P.O. Box 64, FI-00014, Helsinki, Finland

[◆]MEMPHYS− Center for Biomembrane Physics, University of Southern Denmark, DK-5230 Odense, Denmark

Supporting Information

ABSTRACT: The orchestrated recognition of phosphoinositides and concomitant intracellular release of Ca^{2+} is pivotal to almost every aspect of cellular processes, including membrane homeostasis, cell division and growth, vesicle trafficking, as well as secretion. Although Ca^{2+} is known to directly impact phosphoinositide clustering, little is known about the molecular basis for this or its significance in cellular signaling. Here, we study the direct interaction of Ca^{2+} with phosphatidylinositol 4,5-bisphosphate ($PI(4,5)P_2$), the main lipid marker of the plasma membrane. Electrokinetic potential measurements of $PI(4,5)P_2$ containing liposomes reveal that Ca^{2+} as well as Mg^{2+} reduce the zeta potential of liposomes to nearly background levels of pure phosphatidylcholine membranes. Strikingly, lipid recognition by the default $PI(4,5)P_2$ lipid sensor, phospholipase C delta 1 pleckstrin homology domain (PLC δ1-PH), is completely inhibited in the presence of Ca^{2+}, while Mg^{2+} has no effect with 100 nm liposomes and modest effect with giant unilamellar vesicles. Consistent with biochemical data, vibrational sum frequency spectroscopy and atomistic molecular dynamics simulations reveal how Ca^{2+} binding to the $PI(4,5)P_2$ headgroup and carbonyl regions leads to confined lipid headgroup tilting and conformational rearrangements. We rationalize these findings by the ability of calcium to block a highly specific interaction between PLC δ1-PH and $PI(4,5)P_2$, encoded within the conformational properties of the lipid itself. Our studies demonstrate the possibility that switchable phosphoinositide conformational states can serve as lipid recognition and controlled cell signaling mechanisms.

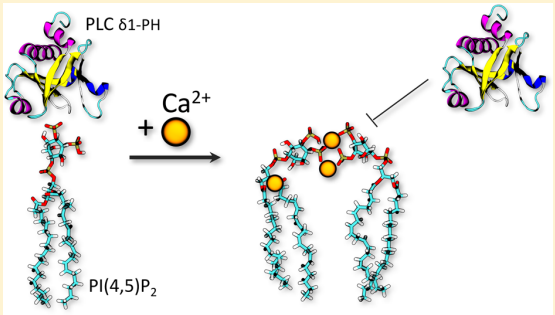

INTRODUCTION

Cell signaling pathways are largely organized via a specific recruitment of signaling effector proteins to their target membranes and a confined release of calcium ions. The quintessential example of this is the action of phospholipase C (PLC) that binds and hydrolyzes phosphatidylinositol 4,5-bisphosphate ($PI(4,5)P_2$) in the plasma membrane to diacylglycerol (DAG) and the water-soluble inositol 1,4,5-trisphosphate (IP3), the latter inducing the release of Ca^{2+} from the endoplasmic reticulum (ER) into the cytosol.[1] Another prominent example is synaptotagmin-1, the main Ca^{2+} sensor of

Received: November 14, 2016
Published: February 8, 2017

DOI: 10.1021/jacs.6b11760
J. Am. Chem. Soc. 2017, 139, 4019−4024

neuronal exocytosis in the presynaptic axon terminal. Synaptotagmin-1 binding to $PI(4,5)P_2$ directly amplifies protein cooperativity and thus sensitivity to Ca^{2+} by a factor of >40. This mutual interplay is a critical step in neurotransmitter release.[2]

$PI(4,5)P_2$ is enriched in the inner leaflet of the plasma membrane[3,4] and constitutes around 1% of the total anionic phospholipid content in cellular membranes.[5] In comparison with other phospholipids, it contains a rather bulky phosphorylated inositol headgroup with a negative charge ranging from −3 *e* to −5 *e*, depending on the pH and the presence of proteins or ions.[6] $PI(4,5)P_2$ and other negatively charged lipids in the cytosolic leaflet are constantly exposed to divalent cations. In resting cells, the free cytosolic Ca^{2+} concentration is approximately 100 nM.[7,8] The cytosolic concentration of Ca^{2+} upon cell signaling has been reported to span a wide range from 0.5 μM to several hundred μM, with a half-life of 500 μs to 26 ms.[9−14] Ca^{2+} influx primarily originates from internal stores within the endoplasmic/sarcoplasmic reticulum or from specialized channels within the plasma membrane providing an essentially infinite supply of extracellular calcium.[9] In all cases, Ca^{2+} is delivered as brief transients, forming microdomains at the membrane site of influx,[10] and thus, local concentrations of Ca^{2+} can be expected to exceed cytosolic concentrations by orders of magnitude.[15] Meanwhile, unlike Ca^{2+}, the levels of free, cytosolic Mg^{2+} are maintained within a fairly narrow concentration range of 0.25−1 mM.[16,17] Interestingly, calcium but not magnesium ions have been ascribed a strong propensity to promote the formation of $PI(4,5)P_2$ clusters as demonstrated in several studies, primarily by using monolayer techniques.[18−22]

While the overall effects of divalent cations, including calcium, on $PI(4,5)P_2$ lateral organization have been intensely studied, the mechanism of Ca^{2+} and $PI(4,5)P_2$ interactions at the molecular level remain unclear. Experiments with pure $PI(4,5)P_2$ monolayers have suggested partial dehydration of both Ca^{2+} and $PI(4,5)P_2$ upon interaction with each other,[23] triggering an electron density increase in the $PI(4,5)P_2$ headgroup region as well as acyl chain region thickening.[24] Interactions between $PI(4,5)P_2$ and Ca^{2+} have also been studied computationally. These studies, however, have typically focused on single $PI(4,5)P_2$ molecules[25] or used simplified coarse-grained models[19] that lack sufficient details to deal with specific chemical features of phosphatidylinositides.

Herein, we combine protein−lipid binding assays and spectroscopic experiments with atomistic molecular dynamics (MD) simulations employing refined state-of-the art force fields to unravel the functional and structural consequences of the interplay between Ca^{2+} and $PI(4,5)P_2$. Our data indicate a hitherto undiscovered role and mechanism for Ca^{2+} in cellular signaling, namely the direct organization of the phosphoinositide headgroup conformation and the selective recognition thereof by the pleckstrin homology (PH) domain of PLC δ1, the canonical $PI(4,5)P_2$ sensor.

RESULTS AND DISCUSSION

Protein−Lipid Binding Assays. To determine the equilibrium dissociation constants (K_D) for divalent cation/$PI(4,5)P_2$ interaction, we employed a simple fluorescent assay using a supported lipid bilayer platform[26−28] containing 5 mol % of $PI(4,5)P_2$ (for details, see the Supporting Information). Significantly, the K_D values differed by less than a factor of 2, with a K_D of 0.6 ± 0.2 mM for Ca^{2+} compared to 1.2 ± 0.2 mM for Mg^{2+} (Figure S1). We therefore decided to use a cation concentration of 1 mM for all follow-up experiments, matching the free Mg^{2+} concentration in the cytosol. In order to systematically study the effects of Ca^{2+} on $PI(4,5)P_2$, we produced 100 nm diameter large unilamellar vesicles (LUVs), facilitating the control of membrane lipid composition and properties. For quality control and physicochemical characterization, all preparations were first subjected to thin layer chromatography (TLC), dynamic light scattering (DLS), and zeta potential measurements (Figure S2). Having the opposite charge of $PI(4,5)P_2$, it is not surprising that Ca^{2+} and Mg^{2+} equally reduce the zeta potential of POPC liposomes containing 5 mol % of $PI(4,5)P_2$, the former being described previously.[29] In fact, the presence of either cation attenuates the electrokinetic potential of the membrane down to the level of POPC alone (Figure S2c).

Because of its extraordinary stereospecificity, the PLC δ1-PH domain is widely used as the canonical reporter for cellular $PI(4,5)P_2$ levels at the plasma membrane as well as with *in vitro* assays.[30−34] We therefore used recombinant PLC δ1-PH domain to follow $PI(4,5)P_2$ binding to synthetic liposomes. Size-exclusion chromatography and DLS confirmed that the purified PLC δ1-PH domain (Figure S3a,b) was monomeric in solution, even in the presence of Ca^{2+} and Mg^{2+} (Figure S3c,d). Next, we performed liposome flotation assays to follow PLC δ1-PH binding efficiency to POPC/$PI(4,5)P_2$ vesicles. Interestingly, preincubation with 1 mM Ca^{2+} but not 1 mM Mg^{2+} fully inhibited liposome binding (Figure 1a,b). Moreover, PLC δ1-PH did not bind to pure POPC liposomes, highlighting its specificity to $PI(4,5)P_2$.

Circular dichroism (CD) spectroscopy excluded a direct effect for cations on the secondary structure of the protein (Figure S3e,f). As such, although Ca^{2+} and Mg^{2+} bind to $PI(4,5)P_2$ with comparable K_D values and reduce electrokinetic membrane properties in an equal manner, only Ca^{2+} was capable of inhibiting PLC δ1-PH binding. This indicates that $PI(4,5)P_2$ recognition by proteins cannot be solely based on electrostatic interactions.

Because a concentration of 1 mM Ca^{2+} corresponds to twice its K_D for $PI(4,5P)_2$ interaction, we performed additional flotation assays with lower Ca^{2+} concentrations. Here, a significant reduction in protein binding could be observed already at a concentration of 0.6 mM Ca^{2+} (Figure S4). In this context, recent data by Milovanovic and colleagues show that Ca^{2+} but not Mg^{2+} promotes syntaxin-1/$PI(4,5)P_2$ domain formation by an underlying mechanism in which Ca^{2+} clusters $PI(4,5)P_2$ and syntaxin-1 independently from each other. Moreover, Ca^{2+} acts as a charge bridge that merges multiple syntaxin-1/$PI(4,5)P_2$ clusters into larger domains. Also here, Ca^{2+} was found to be effective at a concentration of 0.5 mM while even 1 mM Mg^{2+} had no effect.[35]

Ca^{2+} binding to membranes has been recently reported to increase with high curvature.[36] We therefore additionally followed the binding of monomeric ECFP-PLC δ1-PH fusion protein to giant unilamellar vesicles (GUVs) (Figure 1c). Despite limited control over membrane lipid composition at the individual GUV level,[37] GUVs provide the most appropriate synthetic approach for flat and freestanding bilayer systems. In this system, the presence of 1 mM Ca^{2+} drastically reduced ECFP-PLC δ1-PH binding (Figure 1d and Figure S5), demonstrating the robustness of the observed effect, irrespective of membrane curvature. Magnesium, however, also reduced ECFP-PLC δ1-PH domain binding, halfway

DOI: 10.1021/jacs.6b11760
J. Am. Chem. Soc. 2017, 139, 4019−4024

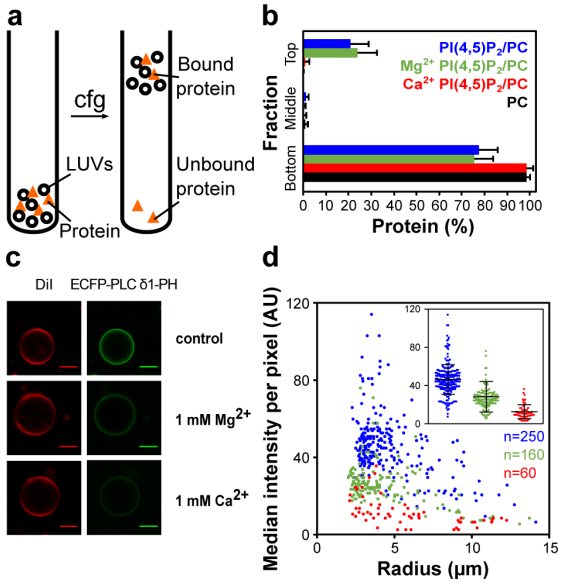

Figure 1. (a) Setup of the LUV flotation assay. (b) PLC δ1-PH binding to LUVs with POPC/PI(4,5P)$_2$ (95/5 mol %). Error bars are standard deviations of three independent experiments. (c) GUVs after ECFP-PLC δ1-PH addition (green) and DiI as membrane marker (red). The scale bar corresponds to 10 μm. (d) The distribution of median ECFP-PLC δ1-PH intensity per pixel of individual GUVs and different sizes of control (blue) and after preincubation with 1 mM Mg^{2+} (green) or Ca^{2+} (red) (data from two additional independent experiments are provided in Figure S5). Each dot represents a single GUV. The number of analyzed GUVs is indicated in the respective color. The median intensity values with mean and standard deviation are depicted in the inset. The Mann–Whitney test was used as significance test (p value <0.0001 for all cases).

toward the Ca^{2+} effect. To understand this result, it is important to note that liposome flotation experiments with proteins are nonequilibrium assays because much of the protein stays in the bottom of the tube. At the same time, cation concentrations remain constant, leading to an additional stoichiometric shift. By contrast, protein binding in the GUV experiment is at equilibrium and binding events are quantified at the individual GUV level.

Vibrational Sum Frequency Spectroscopy. To analyze the molecular basis for the cation specificity, vibrational sum frequency spectroscopy (VSFS) was employed to study the effects of Ca^{2+} and Mg^{2+} on pure PI(4,5)P$_2$ monolayers at the air/water interface. The spectra were recorded over frequency ranges corresponding to the headgroup and acyl-chain portions of the lipid molecules and included the adjacent interfacial water structure.

We present VSFS spectra from the inositol ring and phosphate regions of PI(4,5)P$_2$ in the absence and presence of 1 mM Ca^{2+} and Mg^{2+} (Figure 2a, detailed peak assignments in Figure S6 and Table S1). In the absence of cations in the subphase, both the inositol ring vibrations and the phosphate stretches were rather weak (black data points). This is because of a relatively disordered arrangement of the PI(4,5)P$_2$ headgroups adopted in a pure buffer with a wide range of tilt angles relative to the surface normal. With 1 mM Ca^{2+}, however, the inositol ring signal (961 cm^{-1} and 1012 cm^{-1} peaks from the C–C and C–O coupled vibrations, respectively)[38] increased substantially (red data points). In

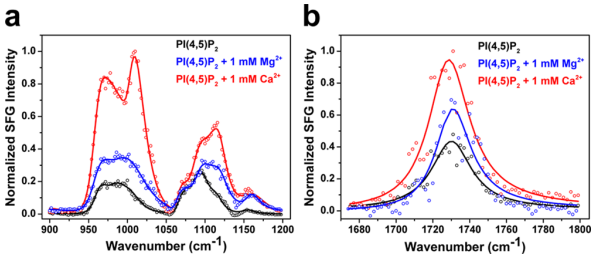

Figure 2. VSFS spectra of (a) the inositol ring and phosphate regions and (b) the carbonyl C=O symmetric stretch region of PI(4,5)P$_2$ on a buffer subphase (black spectra) containing 1 mM $MgCl_2$ (blue spectra) or 1 mM $CaCl_2$ (red spectrum) at a surface pressure of 17 mN/m. The open circles represent VSFS data points, and the solid lines are fits to the data. All spectra were taken with the ssp polarization combination. Spectra of the same data offset along the y-axis are provided in Figure S7. Details of monolayer preparation and images are provided in Figure S14.

fact, the resonances showed 2.7- and 3.6-fold increases, respectively, in oscillator strength (Table S1). These changes reflect both reorientation of the inositol rings and a narrowing of their orientational distribution upon cation binding. Significantly, the changes were not nearly as strong upon the addition of 1 mM Mg^{2+} (blue data points). In that case, the oscillator strength of the inositol ring vibrations was increased by only a factor of 1.5 and 2.1, respectively. Such results indicated that Ca^{2+} rigidified the configuration of the PI(4,5)P$_2$ headgroups much more effectively than Mg^{2+}.

In addition to the inositol ring modes, the phosphate peaks (e.g., $_{sym}PO_3^{2-}$ at 982 cm^{-1}, $_{sym}PO_2^{-}$ at 1086 cm^{-1}, $_{asy}PO_3^{2-}$ at 1115 cm^{-1}, $_{asy}PO_2^{-}$ at 1154 cm^{-1}, detailed assignments in Figure S6 and Table S1) also showed a substantial intensity increase upon the introduction of Ca^{2+} to the subphase. This indicates a strong net orientation and/or ordering of the headgroup phosphates upon Ca^{2+} binding. It should be noted that Ca^{2+} binding may help to deprotonate the second monoesterified phosphate,[25] which would prompt additional changes in the spectra beyond those related to ordering and tilt angle. Moreover, upon the addition of Ca^{2+}, the symmetric PO_3^{2-} stretch exhibited a relatively large 20 cm^{-1} blue shift, while the asymmetric PO_3^{2-} and PO_2^{-} stretches shifted by 6 cm^{-1} and 8 cm^{-1}, respectively (Table S1). The shifts of both PO_3^{2-} peaks are consistent with phosphate dehydration upon cation binding and/or a symmetry change of the C_{3v} point group.[39,40] The shift of the asymmetric PO_2^{-} peak also suggests headgroup phosphate dehydration upon Ca^{2+} binding.[40−42]

The spectral change brought about by 1 mM Mg^{2+} in the phosphate region was much less pronounced overall compared to that with 1 mM Ca^{2+}. The difference in the interactions of Ca^{2+} and Mg^{2+} with phosphate could be explained at least in part by different dehydration penalties for these two cations. It has been suggested that Ca^{2+} binding to phosphate groups is favored because Ca^{2+} is more easily dehydrated than Mg^{2+}.[23] This difference in the hydration shell chemistry may, in turn, act to disfavor the bridging of the inositol rings of PI(4,5)P$_2$, which would weaken the ordering effect of Mg^{2+}.

In addition to phosphate and inositol resonances, VSFS spectra were also obtained in the carbonyl C=O symmetric stretch (1730 cm^{-1})[43] region before and after addition of 1 mM $CaCl_2$ or $MgCl_2$ (Figure 2b). Again, Ca^{2+} showed a more prominent effect on the PI(4,5)P$_2$ than Mg^{2+}. In fact, a 1.6-fold

DOI: 10.1021/jacs.6b11760
J. Am. Chem. Soc. 2017, 139, 4019−4024

increase in the oscillator strength of this peak was observed upon binding of Ca^{2+}, while only a 1.3-fold increase was found for Mg^{2+} (Table S2). This oscillator strength increase should correspond to a backbone ordering effect, thus helping to reinforce a more rigid configuration of the headgroup inositol rings. Ordering of the lipid acyl chains was also observed (Figure S8 and Table S3).[44]

Taken together, the changes in the VSFS spectra provide strong experimental evidence for distinct conformational changes within the lipid headgroup region in the presence of Ca^{2+}, but less with Mg^{2+}. Such results should be important for the PLC δ1-PH domain selectivity of $PI(4,5)P_2$ found above with liposomes and GUVs.

Atomistic Molecular Dynamics Simulations. With the aim of obtaining mechanistic insights into the effects of Ca^{2+} and Mg^{2+} on $PI(4,5)P_2$ molecules at a molecular level, we employed atomistic MD simulations. In order to reduce methodological bias, we used two all-atom force fields (OPLS-AA and CHARMM36) as well as the united-atom force field from Berger (Table S4).[45−47] Importantly, to further account for electronic polarization effects of charged groups in a mean field manner, for Ca^{2+} interacting with $PI(4,5)P_2$ phosphates we also employed the recently developed electronic continuum correction with rescaling (ECCR) method.[48] This, to a large extent, dampens the unrealistically high ion pairing found when employing nonpolarizable force fields.[48] It is particularly useful in the present case where strong electronic polarization can be expected in the vicinity of multiple-charged moieties.

We generated multiple sets of 1 μs long trajectories for different initial $PI(4,5)P_2$ distributions prior to and after the addition of Ca^{2+} or Mg^{2+}. For all simulations, consistently with all force fields used, we find that Ca^{2+} interacts with $PI(4,5)P_2$ and has a pronounced effect on the lipid headgroup orientation (Figure 3 and Figures S9 and S13). Moreover, control simulations with Mg^{2+} showed that the effects induced by magnesium are much weaker than those induced by calcium for all simulations (Figure 3c,d and SI), in full agreement with experiments.

The addition of Ca^{2+} or Mg^{2+} immediately leads to a significant reduction of the area per lipid (Figure S10 and Table S5). This macroscopic effect is in agreement with lateral condensation of the $PI(4,5)P_2$-containing monolayers by Ca^{2+} [20,22−24] and our VSFS analysis of the CH stretches (Figure S8). At the microscopic level, we found that each $PI(4,5)P_2$ molecule binds on average 1.6−3.1 Ca^{2+} molecules, depending on the force field that is employed (Table S5). This is consistent with the water peak spectral changes, which show that each lipid molecule binds more than two Ca^{2+} ions (Figure S8). Ca^{2+} binds mostly to the phosphate groups at positions 4 and 5, but it also penetrates deeper into the lipid bilayer to interact with the carbonyl groups (Figure S11). Ca^{2+} binding to the lipid carbonyl group is consistent with the VSFS data in the carbonyl stretch region, as documented herein (Figure 2b) and elsewhere.[49−53] In agreement with previously published computational and experimental results,[24,50] we observed that Ca^{2+} increases the order parameters of the $PI(4,5)P_2$ acyl chains (Figure S12). The acyl chain ordering is also fully in line with the effects observed in the VSFS spectra (Figure S8).

The most prominent feature observed by simulations is a pronounced headgroup reorientation, primarily caused by the ability of Ca^{2+} to bridge two $PI(4,5)P_2$ headgroups (Figure 3a,b). This result was found regardless of which force field was

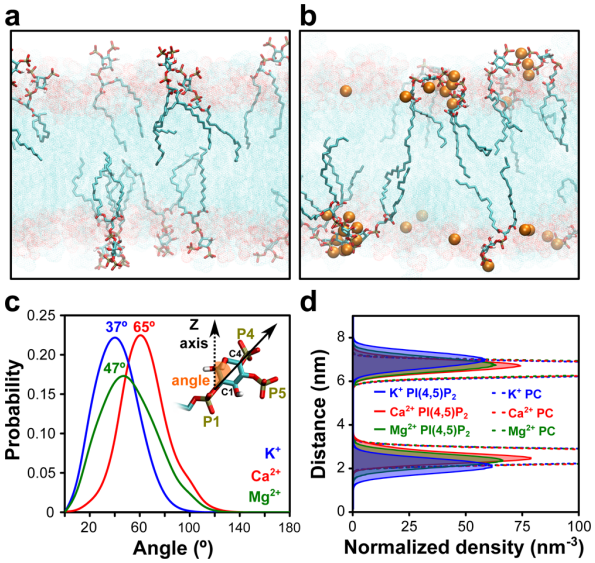

Figure 3. Snapshots from MD simulations of the lipid bilayer taken at 1 μs (a) without and (b) with Ca^{2+}. (c) Tilt angle distribution of the $PI(4,5)P_2$ headgroup and (d) density profiles of lipid headgroups without (blue) and with Mg^{2+} (green) or Ca^{2+} (red). Numbers in (c) represent mean tilt angles for each system. Here, only the results of the Berger force field simulations are presented. Additional force field simulations with similar outcomes can be found in the Supporting Information.

used. To quantitatively analyze the headgroup reorientation, we monitored the tilt angle between the C1−C4 atoms of the $PI(4,5)P_2$ inositol ring and the bilayer normal. The average tilt angle in the control simulation without Ca^{2+} was in the range of 35−41°, depending on the employed force field. This result is in agreement with previously published MD studies.[54−56] In the presence of Ca^{2+} ions, however, the average tilt angle significantly increased for all of the force fields up to 65° (Figure 3c and Figures S9 and S13). Simulations thus consistently showed bending of the $PI(4,5)P_2$ headgroup toward the plane of the bilayer and away from bulk water (Table S5). Moreover, consistent with a narrowing of the inositol ring's distribution as indicated by VSFS results above (Figure 2a), Ca^{2+} slowed $PI(4,5)P_2$ headgroup rotational diffusion as revealed by the rotational correlation function (Figure S9e). The Ca^{2+} effect was also manifested in the density profiles (Figure 3d), where the location of the $PI(4,5)P_2$ headgroups shifted in the presence of calcium toward the bilayer center. Moreover, Ca^{2+} significantly decreased the solvent accessible surface area of $PI(4,5)P_2$, which correlated with a reduced average number of hydrogen bonds between the $PI(4,5)P_2$ headgroups and water molecules (Table S5). These data also match the experimentally observed partial dehydration of $PI(4,5)P_2$ in the presence of Ca^{2+} as measured here by VSFS and elsewhere.[23]

The charge state of $PI(4,5)P_2$ in lipid membranes is highly sensitive to the cellular pH and the presence of proteins and ions.[6,57] By using not only the default parametrization (CHARMM36 and OPLS-AA) but also the ECCR corrected charges for the ions and $PI(4,5)P_2$ phosphate groups (Berger, OPLS-AA), we were able to assess the potential effects of the lipid charge state. Namely, the charge used for $PI(4,5)P_2$ varied from −3.75 to −5, depending on the particular force field (for

DOI: 10.1021/jacs.6b11760
J. Am. Chem. Soc. 2017, 139, 4019−4024

more details, see the SI). Reassuringly, we found semi-quantitatively the same effect of Ca^{2+} on the $PI(4,5)P_2$ tilt angle with Ca^{2+} in all the systems which were tested. This indicates that under the conditions of these investigations the protonation state of $PI(4,5)P_2$ was not particularly critical for the observed effects.

CONCLUSION

By means of protein−lipid binding assays and spectroscopic experiments, together with atomistic MD simulations, we have unraveled and characterized in molecular detail the pronounced effect of Ca^{2+} on $PI(4,5)P_2$ headgroup presentation. First, we confirmed the previously observed increase of the $PI(4,5)P_2$ acyl chain order and $PI(4,5)P_2$ cluster formation,[18−21] as evidenced here by VSFG spectroscopy and MD simulations. Second, we characterized at the molecular level the interactions of Ca^{2+} with $PI(4,5)P_2$ headgroup phosphates, as well as the more deeply seated carbonyl groups. We observed the hitherto unrecognized consequences of Ca^{2+} binding for $PI(4,5)P_2$ at the molecular level. Namely, we observed a dramatic change in the $PI(4,5)P_2$ headgroup tilt angle. By means of liposome flotation and GUV binding assays, we show that Ca^{2+} has a strong propensity to render the $PI(4,5)P_2$ headgroup invisible to the PLC-δ1 PH domain.

Our data lead to the plausible conjecture that the calcium-induced switching of phosphoinositide conformational states may serve as a potential cellular mechanism for lipid recognition and thus play a decisive role in cell signaling and membrane trafficking. A systematic correlation of kinetics and curvature sensitivities at the nanoscale *in vitro*[58] will be key to understanding the general applicability of our data to other proteins and to different endomembranes.

ASSOCIATED CONTENT

Supporting Information

The Supporting Information is available free of charge on the ACS Publications website at DOI: 10.1021/jacs.6b11760.

Detailed materials and methods, additional VSFS spectra, computational and experimental controls (PDF)

AUTHOR INFORMATION

Corresponding Authors

*psc11@psu.edu
*pavel.jungwirth@uochb.cas.cz
*coskun@plid.de

ORCID

Tomasz Róg: 0000-0001-6765-7013
Ilpo Vattulainen: 0000-0001-7408-3214
Paul S. Cremer: 0000-0002-8524-0438
Pavel Jungwirth: 0000-0002-6892-3288
Ünal Coskun: 0000-0003-4375-3144

Author Contributions

¶E.B., R.P., S.R., and S.S. contributed equally.

Notes

The authors declare no competing financial interest.

ACKNOWLEDGMENTS

We thank Milena Stephan, André Nadler, and Alf Honigmann (Max Planck Institute of Molecular Cell Biology and Genetics) for support with GUV image quantification and GUV production protocol; Josef Lazar (C4Sys research infrastructure) for advice on background correction in Fiji; and the light-microscopy facility of the BIOTEC/CRTD at TU Dresden for providing excellent microscopy support and maintenance. We thank Michal Grzybek for skillful experimental advice and support. P.J. thanks the Academy of Finland for the FiDiPro Award. We acknowledge generous computational resources made available by CSC-IT Centre for Science (Espoo, Finland) and the High-Performance Computing Center of the TU Dresden. Financial support was provided by the Deutsche Forschungsgemeinschaft (DFG) "Transregio 83" (Grant No. TRR83 TP18 (Ü.C., A.C., E.B.)), the German Federal Ministry of Education and Research grant to the German Center for Diabetes Research (DZD e.V.) (Ü.C.), the Academy of Finland (Center of Excellence program) (I.V., T.R., S.R.), the European Research Council (Advanced Grant CROWDED-PRO-LIPIDS) (I.V.), a FEBS Short-Term Fellowship (S.R.), the Graduate School program of Tampere University of Technology and Alfred Kordelin Foundation (S.R.), the Polish Ministry of Science and Higher Education (Iuventus Plus 2015−2016 project IP2014 007373) (A.C.), the Dresden International Graduate School for Biomedicine and Bioengineering, granted by the DFG (GS97) (E.B.), the Czech Science Foundation GACR 13-19073S (R.P.), 16-01074S (P.J.), and 17-06792S (L.C.), the National Science Foundation (CHE-1413307 (P.S.C.)), and the Office of Naval Research (N00014-14-1-0792 (P.S.C.)).

REFERENCES

(1) Putney, J. W.; Tomita, T. *Adv. Biol. Regul* **2012**, *52* (1), 152−64.
(2) van den Bogaart, G.; Meyenberg, K.; Diederichsen, U.; Jahn, R. *J. Biol. Chem.* **2012**, *287* (20), 16447−53.
(3) McLaughlin, S.; Wang, J.; Gambhir, A.; Murray, D. *Annu. Rev. Biophys. Biomol. Struct.* **2002**, *31*, 151−75.
(4) Di Paolo, G.; De Camilli, P. *Nature* **2006**, *443* (7112), 651−7.
(5) Nasuhoglu, C.; Feng, S.; Mao, J.; Yamamoto, M.; Yin, H. L.; Earnest, S.; Barylko, B.; Albanesi, J. P.; Hilgemann, D. W. *Anal. Biochem.* **2002**, *301* (2), 243−54.
(6) Wang, Y. H.; Slochower, D. R.; Janmey, P. A. *Chem. Phys. Lipids* **2014**, *182*, 38−51.
(7) Clapham, D. E. *Cell* **2007**, *131* (6), 1047−58.
(8) Usachev, Y. M.; Marchenko, S. M.; Sage, S. O. *J. Physiol.* **1995**, *489*, 309−17.
(9) Berridge, M. J. *J. Physiol.* **1997**, *499*, 291−306.
(10) Berridge, M. J. *Cell Calcium* **2006**, *40* (5−6), 405−12.
(11) Heidelberger, R.; Heinemann, C.; Neher, E.; Matthews, G. *Nature* **1994**, *371* (6497), 513−5.
(12) Llinas, R.; Sugimori, M.; Silver, R. B. *Science* **1992**, *256* (5057), 677−9.
(13) Tengholm, A.; Gylfe, E. *Mol. Cell. Endocrinol.* **2009**, *297* (1−2), 58−72.
(14) Ammala, C.; Eliasson, L.; Bokvist, K.; Larsson, O.; Ashcroft, F. M.; Rorsman, P. *J. Physiol.* **1993**, *472*, 665−88.
(15) Parekh, A. B. *J. Physiol.* **2008**, *586* (13), 3043−54.
(16) Grubbs, R. D. *BioMetals* **2002**, *15* (3), 251−9.
(17) Fujise, H.; Cruz, P.; Reo, N. V.; Lauf, P. K. *Biochim. Biophys. Acta, Mol. Cell Res.* **1991**, *1094* (1), 51−54.
(18) Carvalho, K.; Ramos, L.; Roy, C.; Picart, C. *Biophys. J.* **2008**, *95* (9), 4348−60.
(19) Ellenbroek, W. G.; Wang, Y. H.; Christian, D. A.; Discher, D. E.; Janmey, P. A.; Liu, A. J. *Biophys. J.* **2011**, *101* (9), 2178−84.
(20) Levental, I.; Christian, D. A.; Wang, Y. H.; Madara, J. J.; Discher, D. E.; Janmey, P. A. *Biochemistry* **2009**, *48* (34), 8241−8.
(21) Sarmento, M. J.; Coutinho, A.; Fedorov, A.; Prieto, M.; Fernandes, F. *Biochim. Biophys. Acta, Biomembr.* **2014**, *1838* (3), 822−30.

DOI: 10.1021/jacs.6b11760
J. Am. Chem. Soc. 2017, 139, 4019−4024

(22) Levental, I.; Cebers, A.; Janmey, P. A. *J. Am. Chem. Soc.* **2008**, *130* (28), 9025−30.
(23) Wang, Y. H.; Collins, A.; Guo, L.; Smith-Dupont, K. B.; Gai, F.; Svitkina, T.; Janmey, P. A. *J. Am. Chem. Soc.* **2012**, *134* (7), 3387−95.
(24) Graber, Z. T.; Wang, W.; Singh, G.; Kuzmenko, I.; Vaknin, D.; Kooijman, E. E. *RSC Adv.* **2015**, *5* (129), 106536−106542.
(25) Slochower, D. R.; Huwe, P. J.; Radhakrishnan, R.; Janmey, P. A. *J. Phys. Chem. B* **2013**, *117* (28), 8322−9.
(26) Jung, H.; Robison, A. D.; Cremer, P. S. *J. Am. Chem. Soc.* **2009**, *131* (3), 1006−14.
(27) Huang, D.; Zhao, T.; Xu, W.; Yang, T.; Cremer, P. S. *Anal. Chem.* **2013**, *85* (21), 10240−8.
(28) Robison, A. D.; Sun, S.; Poyton, M. F.; Johnson, G. A.; Pellois, J. P.; Jungwirth, P.; Vazdar, M.; Cremer, P. S. *J. Phys. Chem. B* **2016**, *120* (35), 9287−96.
(29) Toner, M.; Vaio, G.; McLaughlin, A.; McLaughlin, S. *Biochemistry* **1988**, *27* (19), 7435−43.
(30) Balla, T.; Varnai, P. *Sci. Signaling* **2002**, *2002* (125), pl3.
(31) Garcia, P.; Gupta, R.; Shah, S.; Morris, A. J.; Rudge, S. A.; Scarlata, S.; Petrova, V.; McLaughlin, S.; Rebecchi, M. J. *Biochemistry* **1995**, *34* (49), 16228−34.
(32) Saliba, A. E.; Vonkova, I.; Ceschia, S.; Findlay, G. M.; Maeda, K.; Tischer, C.; Deghou, S.; van Noort, V.; Bork, P.; Pawson, T.; Ellenberg, J.; Gavin, A. C. *Nat. Methods* **2013**, *11* (1), 47−50.
(33) Lemmon, M. A.; Ferguson, K. M.; O'Brien, R.; Sigler, P. B.; Schlessinger, J. *Proc. Natl. Acad. Sci. U. S. A.* **1995**, *92* (23), 10472−6.
(34) Lemmon, M. A. *Nat. Rev. Mol. Cell Biol.* **2008**, *9* (2), 99−111.
(35) Milovanovic, D.; Platen, M.; Junius, M.; Diederichsen, U.; Schaap, I. A.; Honigmann, A.; Jahn, R.; van den Bogaart, G. *J. Biol. Chem.* **2016**, *291* (15), 7868−76.
(36) Magarkar, A.; Jurkiewicz, P.; Allolio, C.; Hof, M.; Jungwirth, P. *J. Phys. Chem. Lett.* **2017**, *8* (2), 518−523.
(37) Czogalla, A.; Grzybek, M.; Jones, W.; Coskun, U. *Biochim. Biophys. Acta, Mol. Cell Biol. Lipids* **2014**, *1841* (8), 1049−59.
(38) Isbrandt, L. R.; Oertel, R. P. *J. Am. Chem. Soc.* **1980**, *102* (9), 3144−3148.
(39) Laroche, G.; Dufourc, E. J.; Dufourcq, J.; Pezolet, M. *Biochemistry* **1991**, *30* (12), 3105−14.
(40) Casillas-Ituarte, N. N.; Chen, X.; Castada, H.; Allen, H. C. *J. Phys. Chem. B* **2010**, *114* (29), 9485−95.
(41) Levinson, N. M.; Bolte, E. E.; Miller, C. S.; Corcelli, S. A.; Boxer, S. G. *J. Am. Chem. Soc.* **2011**, *133* (34), 13236−9.
(42) Flach, C. R.; Brauner, J. W.; Mendelsohn, R. *Biophys. J.* **1993**, *65* (5), 1994−2001.
(43) Rzeznicka, II; Sovago, M.; Backus, E. H.; Bonn, M.; Yamada, T.; Kobayashi, T.; Kawai, M. *Langmuir* **2010**, *26* (20), 16055−62.
(44) Gurau, M. C.; Lim, S. M.; Castellana, E. T.; Albertorio, F.; Kataoka, S.; Cremer, P. S. *J. Am. Chem. Soc.* **2004**, *126* (34), 10522−3.
(45) Klauda, J. B.; Venable, R. M.; Freites, J. A.; O'Connor, J. W.; Tobias, D. J.; Mondragon-Ramirez, C.; Vorobyov, I.; MacKerell, A. D., Jr.; Pastor, R. W. *J. Phys. Chem. B* **2010**, *114* (23), 7830−43.
(46) Jorgensen, W. L.; Chandrasekhar, J.; Madura, J. D.; Impey, R. W.; Klein, M. L. *J. Chem. Phys.* **1983**, *79* (2), 926−935.
(47) Berger, O.; Edholm, O.; Jahnig, F. *Biophys. J.* **1997**, *72* (5), 2002−13.
(48) Kohagen, M.; Pluharova, E.; Mason, P. E.; Jungwirth, P. *J. Phys. Chem. Lett.* **2015**, *6* (9), 1563−7.
(49) Porasso, R. D.; Lopez Cascales, J. J. *Colloids Surf., B* **2009**, *73* (1), 42−50.
(50) Bockmann, R. A.; Grubmuller, H. *Angew. Chem., Int. Ed.* **2004**, *43* (8), 1021−4.
(51) Magarkar, A.; Rog, T.; Bunker, A. *J. Phys. Chem. C* **2014**, *118* (33), 19444−19449.
(52) Binder, H.; Zschornig, O. *Chem. Phys. Lipids* **2002**, *115* (1−2), 39−61.
(53) Melcrova, A.; Pokorna, S.; Pullanchery, S.; Kohagen, M.; Jurkiewicz, P.; Hof, M.; Jungwirth, P.; Cremer, P. S.; Cwiklik, L. *Sci. Rep.* **2016**, *6*, 38035.
(54) Li, Z.; Venable, R. M.; Rogers, L. A.; Murray, D.; Pastor, R. W. *Biophys. J.* **2009**, *97* (1), 155−63.
(55) Lupyan, D.; Mezei, M.; Logothetis, D. E.; Osman, R. *Biophys. J.* **2010**, *98* (2), 240−7.
(56) Wu, E. L.; Qi, Y.; Song, K. C.; Klauda, J. B.; Im, W. *J. Phys. Chem. B* **2014**, *118* (16), 4315−25.
(57) Graber, Z. T.; Gericke, A.; Kooijman, E. E. *Chem. Phys. Lipids* **2014**, *182*, 62−72.
(58) Mathiasen, S.; Christensen, S. M.; Fung, J. J.; Rasmussen, S. G. F.; Fay, J. F.; Jorgensen, S. K.; Veshaguri, S.; Farrens, D. L.; Kiskowski, M.; Kobilka, B.; Stamou, D. *Nat. Methods* **2014**, *11* (9), 931−934.

DOI: 10.1021/jacs.6b11760
J. Am. Chem. Soc. 2017, 139, 4019−4024

Tampereen teknillinen yliopisto
PL 527
33101 Tampere

Tampere University of Technology
P.O.B. 527
FI-33101 Tampere, Finland

ISBN 978-952-15-4272-5
ISSN 1459-2045